공학석사 학위논문

Structural Performance of Autoclaved Lightweight Concrete Masonry Walls subjected to Cyclic Lateral Loading

반복 횡 하중을 받는 경량기포콘크리트 조적벽체의 구조적 성능

2019년 2월

서울대학교 대학원

건축학과

김 영 문

Structural Performance of Autoclaved Lightweight Concrete Masonry Walls subjected to Cyclic Lateral Loading

지도 교수 박 홍 근

이 논문을 공학석사 학위논문으로 제출함

2019년 2월

서울대학교 대학원

건축학과

김 영 문

김영문의 공학석사 학위논문을 인준함

2019 년 2 월

위 원 장 _____ (인)

부위원장 _____ (인)

위 원 _____ (인)

Abstract

Structural Performance of Autoclaved Lightweight Concrete Masonry Walls subjected to Cyclic Lateral Loading

Kim, Young moon
Department of Architecture and Architectural Engineering
College of Engineering
Seoul National University

Developed in Europe in 1920, Autoclaved light-weight concrete (ALC) is one of the brick materials and is widely used in small houses because of its light weight and easy construction. Especially after the Second World War (1945), it was useful for restoration of German buildings. Since that time, it has expanded not only in Europe, but also in the US and Asia. In Korea, it started to produce ALC in the early 1990s, and now it is used in various fields such as factories and apartments as well as small houses.

The growing use of Autoclaved lightweight concrete (ALC) in Korea

requires that appropriate design provisions for ALC. At present, such design provisions are not addressed by structural design codes in Korea. In addition, seismic regulations have strengthened recently due to the Gyeongju and Pohang earthquakes. ALC buildings are also subject to these seismic standards. Therefore, building standards for ALC including seismic resistance are required.

This paper focused on the verification of structural performance of ALC walls subjected to cyclic lateral loading. And the material and prism tests were performed before the cyclic wall tests to confirm the basic properties of the ALC wall.

.

Keywords : Autoclaved light-weight concrete, Shearwall, standard, Glassfiber, cyclic

Student Number : 2017-22064

Contents

List of Tables

List of Figures

Chapter 1. Introduction

1.1 Background

Autoclave lightweight concrete (ALC) is a prefabricated concrete manufactured through high temperature and high-pressure steam curing process. There are two types of ALC products, such as blocks and panels. In Korea, blocks are used as walls or partitions, and panels are used as slabs, roofing and finishing materials.

ALC is manufactured by mixing, cutting, high-temperature high-pressure steam curing, and additional cutting as shown in Fig. 1-1. The constituent materials of ALC are usually the same as those of concrete. Its main materials are cement, lime, sand and water. To expand the volume, Aluminum powder is added. The chemical action of the aluminum powder generates gas and expands the volume of ALC. The pore in the ALC account for 80% of the total volume and makes the ALC light weight. Therefore, the dry-density is determined by the blending ratio of the aluminum powder. The next step is to cut the bulked ALC into blocks and panels. After that, ALC block and panel are under high temperature high pressure steam curing (190 ℃, 10 atm). The panel requires a secondary processing with intended use (roof, slab, exterior finishing). After high temperature and high-pressure steam curing, ALC has a high moisture content about 40 ~ 50%, so it is dried outdoors.

As can be seen from the manufacturing process, ALC is lighter than

ordinary concrete and has a lot of pores. Therefore, it is easy to transport and construction. In addition, it has excellent performance as an insulation material due to its low thermal conductivity. However, since the compressive strength and tensile strength are lower than that of ordinary concrete, it is structurally weaker than ordinary concrete. Therefore, a legalized structural standard is needed to make full use of the advantages of ALC through structural validation.

In Korea, seismic regulations have been strengthened since the Gyeongju and Pohang earthquake. Prior to the revision of the Building Code in 2017, seismic design was mandatory only for buildings with more than 16 stories and over 5,000 square meters of floor area. Currently, earthquake-resistant design was applied to buildings of more than 2 stories and 200 square meters of a floor area according to 48-3 of the revised Building Code (Disclosure of buildings' seismic capacity, Dec. 26, 2017). Therefore, it is necessary to verify the performance of ALC buildings because ALC building is also subject to earthquake regulation.

Currently, there are two design Standards for ALC in Korea (ALC Block / Panel Structure Design Standard, Ministry of Construction & Transportation Notice 1997-376). These old design Standards are about only gravity load, and there is no content about seismic design. On the other hand, in Europe and the United States, many studies on ALC have been carried out and related regulations have been established, but the standard about ALC in Korea has not changed. Therefore, it is necessary to confirm the performance of the ALC building through research and experiment.

(a) Mixing raw materials

(b) Cutting

Figure 1-1ALC Manufacturing process

(c) Curing with high temperature and pressure

(d) Additional cutting (Panel)

Figure 1-1ALC Manufacturing process

(e) Drying for adjuting a moiure content

Figure 1-1ALC Manufacturing process

In some parts of the world where earthquakes occur frequently, seismic details for ALC buildings are standardized. These details are different for each country and company, but can be divided into HEBEL and YTONG as shown in Fig. 1-2. These details recommend installing reinforce bars in the beam and the intersection of the wall to ensure the integrity of the ALC structure. The spacing of the vertical Re-bars is set to within 600mm, and the diameter of the column is about 150mm. The spaceing between vertical Re-bars is difficult to actual construction, and the block breaks frequently due to the hole for constructing the vertical Re-bar. Therefore, in this study, the vertical Re-bar was only reinforced at the side of wall and glass-fiber was reinforced at the whole wall to improve the workability, economy, and wall performance.

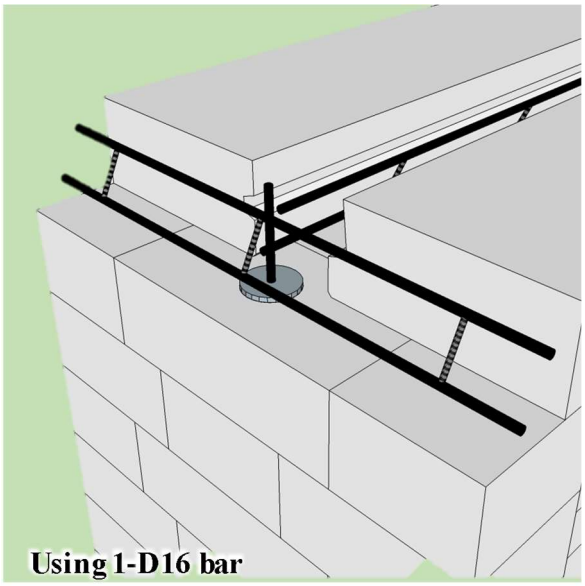

(a) HEBEL

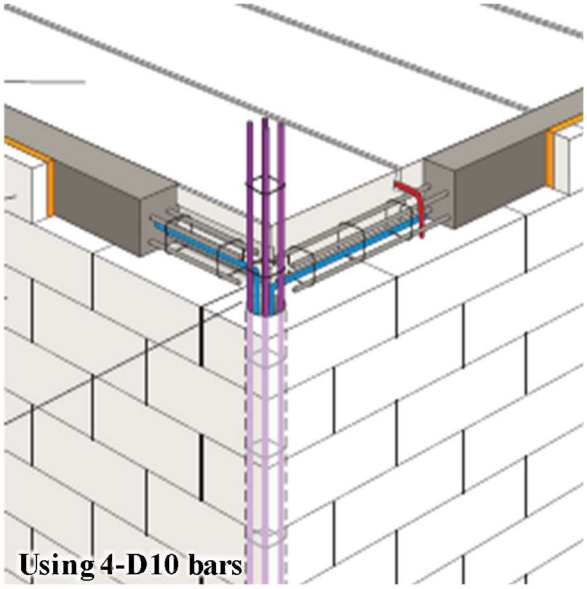

(a) YTONG

Figure 1-2 Reinforcement details of other countries

1.2 Scope and Objectives

This paper verified the structural performance of ALC walls subjected to cyclic lateral loading to improve the workability, economic efficiency, and performance of ALC buildings. Because there are few structural studies related to ALC in Korea, material tests and prism tests were performed to confirm the basic properties of ALC before the cyclic tests of wall.

The purpose of this study is to the structural performance of ALC walls subjected to cyclic lateral loading. To evaluate performance of ALC shear wall, the test results were compared with the code in ACI 523.4R. Because there are very few cyclic tests on ALC walls in Korea, this experiment will provide not only the performance of the ALC wall, but also the basic datas to judge the earthquake resistance ability of the ALC building.

1.3 Outline of the Master's Thesis

This paper described the structural performance of ALC shear walls subjected to cyclic lateral loading. The ALC walls consist of ALC blocks, panels, mortars, reinforcing bars and glass fibers as shown in Fig. 1-3. Therefore, to verify the structural performance of the wall, the experiment was divided into three parts as shown in Fig. 1-4. The first is material test to confirm the properties of ALC block and mortar. The second is a prism test. The third is the cyclic test of wall to confirm the seismic performance of the ALC wall.

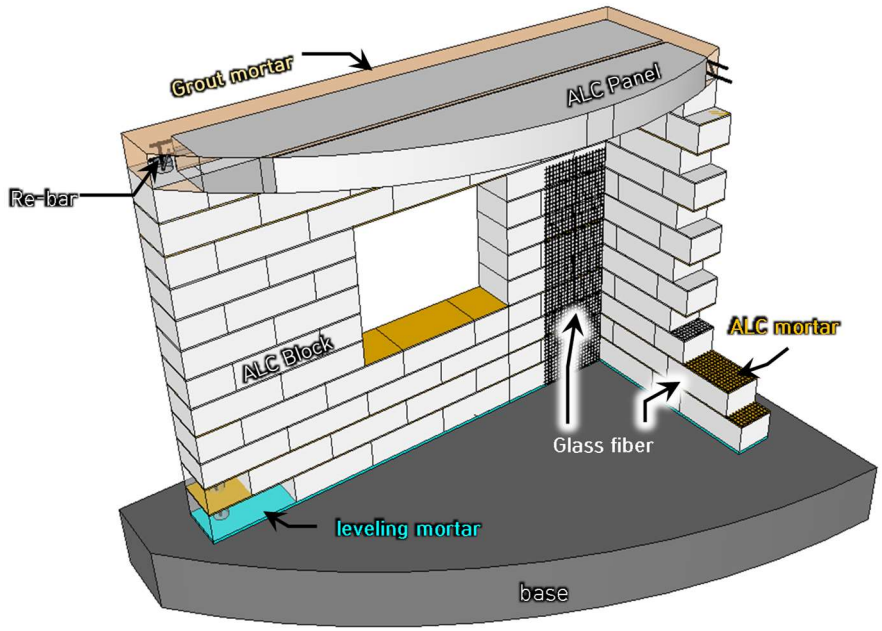

Figure 1-3 Components of a ALC building

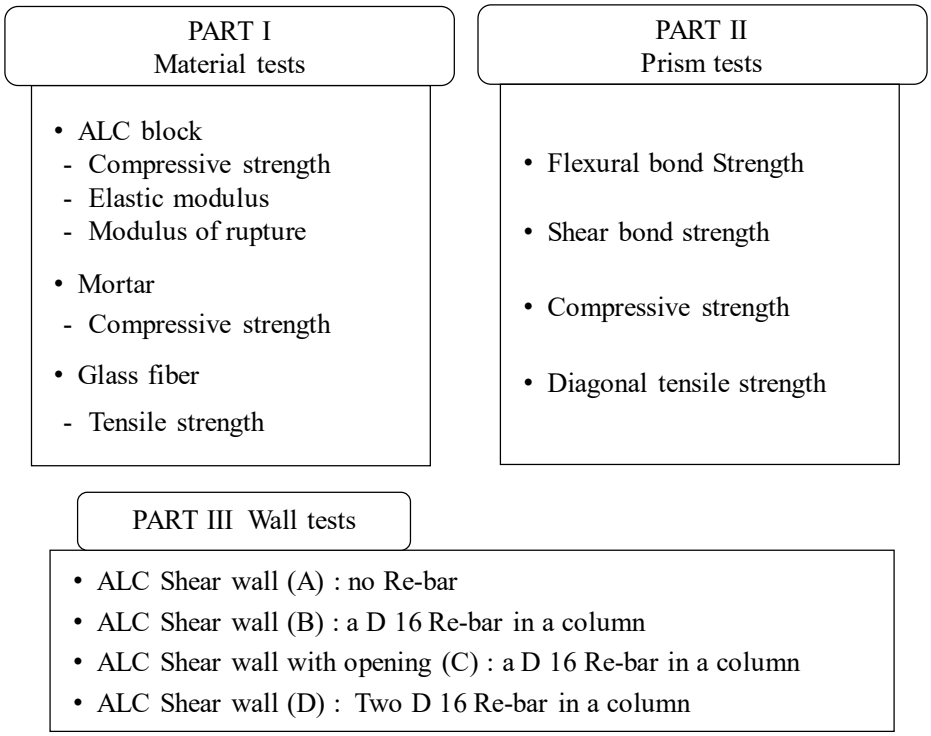

Figure 1-4 Outline of the master's thesis

Chapter 2. Literature Review

2.1 Code Review

2.1.1 Korean (Domestic) standards

Table 2-1 shows the domestic standards for ALC. Among them, the standards related to the block building are ALC block structure design standard (Ministry of Construction & Transportation (MOCT) 1997-373) and ALC block (KS F 2701: 2012).

Table 2-1 Korean Design standard for ALC

Code number	Title
MOCT 1997-376	Design standard for ALC block
MOCT 1997-377	Design standard for ALC panel
KS F 2701: 2012	ALC block
KS F 4914: 2017	ALC Panel

2.1.1.1 Design standard for ALC block (MOCT 1997-376)

The ALC block design standard stipulated by MOCT is only about simple construction methods and basic material properties. This standard covers only gravity design methods and empirical design methods, and there is no part about earthquake resistance.

The ALC block design standard (1997) is based on the allowable stress design method. The equaions in the block design standard (1997) are shown in Table 2-2. The design standard includes Allowable Compressive stress, flexural compressive stress, and shear stress of ALC. In the standard, tensile stress is not allowed, and the shear stress is calculated to be lesser than shear stress in ACI 523.4R.

Table 2-2Allowable Stress in Design standard for ALC block (1997)

Allowable stress	Equation
f_a 2)	$f_a = 0.2 f_{ALC}' \left[1 - \left(\frac{h'}{42t} \right)^3 \right]$
f_b 3)	$f_b = 0.33 f_{ALC}'$ 1)
f_t 4)	Not allowed
f_v 5)	$f_v = 0.09\sqrt{f_{ALC}'}$, $(f_v < 0.12$ MPa)

1) f_{ALC}'= Compressive strength of ALC (MPa), h'= wall height (mm), t= wall thickness (mm)

2) f_a = Allowable compressive stress

3) f_b = Allowable flexural compressive stress

4) f_t = Allowable tensile stress

5) f_v = Allowable Shear Stress

2.1.1.2 ALC block (KS F 2701: 2012)

The ALC block (KS F 2701: 2012) standard defines the quality of ALC block with dry density and compressive strength. As shown in Table 2-3, ALC blocks are classified into 0.5, 0.6, and 0.7 products with dry density and compressive strength. And this criterion focused on dry-density of ALC wall. However, this classification method does not help in designing the structure of ALC buildings. Structural importance is the compressive strength (tensile strength) of ALC, so it is desirable to classify the ALC block with compressive strength as in ACI.523.4R. In addition, classification of ALC blocks based on dry dentsity will prevent the development of ALC products that are lightweight and have excellent compressive strength.

Table 2-3 Classification for ALC block (KS F 2701: 2012)

Classification	Dry density (Ton/m^3)	Compressive strength (MPa)
0.5 product	0.45 ~ 0.55	$f_{ALC}' > 2.9$
0.6 product	0.55 ~ 0.65	$f_{ALC}' > 4.9$
0.7 product	0.65 ~ 0.75	$f_{ALC}' > 6.9$

2.1.2 International standards

The international building standards for ALC are ACI.523.4R in the United States and DIN EN 12602 in Europe. In addition, the BCRSM in the US and EUROCODE 6 in Europe provide standards for all brick buildings and include ALC. In this paper, in addition to the above four international standards, the ASTM standards were used to verify the performance of the ALC block structure (Table 2-4). Among them, ACI 523.4R and ASTM were mainly used for the test. The ACI 523.4R strength equations in Table 2-5 were used to evaluate the material and wall test results.

Table 2-4 International standards about ALC

Code number	Title
ACI 523.4R-09, 2009	Guide for Design and Construction with Autoclaved Aerated concrete Panels
DIN EN 12602 ,2013	Prefabricated Reinforced Components of Autoclaved aerated concrete
BCRSM, 2013	Building Code Requirements and Specification for Masonry Structures
Eurocode 6, 2005	Design of Masonry Structures
ASTM C67-11	Standard Test Methods for Sampling and Testing Brick and Structural Clay Tile
ASTM C78/C78M − 16	Standard Test Method for Flexural Strength of Concrete (Using Simple Beam with Third-Point Loading)
ASTM C91/C91M − 18	Standard Specification for Masonry Cement
ASTM C109/C109M − 16a	Standard Test Method for Compressive Strength of Hydraulic Cement Mortars
ASTM C270 − 14a	Standard Specification for Mortar for Unit Masonry
ASTM C476 − 16	Standard Specification for Grout for Masonry
ASTM E518/E518M − 15	Standard Test Methods for Flexural Bond Strength of Masonry

ASTM E519/E519M − 15	Standard Test Method for Diagonal Tension (Shear) in Masonry Assemblages
ASTM C1660 − 10	Standard Specification for Thin-bed Mortar for Autoclaved Aerated Concrete (AAC) Masonry
ASTM C1692—11	Standard Practice for Construction and Testing of Autoclaved Aerated Concrete (AAC) Masonry
ASTM C1691 − 11	Standard Specification for Unreinforced Autoclaved Aerated Concrete (AAC) Masonry Units
ASTM C1693 − 11	Standard Specification for Autoclaved Aerated Concrete (AAC)

Table 2-5 Equations in ACI.523.4R(2009)

	Equation
f_{ALC}' (MPa) compressive strength,	$f_{ALC}' \geq 2MPa$
f_t (MPa) Splitting tensile strength,	$f_t = 0.2\sqrt{f_{ALC}'}$
f_r (MPa) Modulous of rupture	$f_r = 2f_t$
f_v (MPa) Shear strength	$f_v = 0.15f_{ALC}'$
V_n (kN) Nominal Shear Strength,	$V_n = V_{nALC} + V_{ns}$
V_{SL} (kN) Sliding shear strength	$V_{SL} = \mu P_u$
V_{sh} (kN) Web shear stength	$V_{sh} = 0.133 l_w t\sqrt{f_{ALC}'}\sqrt{1+\frac{P_u}{0.2\sqrt{f_{ALC}'}l_w t}}$
V_{DS} (kN) Diagonal strut compressive stength	$V_{DS} = 0.17 f_{ALC}' t \frac{h l_w^{\,2}}{h^2 + \left(\frac{3}{4}l_w\right)^2}$
M_{cr} (kN·m) Flexural crack stength	$M_{cr} = S_n\left(f_r + \frac{P_u}{A}\right)$

2.2 Literature Review

2.2.1 Design provision for AAC structural system (tenner, 2004)

In tenner's paper, when a wall receives a lateral force, the cracks in the wall exhibit types as shown in Figure 2-1.

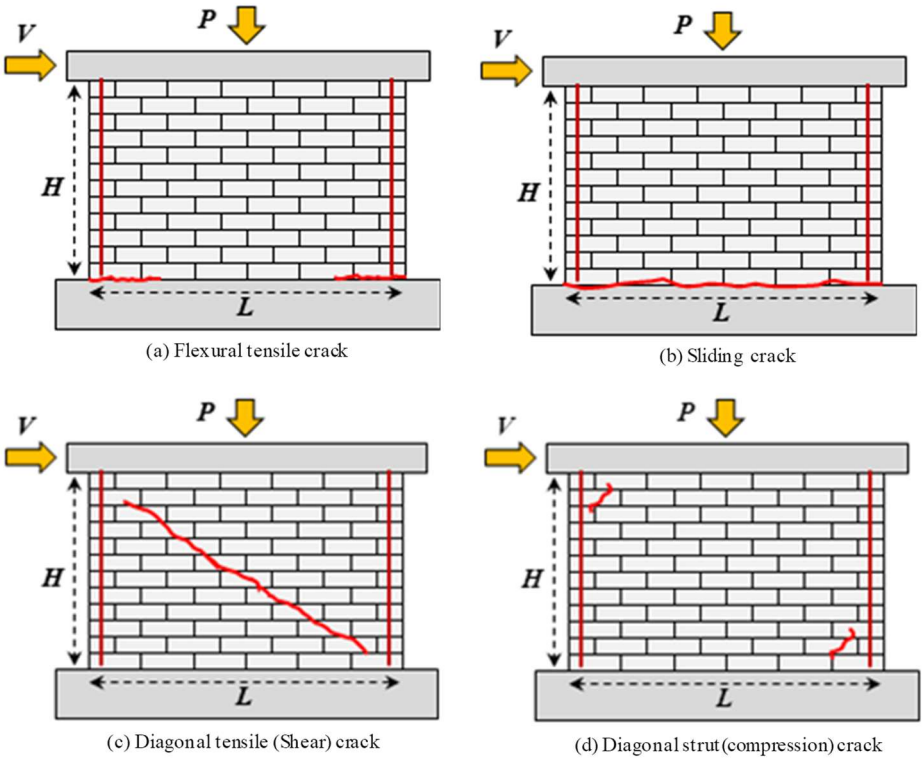

Figure 2-1 Pattern of crack in shear wall

(1) Flexural crack strength

The flexural crack occurs when the flexural tensile stress at bottom of the wall end generated by the lateral force is greater than the flexural bond strength of the leveling mortar between the wall and the foundation and is shown in Eq. 2-1.

$$V_f = \left(f_r + \frac{P}{A} \right) \times \frac{tL^2}{H} \tag{2-1}$$

Where V_f is the flexural crack strength, P is the axial force, A is the cross-sectional area of the wall, t is the wall thickness, and H is the wall height.

(2) Sliding shear strength

Sliding cracks in the ALC Wall occur when the lateral force is greater than the shear friction strength of the mortar and the shear friction strength is as shown in Eq. 2-2.

$$V_{sl} = \mu P + 0.6 f_y A_S \tag{2-2}$$

Where μ is the friction coefficient of the friction surface, f_y is the yield strength of the Re-bar, and A_S is the cross-sectional area of the vertical Re-bar.

(3) Web shaer strength

The web shear strength is the lateral force when the tensile stress of the wall reaches the split tensile strength (f_t) and is given by Eq. 2-3sing Mohr's circle.

$$V_{sh} = \frac{2}{3} L t f_t \sqrt{1 + \frac{P}{f_t L t}} \tag{2-3}$$

Where V_{sh} is web shear strength, L is wall length, t is the wall thickness, and P is the axial load.

In the paper, the 10% lower shear strength of 13 fully mortared walls was 59% of V_{sh} in Eq. 2-3 and, the 10% lower the shear strength of 9 partially mortared walls was 38% of V_{sh} in Eq. 2-3. Therefore, the shear strength of the ALC wall is obtained by multiplying V_{sh} in Eq. 2-3 by the leading coefficient in Table 2-6.

Table 2-6 Leading coefficient of Shear strength

Classification	Leading coeffcient	-
Fully mortared wall	0.59	Based on the lower 10% strength of 13 specimens
Partially mortared wall	0.38	Based on the lower 10% strength of 13 specimens

(4) Crushing of diagonal strut strength

Crushing of diagonal strut strength (V_{ds}) is the lateral force when Strut is compressively fractured in Strut-tie-model made of lateral force and compressive force, and it is expressed by Eq. (2-4). The width of the strut is assumed to be 0.25L in the papaer.

$$V_{ds} = 0.17 \frac{f_{ALC} HL^2}{H^2 + \left(\frac{3}{4}L\right)^2} \tag{2-4}$$

(5) Flexural strength

In the tenner's paper, the flexural strength of the ALC wall could be obtained from conventional flexural theory. The following conditions were considered to determine the flexural strength. The maximum compressive strain of the ALC block was 0.003, the height of the compressive stress block was 0.85 f_{ALC}, and the width of that was $\beta_1 c$ ($\beta_1 = 0.67$). In his tests, ratio of predicted flexural strength to the experimental strength was 1.19. Therefore, the flexural strength of ALC wall could be obtained by conventional flexural theory.

Chapter 3. Material

3.1 Introduction

ALC building consists of ALC block and ALC panel. In Korea, wall is made of ALC block, and slab and roof are made of ALC panel. ALC blocks and panels are bonded with ALC mortar and cement mortar, and ALC mortar is used between ALC blocks. Cement mortar is used between base and wall, column, beam.

Therefore, the material tests were performed before the ALC prism, and the wall test. In material test, ALC block, ALC mortar, cement mortar and glass-fiber were tested. In ALC block tests, compressive strength, elastic modulus and flexural tensile strength were examined. In for ALC mortar and cement mortar tests, compressive strength tests were performed. In the glass-fiber tests, tensile strength tests were conducted and methods with glass-fiber reinforcement were verified.

Because the compressive strength and the flexural tensile strength of the ALC block are vary with the direction of the material, so that the load is applied perpendicular to the direction of rise of specimen. (ASTM C 1693 recommends testing in the direction perpendicular to the material's rise)

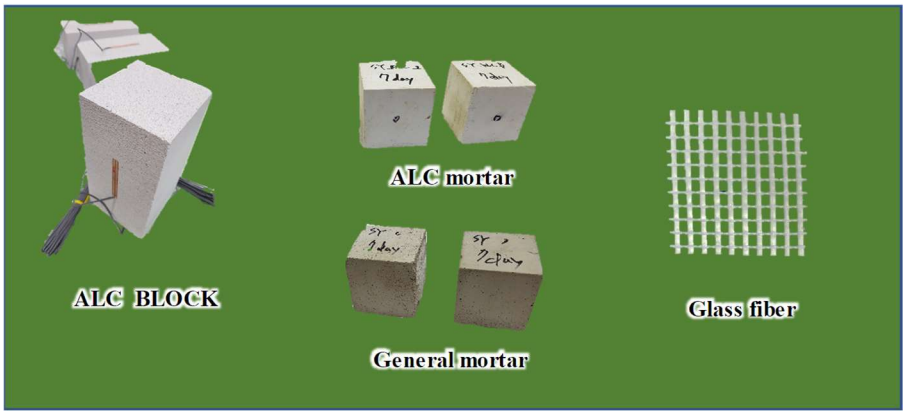

Figure 3-1 Kinds of material

3.2 ALC block

3.2.1 ALC Block Compressive Strength

(1) Variables

The variables affecting the compressive strength of ALC block are density and moisture content. According to existing studies and current standards, the compressive strength increases as the density increases or the water content decreases. The density means the weight per unit volume, and the density of the material varies depending on the amount of aluminum powder added during the mixing process of ALC. The moisture content (M.C) means the water content of dried ALC. The lower the moisture content, the more the compressive strength increases. Since the ALC moisture content after steam curing usually is about 50%, drying enough is necessary to satisfy the water content of 8 ~ 10 % (KS standard) or 10 ~ 15% (ASTM standard) which can be used as building material.

In addition, a factor that can affect the ALC compressive strength is the location of the specimen. The specimens for compressive strength test according to KS standards are to be taken from the center of the block. This is because strength can be changed depending on the position of the specimen. The reason for the different strengths with the position is that the gas generated by the chemical reaction of the aluminum powder. The gas rises to the upper part of the ALC block, and many pores are located at the upper part of the ALC block. Therefore, the strength of the upper part is lower than that of the lower part.

In this study, the moisture content was controlled from 10 % to 15 % as shown in Table 3-1, and the density and the location of the ALC block were considered as variable. The test specimens with high moisture content were dried in an oven at 70 ° C to lower the moisture content. For the compressive strength test of ALC block, 0.35, 0.5, and 0.6 specimens made by SYC Co and 0.5, 0.6 specimens made by Sung Eun Co were tested. The specimens were collected from the top, middle, and bottom of five different molds as shown in Fig 3-2. 15 specimens were collected from each mold and 75 specimens were tested to examine compressive strength of ALC block. (In the KS standard, compressive strength is measured only in the middle of the block. In ASTM C 1693, compressive strength is tested the upper, middle, and lower parts of ALC). In this test, all specimens were collected according to ASTM C 1693. The size of each specimen is 100mm * 100mm * 100mm (cube).

Table 3-1 variables of ALC block compression strength test

Company	Density (Ton/m^3)	location	M.C	Quantity
SYC	0.35	Upper Middle Lower	10~15%	15
	0.5			15
	0.6			15
Sung Eun	0.5			15
	0.6			15

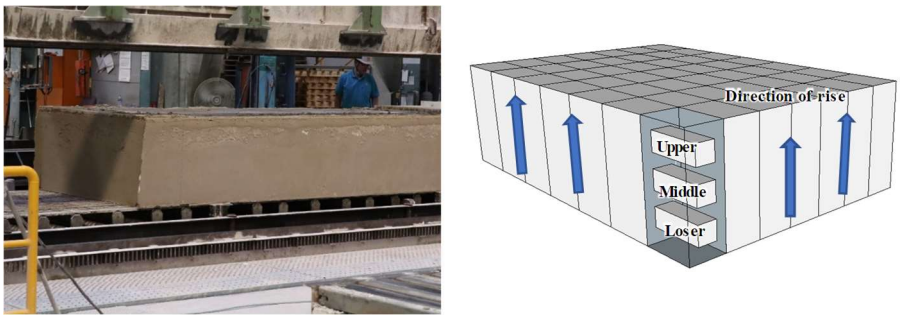

Figure 3-2 Cake of ALC (left), location of specimens (right)

(2) Test Setup

To evaluate the compressive strength of the ALC block, a monotonic incremental compressive strength tests were conducted according to ASTM C1693 using a 2,000 kN capacity universal testing machine (UTM) as shown in Fig. 3-3.

Figure 3-3 test setup for compressive strength of ALC block

(3) Test Results

The relationships between the compressive strength of the ALC block with the dry density (Ton / m^3) are shown in Fig. 3-4. The horizontal axis of the graph represents the dry density and the vertical axis represents the compressive strength. Classifying with ALC block sampling position, the upper part of was represented by a red circle, the middle part was indicated by a white triangle, and the lower part was indicated by a blue square. The required compressive strength and dry density in Low-rise building stuructural standard (Table 3-2) are indicated by black dotted line.

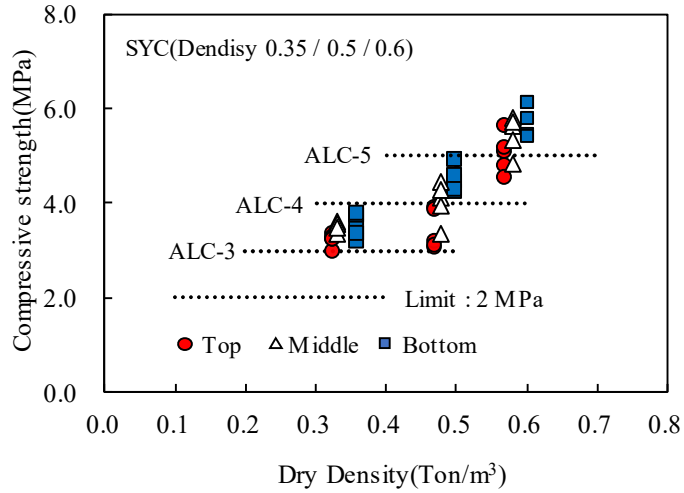

(a) SYC Co.

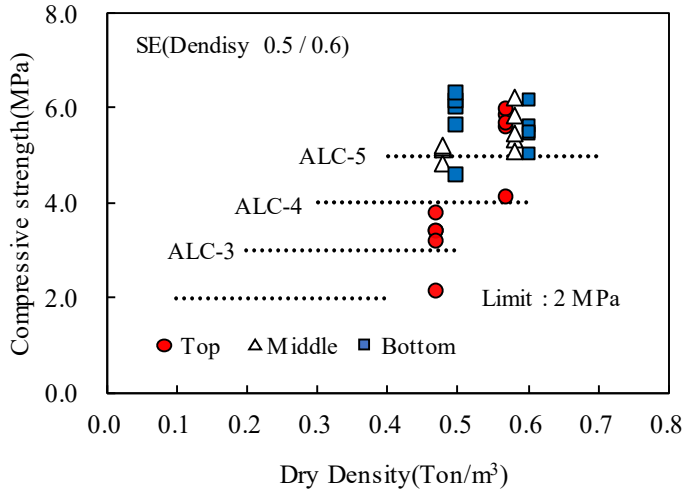

(b) Sung Eun Co.

Figure 3-4 Compressive Strength-Dry density relationships of testspecimen

Table 3-2 classification of ALC block with compressive strength and dry density(Low-rise building standard)

Classification	Demand compressive strength (MPa)	Dry density (Ton/m^3)
ALC-2	2.0	0.25-0.45
ALC-3	3.0	0.35-0.55
ALC-4	4.0	0.45-0.65
ALC-5	5.0	0.55-0.75
ALC-6	6.0	0.55-0.75

Compressive strength of the ALC blocks of both companies increased with increasing dry density. The ALC blocks made by SYC Co. showed small deviation (Gap between maximum and minimum strength difference = 2.0 MPa or less) with positions (upper, middle, lower) in the same product. On the other hand, the 0.5 (Ton/m^3) ALC blocks made by Sung Eun showed large the deviation (Gap between maximum and minimum strength difference = 4.0 MPa).

As shown in the test results, the compressive strength of the ALC block were affected by sampling the position and dry density of the specimen. Although not tested, the compressive strength coulde vary with the water content. Therefore, before measuring the compressive strength of the ALC block, all parameters should be considered.

Table 3-3 Test results of compressive strength of ALC block (SYC Co.)

Specimen Location	Mold NO.	M.C (%)	Compressive Strength (MPa)	A.V. Compressive Strength (MPa)	C.O.V (%)	A.V. Compressive Strength (MPa)	C.O.V (%)
0.35 Product							
Upper	1	12.9	3.35	3.20	0.05	3.40 MPa	0.06
	2	13.2	3.25				
	3	14.5	2.95				
	4	16.0	3.23				
	5	13.5	3.22				
Middle	1	10.0	3.32	3.50	0.03		
	2	10.0	3.58				
	3	17.3	3.54				
	4	17.6	3.57				
	5	10.6	3.46				
Lower	1	3.9	3.49	3.50	0.07		
	2	7.1	3.17				
	3	10.0	3.73				
	4	11.1	3.76				
	5	8.3	3.32				
compressive strength corresponding to 5% lower fractile = 3.35 MPa							
0.5 Product							
Upper	1	10.6	3.88	3.41	0.12	3.97	0.14
	2	5.5	3.06				
	3	7.0	3.17				
	4	10.4	3.85				
	5	9.1	3.08				
Middle	1	12.3	3.33	4.01	0.11		
	2	10.0	4.43				
	3	11.3	4.11				
	4	10.0	3.92				
	5	10.2	4.27				
Lower	1	11.4	4.25	4.48	0.06		
	2	15.8	4.92				
	3	13.2	4.44				
	4	11.0	4.55				
	5	15.8	4.26				
compressive strength corresponding to 5% lower fractile = 3.56 MPa							

0.6 Product							
Upper	1	6.8%	4.77	5.03	0.08	5.42	0.08
	2	9.6%	5.06				
	3	8.1%	5.16				
	4	7.2%	5.61				
	5	8.9%	4.54				
Middle	1	9.1%	5.80	5.45	0.07		
	2	7.4%	5.60				
	3	6.9%	5.72				
	4	7.4%	4.80				
	5	7.6%	5.34				
Lower	1	12.3%	6.11	5.78	0.06		
	2	12.5%	6.11				
	3	11.0%	5.47				
	4	5.7%	5.78				
	5	13.0%	5.40				
compressive strength corresponding to 5% lower fractile = 5.17 MPa							

Table 3-4 Test results of ALC compressive strength of ALC block (Sung Eun)

Specimen Location	Mold NO.	M.C (%)	Compressive Strength (MPa)	A.V. Compressive Strength (MPa)	C.O.V (%)	A.V. Compressive Strength (MPa)	C.O.V (%)
0.5 Product							
Upper	1	8.7	3.40	3.44	0.18	4.76	0.25
	2	7.9	2.13				
	3	11.3	3.77				
	4	10.0	3.41				
	5	11.7	3.20				
Middle	1	11.5	5.18	5.10	0.03		
	2	10.0	5.13				
	3	7.9	5.18				
	4	9.0	4.83				
	5	7.1	5.21				
Lower	1	10.4	6.04	5.74	0.12		
	2	11.6	4.58				
	3	10.2	5.64				
	4	12.0	6.13				
	5	12.0	6.33				
compressive strength corresponding to 5% lower fractile = 3.08 MPa							
0.6 Product							
Upper	1	11.6	4.10	5.44	0.14	5.53	0.09
	2	11.9	5.59				
	3	8.8	5.85				
	4	10.7	5.97				
	5	11.2	5.69				
Middle	1	12.1	6.22	5.58	0.08		
	2	9.8	5.84				
	3	11.2	5.35				
	4	12.1	5.45				
	5	14.0	5.07				
Lower	1	11.8	5.47	5.56	0.07		
	2	8.5	6.17				
	3	9.3	5.62				
	4	11.0	5.50				
	5	14.2	5.05				
compressive strength corresponding to 5% lower fractile = 5.41 MPa							

3.2.2 Elastic modulus

(1) Variables

To measure the modulus of elasticity of the ALC block, the compressive strength and the strain of the ALC block were measured together to confirm the elastic modulus. As the main variables, the density of the ALC block and the location of specimen were considered as shown in Table 2-5. The size of the specimen was 100 × 100 × 200 mm^3 according to ASTM C 1693.

Table 3-5 Variables of ALC block elastic modulus test

Company	Density (Ton/m^3)	Location	M.C	Quantity
SYC	0.35	Upper Middle Lower	5~15%	15
	0.5			15
	0.6			15
Sung Eun	0.5			15
	0.6			15

(2) Test setup

For the measurement of the compressive strength and strain of the ALC block, a compressive strength tests were performed according to ASTM C1693 using a 2,000 kN UTM as shown in Fig. 3-5. Two strain gauges were attached to the opposite sides of the block.

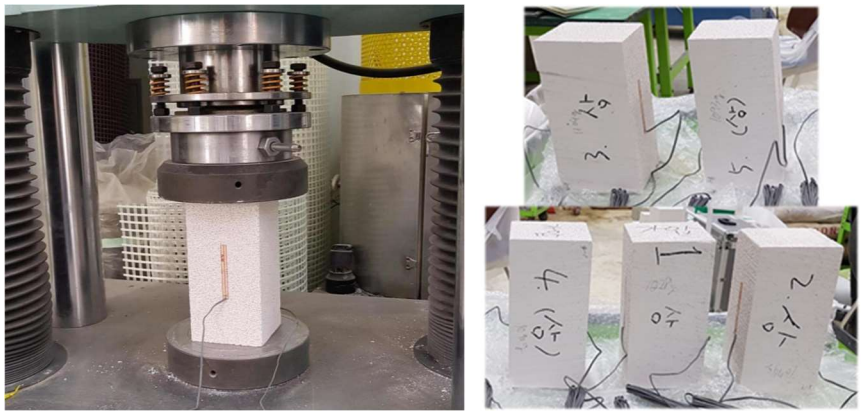

Figure 3-5 ALC block compression strength test set-up

(3) Test Result

The elastic modulus of the ALC block was calculated from the slope of the line connecting the points at 5% and 33% of the maximum stress in the stress-strain curves as shown in Fig. 3-6.

$$E = \frac{\sigma_{33\%} - \sigma_{5\%}}{\varepsilon_{33\%} - \varepsilon_{5\%}} \tag{3-1}$$

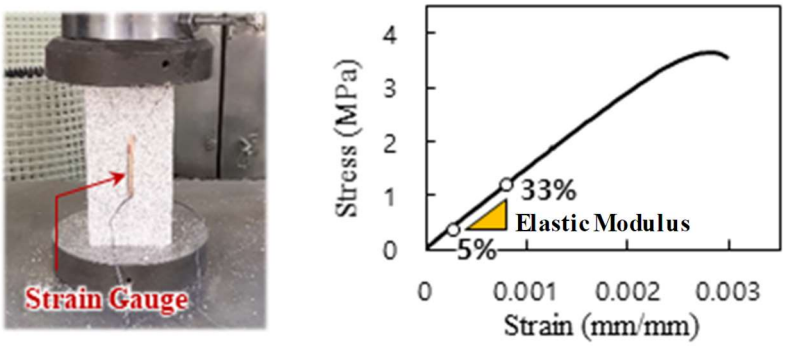

Figure 3-6 Measurement method of elastic modulus of ALC block

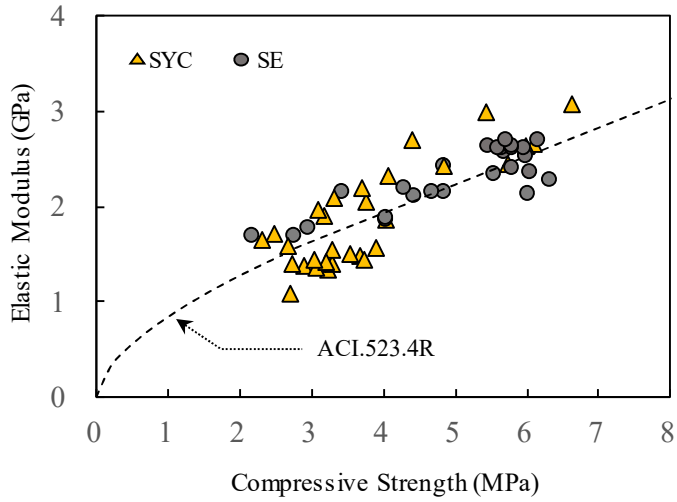

(a) Relationships of Elastic modulus and Compressive strength

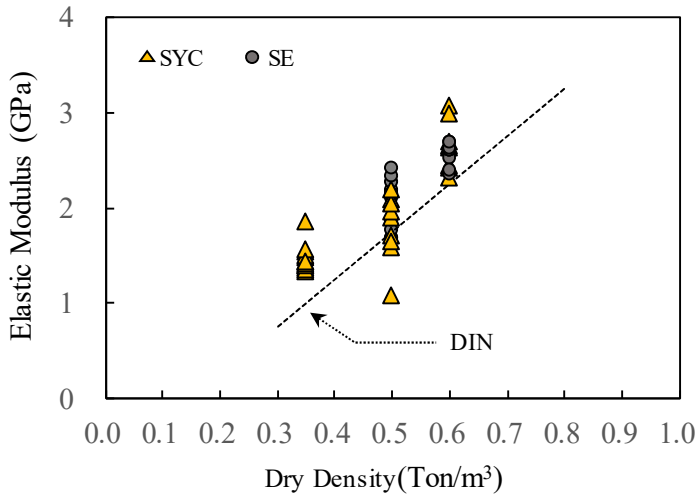

(b) Relationships of Elastic modulus and Dry-density

Figure 3-7 Tendency of elasticic modulus

The relationships of elastic modulus with the compressive strength as shown in Fig.3-7(a) and the prediction by ACI 523.4R was indicated by dashed line. And the relationships of elastic modulus with the dry density as shown in Fig

3-7(b) and the prediction by DIN was indicated by dashed line. The results of the ALC block made by SYC were indicated by yellow triangles and those of Sung Eun were indicated by gray circles. The predictions in ACI 523.4R and DIN standards are as follow equations.

$$E_{ACI523} = 840(f_{ALC}')^{0.6} \tag{3-2}$$

$$E_{DIN} = 5(\rho_{ALC} - 150), \qquad \text{UNIT}: \text{MPa}, \text{kg/m}^3 \tag{3-3}$$

Where, f_{ALC} is the compressive strength of the ALC block, ρ_{ALC} is the density of the ALC block (Ton/m^3). The test results of the elastic modulus were detailed in Tables 3-6 and Fig. 3-8.

In test results, the elastic modulus increased with increasing compressive strength and dry density. In Fig. 3-7(left), the Eq. 3-2 predicted test results well. (Mean = 1.19, S.D = 0.14). However, In ALC block made by SYC, the elastic modulus of block with 2.5 ~ 4.0MPa compressive strength was unsafe because of its low density. In Fig. 3-7(right), Eq. 3-3 proposed by DIN also predicted test results well (mean = 1.22, S.D = 0.16). Among them, the Eq 3-2 proposed by ACI 523.4R predicted the elastic modulus better than that of DIN.

Table 3-6 Test results of Elastic modulus

Classification		Mean	Upper					Middle					Lower			
			1	2	3	4	5	1	2	3	4	5	1	2	3	4
SYC 0.35	Elastic modulus (MPa)	1478	1394	1335	1416	1556		1494	1368	1450	1396	1421	1501	1565	1862	1453
	Compressive strength (MPa)	3.35	2.88	3.23	3.29	3.27		3.66	3.06	3.73	2.74	3.19	3.55	3.89	4.03	3.04
	Density (Ton/m^3)	771.2	770.0	770.0	809.0	735.0		734.0	792.0	736.0	816.0	760.0	757.0	759.0	809.0	778.0
	M.C (%)	10.2	13.2	13.2	19.0	8.1		4.9	13.1	5.1	16.6	8.6	5.1	5.4	12.4	8.1
SYC 0.5	Elastic modulus (MPa)	1813	1720	1604	1664			1912	1975	1085			2106	2049	2201	
	Compressive strength (MPa)	3.02	2.49	2.67	2.32			3.16	3.09	2.69			3.32	3.75	3.70	
	Density (Ton/m^3)	1092.8	1029.0	1027.0	1015.0			1105.0	1091.0	1095.0			1143.0	1158.0	1172.0	
	M.C (%)	13.0	9.5	9.3	8.0			15.1	13.6	14.1			14.3	15.8	17.2	
SYC 0.6	Elastic modulus (MPa)	2661	2333	2446				3078	2996	2656			2649	2711	2421	
	Compressive strength (MPa)	5.40	4.05	5.73				6.63	5.43	6.09			5.97	4.40	4.85	
	Density (Ton/m^3)	1291.8	1226.0	1216.0				1240.0	1262.0	1260.0			1399.0	1422.0	1309.0	
	M.C (%)	10.3	7.5%	6.7				6.9	8.8	8.6			16.6	18.5	9.1	
Sung Eun 0.5	Elastic modulus (MPa)	2066	1699	1706	1862	1785	1883	2154	2112	2200	2168	2135	2276	2351	2159	2437
	Compressive strength (MPa)	4.31	2.76	2.17	4.03	2.96	4.04	4.85	4.42	4.28	4.67	6.02	6.32	5.53	3.42	4.83
	Density (Ton/m^3)	1071.3	1028.0	1074.0	1109.0	1090.0	1093.0	1042.3	1073.0	1068.0	996.0	1032.0	1098.3	1114.0	1092.0	1089.0
	M.C (%)	11.1	9.4	14.3	18.0	16.0	16.3	8.6	11.8	11.3	3.8	7.5	9.8	11.4	9.2	8.9
Sung Eun 0.6	Elastic modulus (MPa)	2587	2575	2620	2541	2369		2639	2708	2624	2614		2611	2407	2636	2695
	Compressive strength (MPa)	5.80	5.68	5.65	5.99	6.05		5.45	6.16	5.95	5.60		5.79	5.79	5.79	5.70
	Density (Ton/m^3)	1318.3	1300.0	1280.0	1300.0	1280.0		1320.0	1340.0	1320.0	1300.0		1360.0	1360.0	1340.0	1320.0
	M.C (%)	13.0	14.0	12.3	14.0	12.3		13.8	15.5	13.8	12.1		13.3	13.3	11.7	10.0

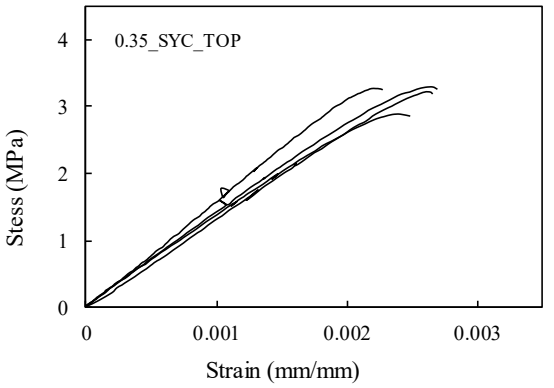

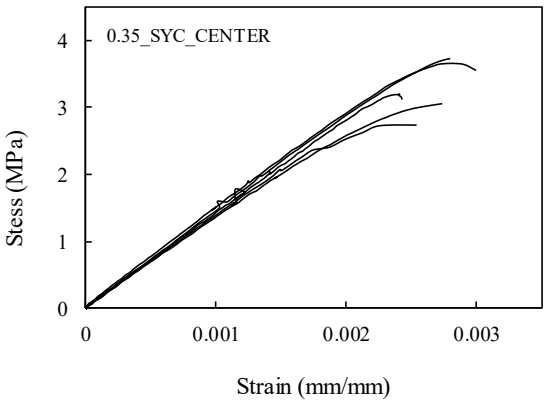

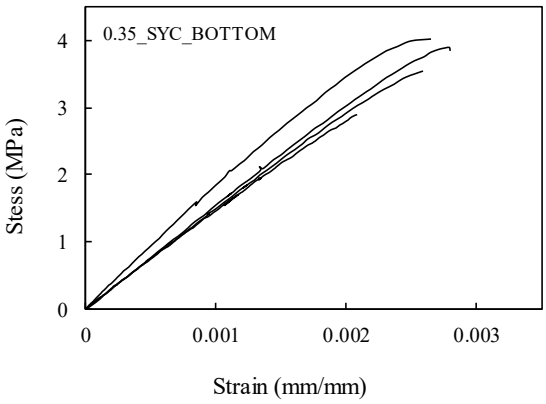

(a) 0.35 Ton/m^3 ALC Block made by SYC Co.

Figure 3-8 Stress-Stress relationships (ALC block)

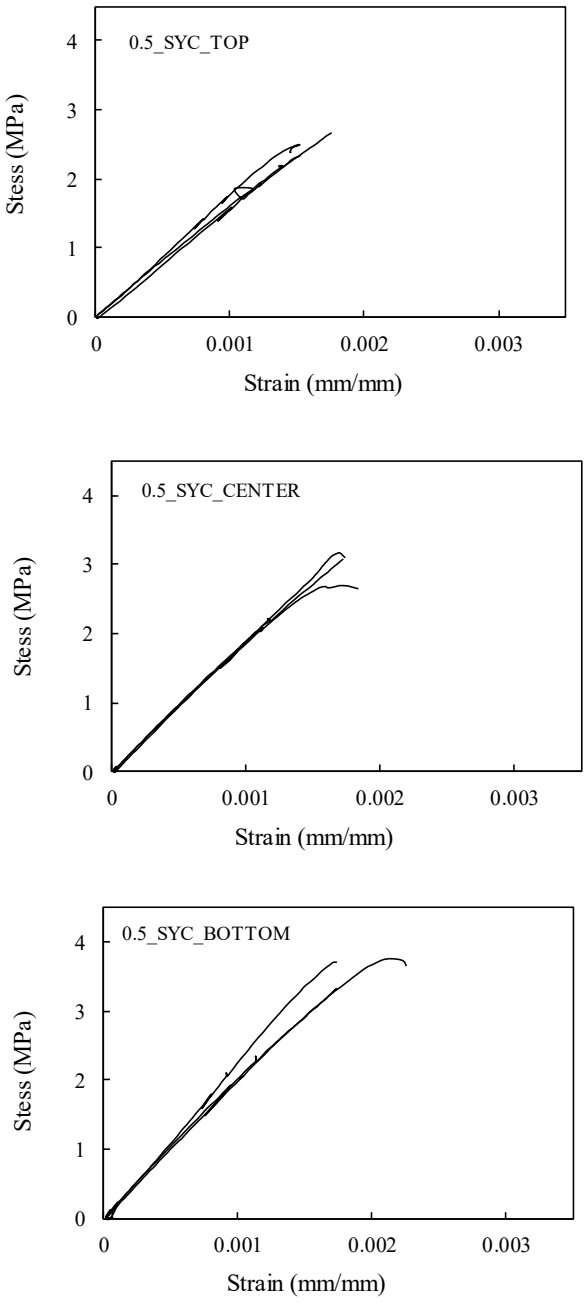

(b) 0.5 Ton/m^3 ALC Block made by SYC Co.

Figure 3-8 Stress-Stress relationships (ALC block)

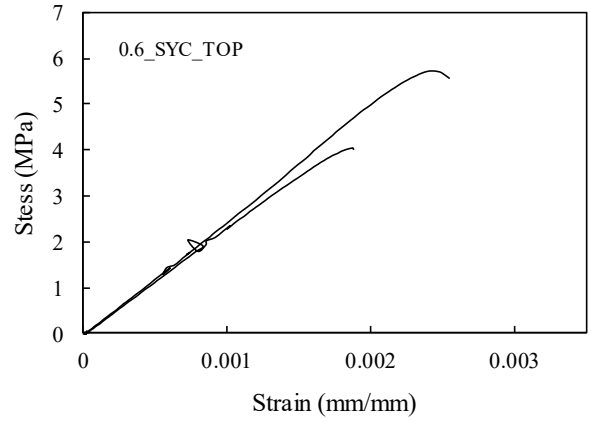

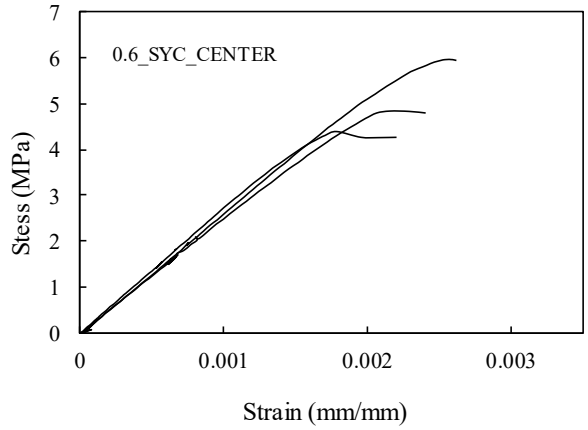

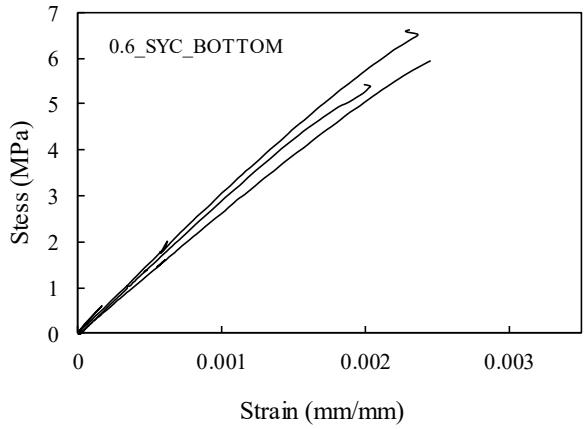

(c) 0.6 Ton/m^3 ALC Block made by SYC Co.

Figure 3-8 Stress-Stress relationships (ALC block)

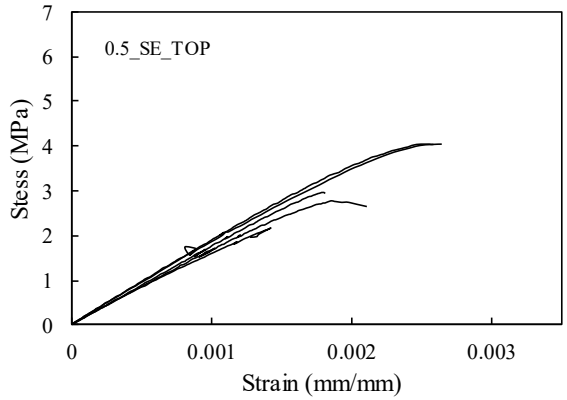

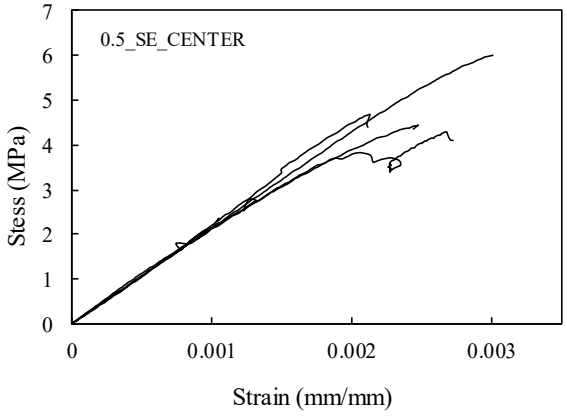

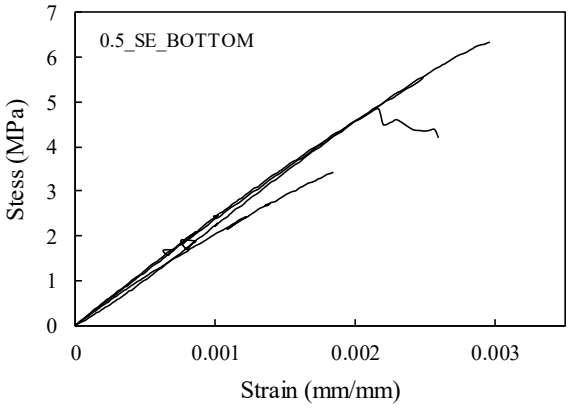

(d) 0.5 Ton/m^3 ALC Block made by Sung-Eun Co.

Figure 3-8 Stress-Stress relationships (ALC block)

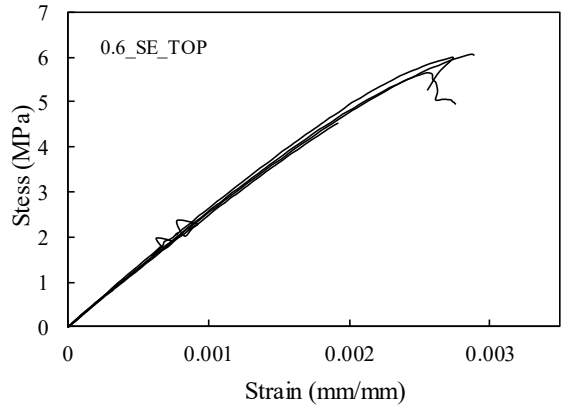

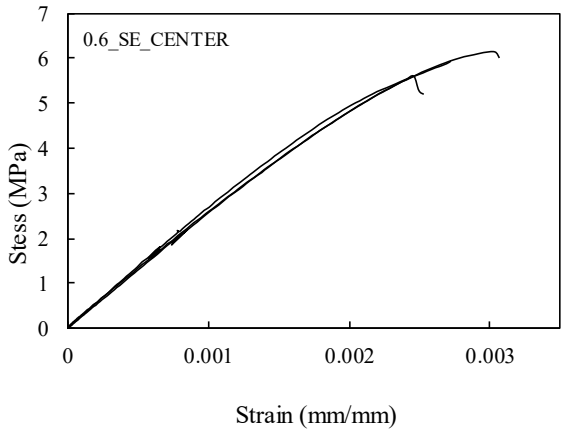

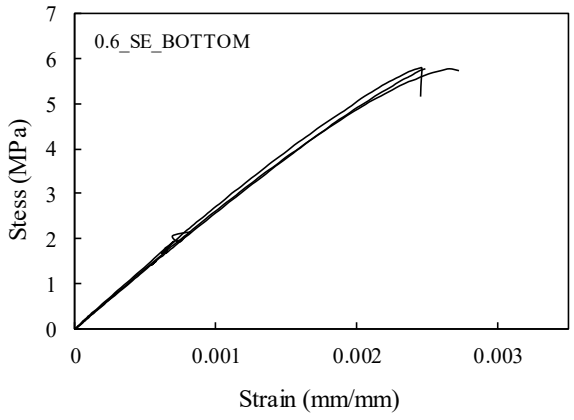

(e) 0.6 Ton/m^3 ALC Block made by Sung-Eun Co.

Figure 3-8 Stress-Stress relationships (ALC block)

3.2.3 Modulus of ruptrue (MOR, Flexural tensile strength)

(1) Variables

The tensile strength of the ALC block is important properties as well as the compressive strength. To evaluate flexural tensile strength of ALC block, flexure tensile strength tests were performed with dry density as shown in Table 3-7. The tests were first carried out on the 0.35 ALC block made by SYC Co. and the 0.5 ALC block made by Sung Eun. After that, the 0.35, 0.5 and 0.6 ALC block made by SYC Co. and 0.5, 0.6 ALC block made by Sung Eun were tested to check the flexural tensile strength of blocks with various dry densities. The size of each specimen was 150 × 150 × 600 mm^3 as shown in Fig. 3-9.

Table 3-7 variables of ALC block in flexural tensile strength test

Company	Density (Ton/m^3)	M.C(%)	Quantity	
			1st	2nd
SYC	0.35	5~15	5	6
	0.5		-	6
	0.6		-	6
Sung Eun	0.5		5	6
	0.6		-	6

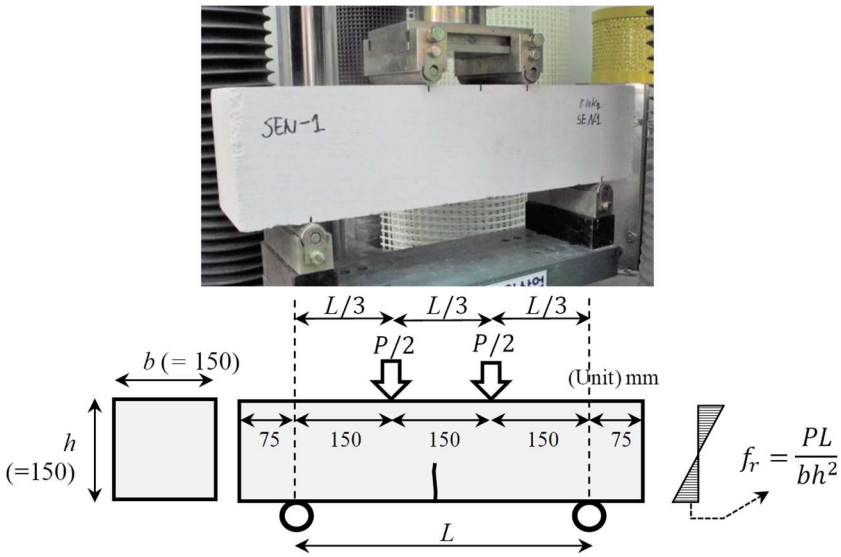

Figure 3-9 Test set-up for MOR

(2) Test Set-up

Because the direct tensile strength (f_t) of the ALC block was difficult to test, so that the modulus of rupture (f_r) was tested to verify the tensile strength. In ACI 523.4R, the relation between the flexural tensile strength and the splitting tensile strength is shown in Eq. 3-4.

$$f_r = 2f_t \tag{3-4}$$

To test the flexural tensile strength(=M.O.R), load was applied to the specimen at 2 points according to ASTM C78 using 2,000 kN capacity UTM as shown in Fig. 3-9. The flexural tensile strength (f_r) is the tensile stress at the bottom of block when the crack was occurred in the ALC block and is calculated by Eq. 3-4.

$$f_r = \frac{PL}{bh^2} \tag{3-4}$$

Where, b is the width of the block, h is the height of the block, P is the load, and L is the distance between the supports.

(3) Test Result

The flexural tensile strength with the compressive strength of the ALC block is shown in Fig. 3-10. The results of SYC block are shown in yellow triangles, and those of Sung Eun are shown in gray circles. To compare the strengths of the test results with those of the current international standards, the strength proposed by RILEM, UT Austin (AIC 523.4R), and DUTCH are also shown in the Fig.3-10. The predition in RILEM was indicated by a green dotted line, that in UT Austin was indicated by a red solid line, and that in DUTCH was indicated by a blue dotted line. The compressive strength, flexural tensile strength, water content, and fracture type of each specimen are detailed in Table 3-8.

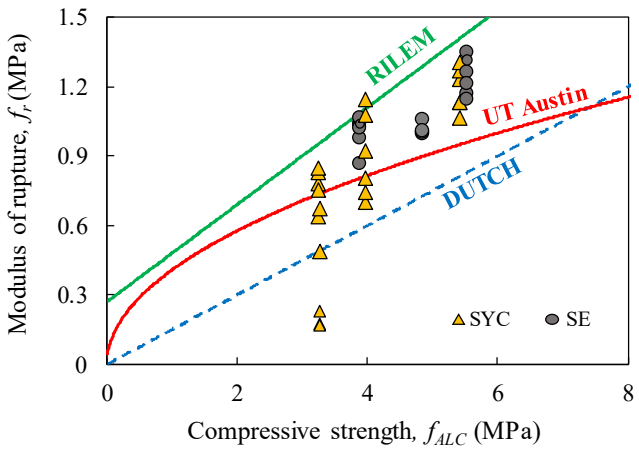

Figure 3-10 Relationship of compressive strength - Modulus of rupture

Test results showed that the flexural tensile strength tends to increase with increasing compressive strength. Comparing the test results with the current standards, RILEM overestimated the test results so that almost all the specimens were unsafe (mean = 0.78, S.D = 0.26) and DUTCH predicted all the specimens safely but underestimated (mean = 1.42, S.D = 0.26). The UT Austin predictions used in ACI 523 predicted the best (mean = 1.09, SD = 0.27). Therefore, the Eq.3-6 proposed by UT Austin best matched the test results.

$$f_r = 0.27 + 0.21 f_{ALC} \text{ (RILEM)} \tag{3-5}$$

$$f_r = 0.4\sqrt{f_{ALC}} \text{ (UT. Austin)} \tag{3-6}$$

$$f_r = 0.15 f_{ALC} \text{ (DUTCH)} \tag{3-7}$$

Table 3-8 Test results of Modulus of rupture

Product	f_{ALC} (MPa)	-	Mean	Specimen					
				1	2	3	4	5	6
SYC (0.35)	3.28	MOR(MPa)	0.34	0.17	0.23	0.67	0.49	0.16	
		M.C(%)	15.17	15.90	18.52	12..96	9.88	16.36	
		failure mode	-	flexure	flexure	flexure	flexure	flexure	
Sung Eun (0.5)	4.85	MOR(MPa)	1.02	1.00	-	1.00	1.06	1.01	
		M.C(%)	17.15	19.11	18.89	16.44	16.89	14.44	
		failure mode	-	flexure	flexure	flexure	flexure	flexure	
SYC (0.35)	3.25	MOR(MPa)	0.73	0.64	0.78	0.75	0.83	0.85	0.55
		M.C(%)	13.65	13.17	13.58	12.35	13.99	12.76	16.05
		failure mode	-	flexure	flexure	flexure	flexure	flexure	shear
SYC (0.5)	3.97	MOR(MPa)	1.19	1.13	1.23	1.27	1.30	1.06	1.13
		M.C(%)	16.94	17.04	17.93	17.33	16.44	15.85	17.04
		failure mode	-	flexure	flexure	flexure	flexure	flexure	flexure
SYC (0.6)	5.42	MOR(MPa)	1.19	1.13	1.23	1.27	1.30	1.06	1.13
		M.C(%)	10.04	11.36	12.84	9.38	8.40	8.40	9.88
		failure mode	-	flexure	flexure	flexure	flexure	flexure	flexure
Sung Eun (0.5)	4.85	MOR(MPa)	1.00	0.86	1.04	1.03	0.98	1.06	1.02
		M.C(%)	20.89	20.00	20.59	23.85	22.96	20.59	17.33
		failure mode	-	flexure	flexure	flexure	flexure	flexure	flexure
Sung Eun (0.6)	5.53	MOR(MPa)	1.24	1.26	1.17	1.21	1.14	1.31	1.35
		M.C(%)	12.10	13.09	12.35	12.10	12.84	10.37	11.85
		failure mode	-	flexure	flexure	flexure	flexure	flexure	flexure

3.3 Mortar

3.3.1 ALC Mortar

(1) Variables

To confirm the characteristics of the ALC mortar for attaching the ALC block, the compressive strength tests of the ALC mortar were performed. Test variables were classified with ALC mortar type and curing period. The size of the specimen was 50 × 50 × 50 mm^3, and 24 specimens were tested according to ASTM C109.

Table 3-9 variables of ALC mortar compressive strength test

Company	Curing day	Qauntity	
SYC	7 days	3	Total 24 specimens
	14 days	3	
	21 days	3	
	28 days	3	
Sung Eun	7 days	3	
	14 days	3	
	21 days	3	
	28 days	3	

(2) Test Set-up

To measure the compressive strength of ALC mortar, compressive strength tests were performed according to ASTM C109 using 2,000 kN UTM as shown in Fig. 3-11.

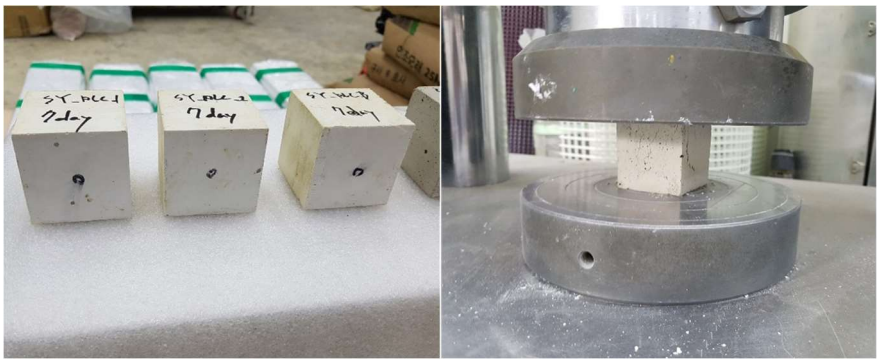

Figure 3-11 Test set-up for ALC mortar compressive strength

(3) Test Result

The relationship between ALC mortar compressive strength and curing period is shown in Figure 3-12. The horizontal axis of the graph represents the curing period and the vertical axis represents the compressive strength. The test results of SYC Co. are shown in yellow triangles, and shose of Sung Eun are shown in gray circle. The dashed line is the required strength of the S-Type mortar shown in ASTM C 91 and ASTM C 1329. S-Type mortar is recommended to use for the load bearing wall as shown in Table 3-10, and is useful for wind load and earthquake. The strength of the mortar was evaluated based on the S-Type in ACI.523.4R. The required strength of S-Type mortar is more than 9 MPa at 7 curing day and more than 14.5 MPa at 28 curing days.

Table 3-10 Demand Strength of Mortar (ASTM C 1329)

Classification	Compressive strength (MPa)		Flexural bond strength (MPa)
	7 days	28 days	
M-Type	**12.4MPa**	**20.0MPa**	**0.8MPa**
S-Type	**9.0MPa**	**14.5MPa**	**0.7MPa**
N-Type	3.5MPa	6.2MPa	0.5MPa

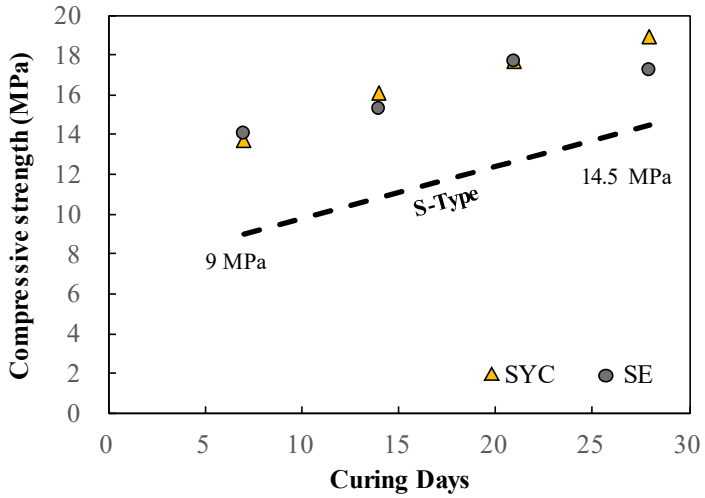

Figure 3-12 Relationships of ALC mortar compressive strength - curing day

The test results showed that the compressive strength increased with the lapse of curing time, and the strength increased slightly after 21 days. The compressive strength of ALC mortar with curing days was higher than the demand strength of S-type mortar in both companies.

3.3.2 Cement Mortar

(1) Variables

As shown in Fig. 3-13(left), the compressive strength test was performed to confirm the characteristics of the cement mortar applied between the wall and foundation of ALC. The test variables were the mortar type and curing period, such as the previously tested ALC mortar. The size of the specimen was 50 × 50 × 50 mm^3, and 24 specimens were tested according to ASTM C109.

Table 3-11 Variables of Cement mortar in compressive strength test

Company	Curing day	Qauntity	
SYC	7 days	3	Total 24 specimens
	14 days	3	
	21 days	3	
	28 days	3	
Sung Eun	7 days	3	
	14 days	3	
	21 days	3	

Figure 3-13 Uses of cement mortar (Left), Cement mortar specimens (Right)

(2) Test Set-up

The compressive strength of cement mortar was tested by the same method as that of the previous ALC mortar, and the compressive strength test was performed according to ASTM C109 using a 2,000 kN capacity UTM

(3) Test Result

Figure 3-14 shows the relationships between compressive strength and curing days of cement mortar. The test results of SYC Co. are shown in yellow triangles, and those of Sung Eun are shown in gray circle. The long-dashed line indicates the required strength of the S-type mortar, and the short dashed line indicates the required strength of the N-type mortar. The strength values shown in the graph are the required compressive strengths of S-Type and N-Type mortar on the 7th and 28th days.

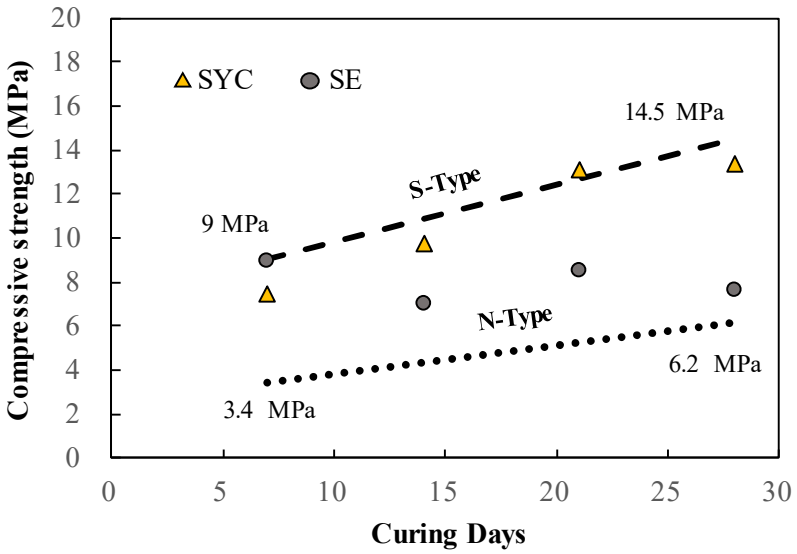

Figure 3-14 Relationships of cement mortar compressive strength - curing day

From the test results, the compressive strength of the cement mortar did not satisfy the required strength of the S-type. Cement Mortar made by Sung Eun has lower compressive strength than SYC Cement Mortar. Therefore, it is necessary to manage the strength of cement mortar to satisfy the required strength of S-Type.

The compressive strength of cement mortar was lower than that of ALC mortar. This means that the strength between the foundation and the wall (where the cement mortar is applied) is weaker than the strength between the blocks (where the ALC mortar is applied). Therefore, when the wall receives a lateral force, it is easy to occure a fracture between the wall and the foundation.

3.4 Glass-fiber

3.4.1 Tensile stength test

(1) Variables

To verify the tensile strength of the glass-fiber used for reinfoecement in a wall, tensile strength test was performed with the type of glass-fiber. The glass-fiber mesh used in the test was E-GLASS MESH, which was manufactured in Korea fastener. Co. The distance between fibers in A-type glass-fiber and B-type glass-fiber is 4.5mm, and the distance between fibers in C-type fiber-glass is 9.5mm. Glass-fiber A-type and B-type were used for reinforcement of wall side, and C-type was used at bed-joint. Each glass-fiber specimens were cut into 500 mm × 50 mm in the direction of weft and warp.

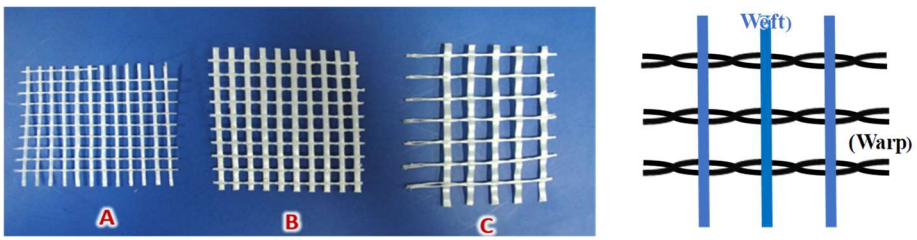

Figure 3-15 Types of Glass-fiber (left), direction of glass-fiber(right)

Table 3-12 variables of tensile strength test of glass-fiber

Classification	Spacing	Thickness	Uses for	drection	Quantity
Type-A	4.5mm	0.16mm	Side of wall	Warp/Weft	Total 18
Type-B	4.5mm	0.30mm	Side of wall		
Type-C	9mm	0.30mm	Bedjoint		

(2) Test set-up

To examine the tensile strength of the glass-fiber, a glass-fiber tensile test was performed according to ASTM D4595 using 2,000 kN UTM as shown in Fig. 3-16 (right). The test specimen was made 500 mm × 50 mm for each fiber direction (weft, warp) as shown in Fig. 3-16 (left). The length of 100 mm of both ends of the specimen is to tighten the specimen.

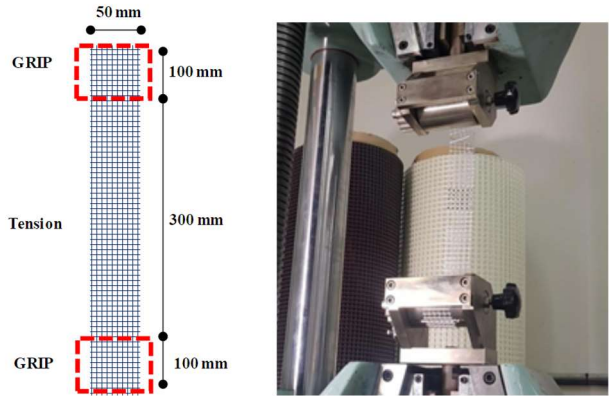

Figure 3-16 Glass-fiber specimen (left), Test set-up (right)

(3) Test Result

The test results are shown in Table 3-13, and the tensile strength of the glass-fiber was maximum load per width of 50 mm (N / 50 mm). Test results showed that Type-B glass-fiber has the highest strength in the weft direction and Type-C glass-fiber has the highest strength in the warp direction.

Table 3-13 Test result of tensile strength of glass-fiber

classificaion	Mean tensil strength(N/50mm)		
	Type-A	Type-B	Type-C
Weft	1,976	3,857	3,440
Warp	1,267	1,410	1,982

3.4.2 Flexural tensile strength of ALC Block reinforced with glass-fiber

(1) Variables

Flexural tensile strength test was performed to verify the effect of glass-fiber applied on the side wall. As shown in Table 3-14, glass-fiber type and mortar thickness were used as variables. In addition, FR-A-5 (T), FR-B-5 (T) and FR-C-5 (T) specimens were planned to confirm the effect of tacker to increase adhesion between glass-fiber mesh and ALC block.

Table 3-14 Test results of tensile strength of glass-fiber

Specimen	Co.	Glass-fiber Type	Mortar thickness (mm)	Quantity	-
FR(0.35)-A-3	SYC	A-Type	1~3	2	Total 22 specimens
FR(0.35)-A-5		A-Type	3～5	2	
FR(0.35)-B-5		B-Type	3～5	2	
FR(0.35)-C-5		C-Type	3～5	2	
FR(0.35)-A-5(T)		A-Type	3～5	1	
FR(0.35)-B-5(T)		B-Type	3～5	1	
FR(0.35)-C-5(T)		C-Type	3～5	1	
FR(0.5)-A-3	Sung Eun	A-Type	1~3	2	
FR(0.5)-A-5		A-Type	3～5	2	
FR(0.5)-B-5		B-Type	3～5	2	
FR(0.5)-C-5		C-Type	3～5	2	
FR(0.5)-A-5(T)		A-Type	3～5	1	
FR(0.5)-B-5(T)		B-Type	3～5	1	
FR(0.5)-C-5(T)		C-Type	3～5	1	

Notes : FR(0.5)-A-5(T) ; FR=Flexural tensile strength test, (0.5)=density, A=Type of glass-fiber, 5=mortar thickness, (T) = Tacker

(2) Test set-up

To test the flexural tensile strength of ALC block reinforced with glass-fiber, load was applied to the specimen at 2 points according to ASTM C78 using 2,000 kN capacity UTM as shown in Fig. 3-17. The flexural tensile strength (f_r) is the tensile stress at the bottom of the block at the time of cracking at the center of the ALC block, and can be calculated by Eq. 3-6, same as Eq. 3-4 in section.

$$f_r = \frac{PL}{bh^2} \tag{3-6}$$

As shown in Fig. 3-17, the glass-fiber was attached to the ALC block with ALC mortar. This reinforcement method is called Textile Reinforced Mortar (TRM). There is another reinforcing method with epoxy. Epoxy, an organic adhesive, is vulnerable to fire and is not environmentally friendly, making it unsuitable for residential use.

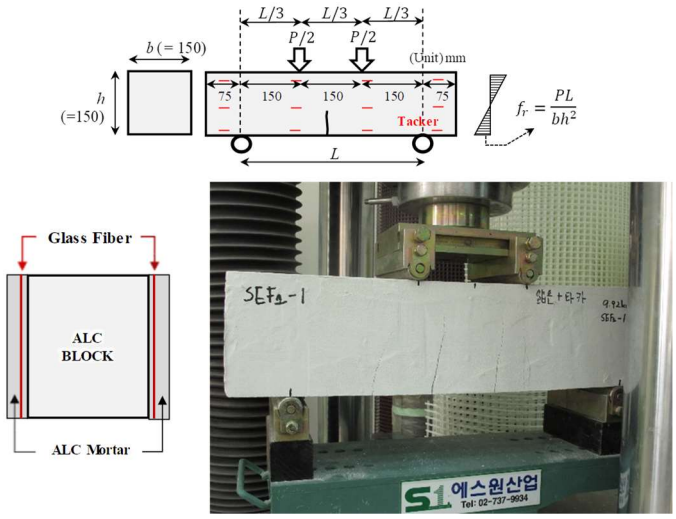

Figure 3-17 Test set-up for M.O.R. of ALC block with glass-fiber

(3) Test Results

(a) Flexural Tensile Strength with Mortar Thickness

To compare the flexural tensile strength of the ALC block reinforced with glass-fiber with the mortar thickness, the Load-displacement grape was shown in Fig 3-18. The horizontal axis of the graph represents the UTM displacement, and the vertical axis represents the load. The test results of 0.35(Ton/m^3) ALC blocks were shown on the left, and the test results of 0.35(Ton/m^3) ALC blocks were shown on the right. The specimens (FR(0.35/0.5)-A-3) with mortar thickness of 3 mm were indicated by a solid red line and the specimens (FR(0.35/0.5)-A-5) with mortar thickness of 5 mm were indicated by a blue dashed line. The point when the initial crack occurred in ALC block was indicated by a yellow circle.

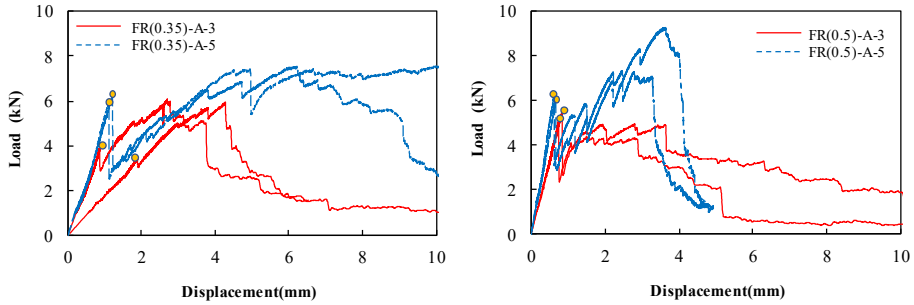

Figure 3-18 Relationships of load-displacement with different mortar thickness

The maximum flexural tensile strength increased with increasing mortar thickness. The flexural strength (mean=1.02 MPa) of FR(0.35)-A-5 was 30% higher than the flexural strength (mean=0.78 MPa) of FR(0.35)-A-3. The maximum flexural strength (mean=1.11 MPa) of FR(0.5)-A-5 was 78% more

than the maximum flexural strength (mean=0.62 MPa) of FR(0.5)-A-3.

As shown in Table 3-15, The peak loads after block cracking were almost higher than the load when the block cracking. This was because the glass-fiber received a tensile force greater than that of the flexural tensil strength of ALC block. However, in the FR(0.5)A-3 specimen, the peak load after the block cracking was lower than the load at block cracking. This was because the bond strength of mortar was weaker than others, and the glass-fibers failed to exert their tensile strength.

Reinforcing glass-fiber with thick mortar was effective in increasing flexural tensile strength. In other words, the adhesion of glass-fiber increased with increasing thickness of mortar. Therefore, it is effective to reinforce ALC Block with thick mortar (3~5mm) than mortar thickness (1~3mm) currently applied.

Table 3-15 Test results of flexural tensile strength of ALC block with mortar thickness

Specimen	f_{r1} [1] (MPa)	f_{r2} [2](MPa)	f_{r1}/ f_{r2} (%)	Failure mode
FR(0.35)-A-3	0.49	0.77	157%	flexure
	0.46	0.79	172%	flexure
FR(0.35)-A-5	0.83	1.00	120%	flexure
	0.78	1.03	132%	flexure
FR(0.5)-A-3	0.73	0.58	79%	flexure
	0.68	0.66	97%	flexure
FR(0.5)-A-5	0.81	1.23	152%	flexure
	0.84	0.98	117%	flexure

1) f_{r1} =flexural tensile strength when first flexural crack occured

2) f_{r2} = peak flexural tensile strength after f_{r1}.

(b) Flexural Tensile Strength with glass-fiber type

Figure 3-19 shows the comparison of the flexural tensile strength of glass-fiber-reinforced ALC blocks for different glass-fiber types. The specimen reinforced with A-type glass-fiber(FR(0.35/0.5)-A-5) is shown in red solid line, the specimen reinforced with B-type glass-fiber(FR(0.35/0.5)-B-5) is shown in blue pointed line, and the specimen reinforced with C-type glass-fiber(FR(0.35/0.5) -C-5) is shown in black dashed line.

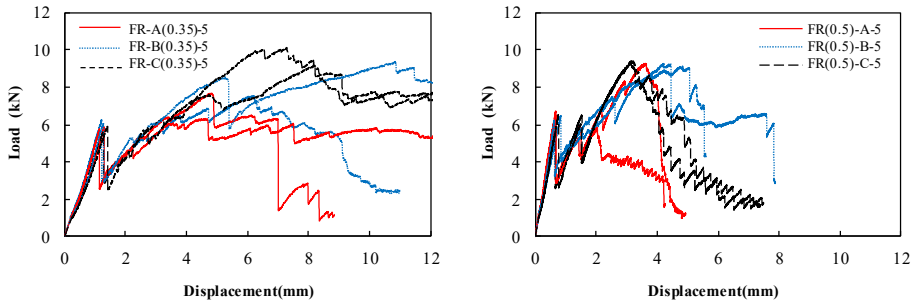

Figure 3-19 Relationships of load-displacement with different mesh types

The test results showed that the specimens reinforced with C-type glass-fiber showed the highest flexural tensile strength as shown in Table 3-16. The flexural tensile strengths of FR(0.35)-B-5 and FR(0.35)-C-5 were 11.8% and 33.0% higher than those of FR(0.35)-A-5, respectively. And the flexural tensile strengths of FR(0.5)-B-5 and FR(0.5)-C-5 were 10.8% and 16.7% higher than those of FR(0.5)-A-5, respectively.

Failure mode can be classified as shown in Fig. 3-20 depending on the type of glass-fiber, and specimens with A-type and C-type glass-fiber showed the best failure mode (tensile failure of glass-fiber). In FR(0.35/0.5)-A-5 and FR(0.35/0.5)-C-5 specimens, tensile failure of glass-fiber occurred before

mortar failure. On the other hand, mortar fracture occurred earlier than a failure of glass-fiber in FR(0.35/0.5)-B-5 specimens.

(a) A-Type glass-fiber

(b) B-Type glass-fiber

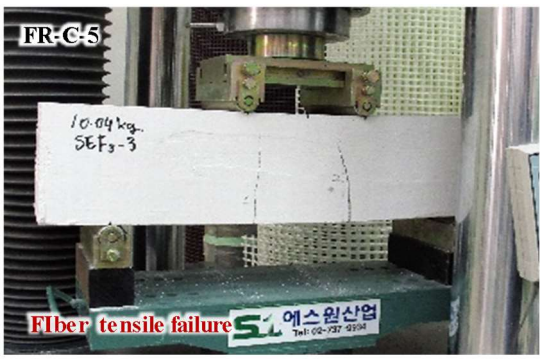

(a) C-Type glass-fiber

Figure 3-20 Failure modes of reinforced ALC block

The specimen reinforced with the C-type glass-fiber showed the highest flexural tensile strength and ideal fracture shape. Therefore, to increase the flexural tensile performance of the wall, it is necessary to use C-type glass-fiber instead of A-type glass-fiber for wall reinforcement. Therefore, the fiberglass reinforcing method was most effective when reinforcing a wall with C-type glass-fiber, and the thickness of the mortar was 3 ~ 5mm.

Table 3-16 Test results of flexural tensile strength of ALC block with types of glass-fibers

Specimen	f_{r1} (MPa)	f_{r2} (MPa)	f_{r1}/f_{r2} (%)	Failure mode
FR(0.35)-A-5	0.83	1.00	120%	flexure
	0.78	1.03	132%	flexure
FR(0.35)-B-5	0.78	1.02	131%	flexure
	0.81	1.25	154%	flexure
FR(0.35)-C-5	0.74	1.36	184%	flexure
	0.78	1.34	172%	flexure
FR(0.5)-A-5	0.81	1.23	152%	flexure
	0.84	0.98	117%	flexure
FR (0.5)-B-5	0.86	1.21	141%	flexure
	0.83	1.24	149%	flexure
FR(0.5)-C-5	0.86	1.25	145%	flexure
	0.81	1.33	164%	flexure

(c) Flexural Tensile Strength with Tacker reinforcement

The comparison of the flexural tensile strength with the tacker reinforcement, the Load-displacement grape was is shown in Fig. 3-21. The test results of the specimens reinforced with tackers were shown in red solid lines, and the test results of specimens without tackers were shown in blue dashed lines.

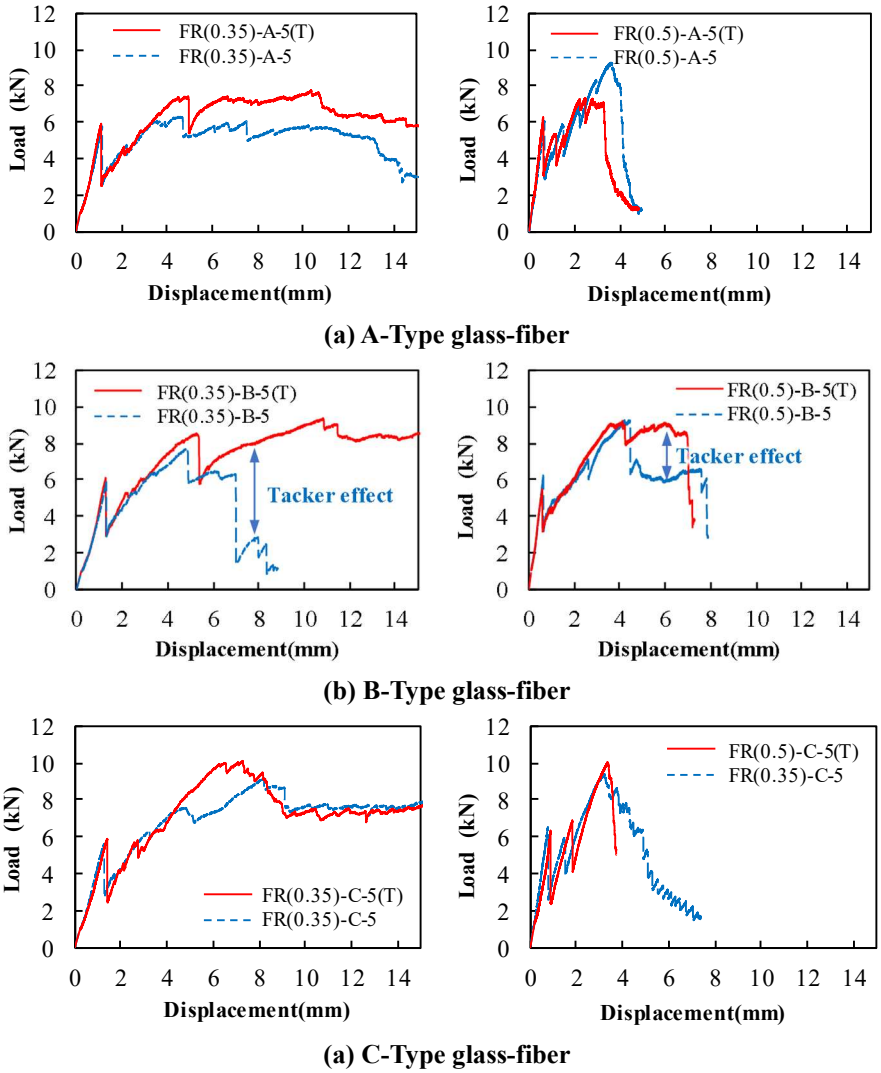

Figure 3-21 Relationships of load and displacement

In the test results, the effect of tacker was not significant in the specimens reinforced with Type-A and Type-C glass-fibers, but the effect of tacker was effective in the specimens reinforced with Type-B glass-fiber. In the specimens reinforced with Type-B glass-fiber, the mortar was destroyed early, and tacker grabbed the glass-fiber after mortar fracture. Thus, the mechanical attachment of the tacker maintains the tensile strength of the glass-fiber.

3.5 Disscussion

In the material test, the materials in the ALC building were tested to verify the material properties. The compressive strength tests and the flexural tensile strength tests were performed for the ALC block, and the compressive strength tests was performed for the mortar. Tensile tests were carried out for glass-fibers basically and flexural tensile strength tests were carried out on ALC blocks reinforced with glass-fiber on the outside.

(1) ALC blocks showed 3~5MPa compressive strength with dry density. The elastic modulus and flexural tensile strength of ALC block increased with increasing compressive strength and dry density of ALC block. The predictions in ACI 523.4R matched well with test results. These predictions showed elastic modulus and flexural tensile strength of ALC block with compressive strength of ALC block. The compressive strength, elastic modulus and flexural tensile strength of the ALC block varied with the position of the block even if the block

had the same dry density. Therefore, before the performance of the structure is evaluated, the compressive strength of the ALC block should be confirmed.

(2) The compressive strength of ALC mortar satisfied the required strength of S-type mortar proposed in ACI 523.4R, but the cement mortar was not satisfied. Therefore, although the adhesion performance of the mortar with the compressive strength of the mortar was not verified through the prism and the wall test, quality of the mortar should be managed to satisfy the S-type mortar required strength.

(3) An effective glass-fiber reinforcement method was investigated by the flexural tensile strength test of ALC block reinforced with glass-fiber. When the thickness of mortar was 3 ~ 5mm and C-type glass-fiber (tensile strength = 2kN / 50mm, spacing between fibers = 9.5mm) was used, the flexural tensile strength and mortar adhesion of ALC block were the highest. In addition, when the glass-fiber was fixed with tackers an interval of 200 mm, adhesion of the glass-fiber was improved.

Chapter 4. Prism tests

4.1 Introduction

ALC walls are made of ALC block and mortar. Therefore, prism specimens made of ALC block and mortar could reflect wall performance well rather than ALC material. Therefore, before the wall experiment, the flexural bond strength, the shear bond strength, the compressive strength, and the diagonal tension (shear) strength of the ALC prism specimens were tested to evaluate the performance of each part of wall.

The crack patterns that could occur in gravity load (axial force) and seismic load (lateral force) at the same time were divided into four types as shown in Fig. 4-1. The first is the flexural tensile crack at the bottom (A) between the mortar due to the moment and the second is the horizontal crack (B) due to the lateral shear force between the bed-joints at the bottom of the wall. The third is the compressive crack (C) due to gravity load and moment, and the last is the diagonal shear crack (D) at the center of the wall.

In chapter 4, to evaluate the strength with the failure modes that could occur in the wall, flexural bond strength (A), shear bond strength (B), prism compressive strength (C), and prism diagonal tensile strength (D) Respectively.

To evaluate the performance of the prisms with the glass-fiber reinforcement, the glass-fiber reinforced methods (bed-joint / external wall / bed-joint and

esternal wall) were used as variables. As a result of the flexural tensile strength test with the glass-fiber in Section 3.4.2, C-type glass-fiber and mortar thickness of 3 ~ 5mm were selected as reinforcement method. However, in the prism flexural bond strength and prism compression strength test, A-type glass-fiber was reinforced on the external wall and the mortar thickness of 2 mm, because specimens of the two prisms were planned before the verification of glass-fiber reinforcement method.

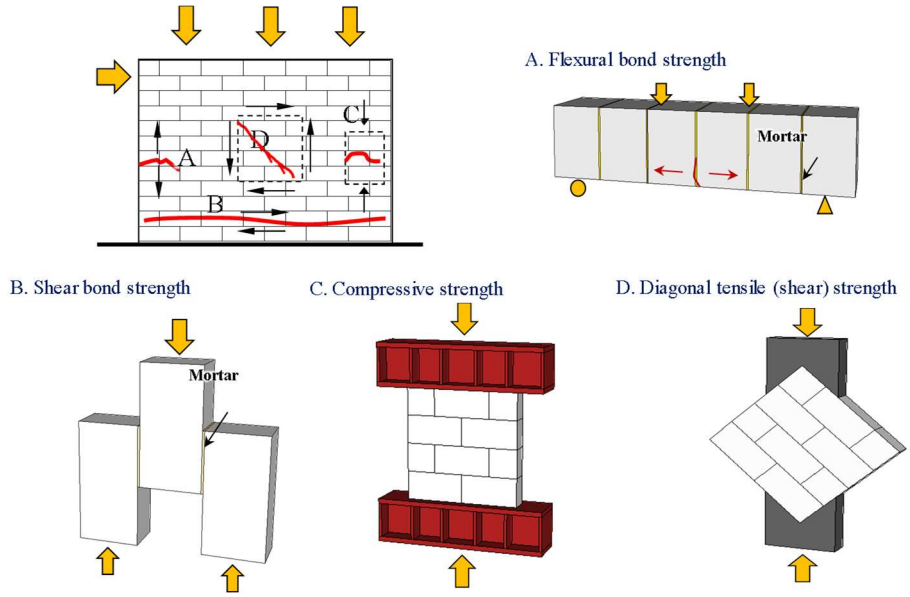

Figure 4-1Kinds of Prism tests

4.2 ALC Flexural Bond Strength of ALC Mortar

4.2.1 Variables

To verify the flexural bond strength of the ALC mortar, the flexural bond strength tests were performed with dry density of ALC block and glass-fiber reinforcement as the variables as shown in Table 4-1.

The FB(0.35)-UU specimen was compared with the FB(0.5)-UU specimen to examine the flexural bond strength of mortar with different dry density of ALC block. FB (0.35/0.5)-FU specimens were tested to confirm the effects of glass-fiber embeded in bed-joint. In addition, to confrim the effect of A-type glass-fiber reinforced at bed-joints and on the side of wall, FB(0.35/0.5)-FF specimens were tested. A-type glass-fiber as shown in Fig. 3-15 (a) was used as the glass-fiber for reinforcing the external wall, and C-type glass-fiber was used as reinforcement embeded in bedjoint of ALC wall. The joint thickness was 2 mm (± 1mm).

Table 4-1 Variables of flexural bond strength tests

Specimen	ALC Density	Glass-fiber		Mortar Thickness	Quatntity
		Bed-joint	Sides		
FB(0.35)-UU	0.35 (Ton/m^3)	-	-	(bedjont) 1~3mm (sides) 1~3mm	3
FB(0.35)-FU		C-Type	-		3
FB(0.35)-UF		C-Type	A-Type		3
FB(0.5)-UU	0.5 (Ton/m^3)	-	-	(bedjont) 1~3mm (sides) 1~3mm	3
FB(0.5)-FU		C-Type	-		3
FB(0.5)-FF		C-Type	A-Type		3

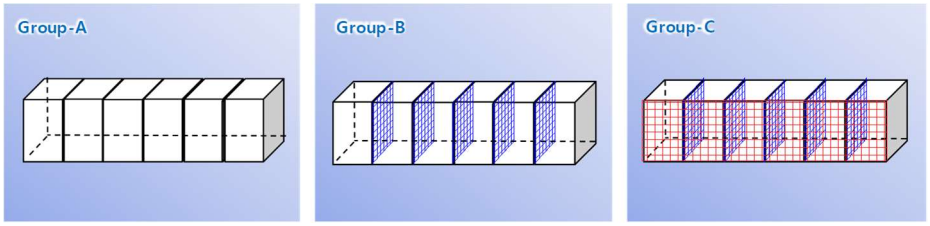

Figure 4-2 Gruops for flexural bond strength tests

4.2.2 Test set-up

The specimens were made by attaching six ALC blocks which size was 150 mm × 150 mm × 100 mm, as shown in Fig 4-2. The size of each specimen was 150 mm × 150 mm × 600 mm, which was the same as the size of the flexural tensile specimen (Figure 3-9).

The test was carried out according to ASTM-E518, and the load was applied to two points at one-third of the distance (L). The flexural bond strength (f_{bond}) is the tensile stress at the bottom of the specimen and shown as Eq. 4-1.

$$f_{FB} = \frac{PL}{bh^2} \tag{4-1}$$

Where b is the width of the block, h is the height of the block, P is the load, and L is the distance between the supporters.

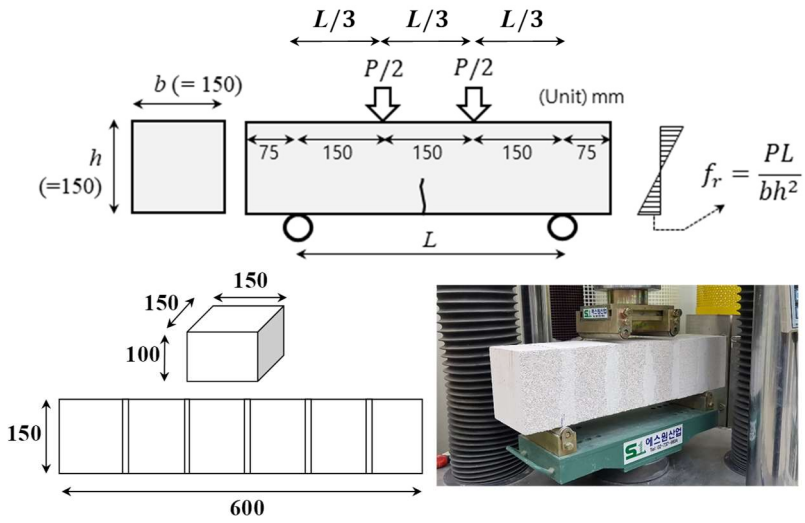

Figure 4-3 Test set-up for flexural bond strength tests

4.2.3 Test Results

(1) Flexural bond strength of ALC mortar

The flexural bond strength with the group of ALC blocks was shown in Fig. 4-4. The horizontal axis of the graph is the group of the test specimen, the group A is the non-reinforced specimens (FB(0.35/0.5)-UU), the group B is specimens reinforced with glass fibe at bed-joint (FB(0.35/0.5)-FU), the group C is specimens reinforced with glass-fiber at the bed-joint and the sides of the specimens(FB (0.35/0.5)-FF). The vertical axis represents the flexural bond strength. When the specimen was fractured at the mortar, it is marked with a red circle. When the specimen was fractured in the ALC block, it is marked with a blue triangle. The gray dotted line shows the required flexural bond strength 0.552 MPa in ACI 523.4R. This is equivalent to the minimum flexural tensile strength of the ALC block with a compressive strength of from 3.10 MPa to 4.83 MPa.

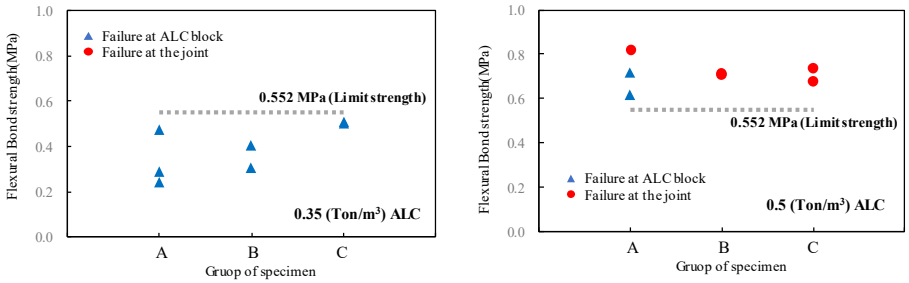

(a) 0.35(Ton/m^3) ALC block **(b) 0.5(Ton/m^3) ALC block**

Figure 4-4 Frexural bond strength of mortar with types of specimen

As shown in Fig. 4-5 (a), the 0.35(Ton/m^3) specimens were fractured in the ALC block and the maximum flexural tensile strength was 0.51 MPa. Since no fracture occurred in the mortar, the flexural bond strength of the mortar can be expected to be 0.51 MPa or more. 0.5 (Ton/m^3) specimens were fractured in mortar as shown in Fig. 4-5 (b). The minimum flexural bond strength of mortar was 0.82 MPa and it satisfied the flexural bond strength 0.552 MPa required in ACI 523.4R.

(a) 0.35(Ton/m^3) ALC block

Figure 4-5 Failure mode (Flexural bond strength test)

(b) 0.5(Ton/m^3) ALC block

Figure 4-5 Failure mode (Flexural bond strength test)

Table 4-2 Test results of flexural bond strength test

ALC block with 0.35(Ton/m^3) Density				
Specimen	Peak load(kN)	Flexural bond strength (MPa)	Section of fracture	Frature mode
FB(0.35)-UU	1.80	0.24	ALC	flexure
FB(0.35)-UU	2.14	0.29	ALC	flexure
FB(0.35)-UU	3.54	0.47	ALC	flexure
FB(0.35)-FU	2.28	0.30	ALC	flexure
FB(0.35)-FU	3.02	0.40	ALC	flexure
FB(0.35)-UF	3.75	0.50	ALC	flexure
FB(0.35)-UF	3.80	0.51	ALC	flexure
ALC block with 0.5(Ton/m^3) Density				
Specimen	Peak load(kN)	Flexural bond strength (MPa)	Section of fracture	Frature mode
FB(0.35)-UU	5.36	0.71	ALC	flexure
FB(0.35)-UU	4.62	0.62	ALC	flexure
FB(0.35)-UU	6.12	0.82	Mortar	flexure
FB(0.35)-FU	5.30	0.71	Mortar	flexure
FB(0.35)-FU	5.32	0.71	Mortar	flexure
FB(0.35)-UF	5.50	0.73	Mortar	flexure
FB(0.35)-UF	5.08	0.68	Mortar	flexure

(2) Effect of glass-fiber in flexural bond strength

The relationship between the load-displacement of the glass-fiber reinforced specimen is shown in Fig. 4-6. The vertical axis represents the load (kN), and the horizontal axis represents the vertical displacement (mm) of the UTM head. In the graph, the point at which the first crack occursed is marked with a yellow circle.

The brittle fracture of the block occurred in the group A without glass-fiber reinforcement and the group B with glass-fiber reinforced at the bed-joints. On the other hand, the specimen reinforced with glass-fiber on the sides and bed-joint showed ductility without brittle fracture even after the initial crack occurred. Therefore, the glass-fiber on the side of block had the effect of preventing brittle fracture and the increases flexural strength of ALC block.

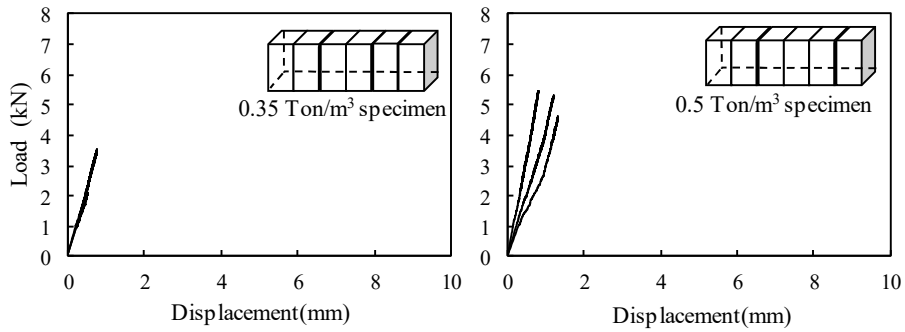

(a) Unreinforced specimens

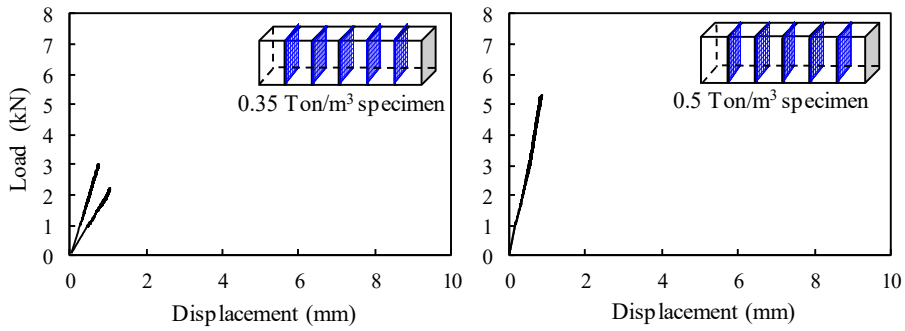

(b) Reinforeced specimens at the bed joints

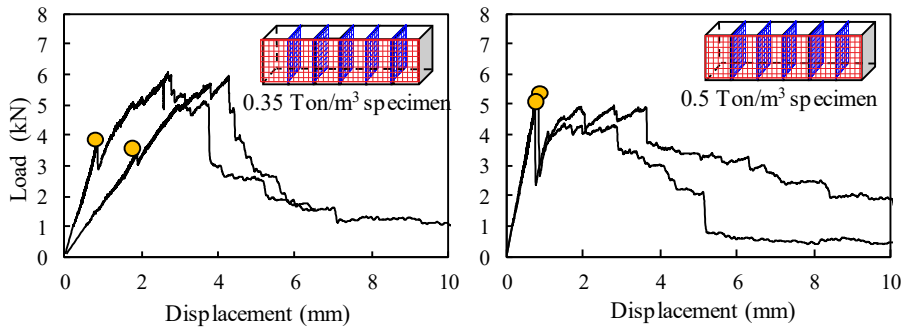

(b) Reinforeced specimens at the bed joints and sides

Figure 4-6 The relationship between the load-displacement in flexural bond strength test

4.3 Shear Bond Strength of ALC Mortar

4.3.1 Variables

The ALC shear bond strength test specimens were classified into 6 types as shown in Fig. 4-7. SB (0.35/0.5)-UU specimens were used to confirm the shear bond strength of the non-reinforced wall, and the axial loads ratios were 0 %, 5 %, 10 % and 15 %. SB (0.35/0.5)-FU specimens were tested to confirm the shear bond strength of ALC wall reinforced with fiber glass at bed-joint, and axial load ratios were 0 % and 10 %. SB(0.35/0.)-UF specimens were tested to confirm the shear bond strength of ALC wall reinforced with glass-fiber on the sides of wall, and axial load ratios were 0% and 10%. SB(0.35/0.5)-FF specimens were tested to determine the shear bond strength of ALC wall reinforced with the glass-fiber at bedjoint and on the sides of wall, and axial load ratio was 0% and 10%, respectively. The SB(0.35/0.5) -SU was a specimen with a rcolumn inside and the SB(0.3/0.5) -PU was a panel specimen, they were tested without axial load.

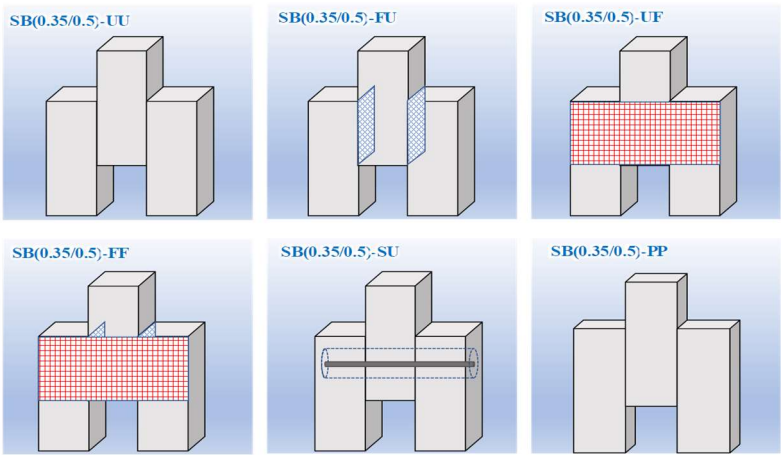

Figure 4-7 Types of specimens in shear bond strength test

Table 4-3 Variables of flexural bond strength test

Specimen	Fiber-glass		Axial load ratio	quantity
	Bed-joint	Sides of wall		
SB (0.35)-UU	-	-	0%	2
			5%	1
			10%	2
			15%	1
SB (0.35)-FU	C type	-	0%	1
			10%	1
SB (0.35)-UF	C type	-	0%	1
			10%	1
SB (0.35)-FF	C type	C type	0%	2
			10%	2
SB (0.35)-SU	-	-	0%	1
SB (0.35)-PU	-	-	0%	2
SB (0.5)-UU	-	-	0%	2
			5%	1
			10%	2
			15%	1
SB (0.5)-FU	C type	-	0%	1
			10%	1
SB (0.5)-UF	C type	-	0%	1
			10%	1
SB (0.5)-FF	C type	C type	0%	2
			10%	2
SB (0.5)-SU	-	-	0%	1
SB (0.5)-PU	-	-	0%	2

Notes : SB(0.35)-FF(5), SB(Shear bond strength test), 0.35(dry density of ALC block), F-(Reinforcement at bedjoint), - F(Reinforcement on the sides of ALC block),5(axial load ratio)

4.3.2 Test set-up

The specimen was attached with three blocks as shown in Fig. 4-8. The size of one block was 200mm × 300mm × 600mm (width × thickness × height). The upper block at center was 200mm × 300mm × 400mm (width × thickness ×

height) and was placed under the acturator and receives the load. The lower block is 200mm × 300mm × 100 mm (width x thickness x height), with both side buttresses, placed between side blocks to keep the specimen from moving. To confirm the shear bond strength with the axial load ratio, the clamping force was applied using a steel wire and nuts as shown in Fig. 4-8 (c).

(a) Test set-up **(b) Test view** **(c) Clamping force**

Figure 4-8 Test set-up for shear bond strength tests

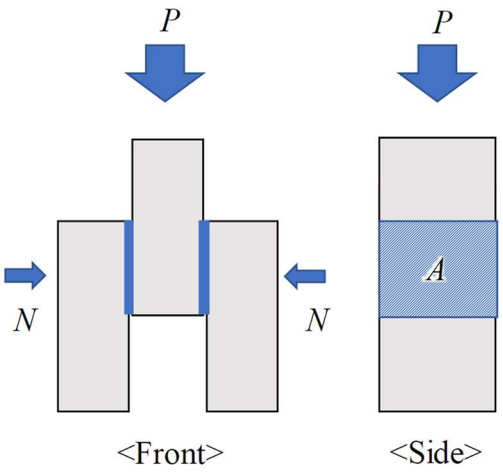

Figure 4-9 mearsurement of shear bond strength

4.3.3 Test results

The shear bond strength was calculated at first crack of both mortars in Figure 4-10. The failure mode in the shear bond strength test was continuous failure or simultaneous failure of joints. When the joints were fractured continuously, the load-displacement graph showed the two peak points (first and second cracks). When the joints are fractured at same time, the load-displacement graph showed one peak point. The load applied to the joint before the crack occurs is the shear bond strength, and the load applied after the crack occurs is the shear friction strength. Therefore, to measure the shear bond strength, the load at the first crack was used and it was calculated Eq. 4-2. The coefficient of friction was calculated by the following Eq. 4-3 using the constant load and clamped force after fracure of both joints.

$$f_{SB} = \frac{P}{2A} \tag{4-2}$$

$$\mu = \frac{P}{2N} \tag{4-3}$$

Where f_{SB} is the shear bond strength of the specimens, P is the load, A is the adhesion area of the mortar, N is the clamping force between the ALC blocks, and μ is the friction coefficient.

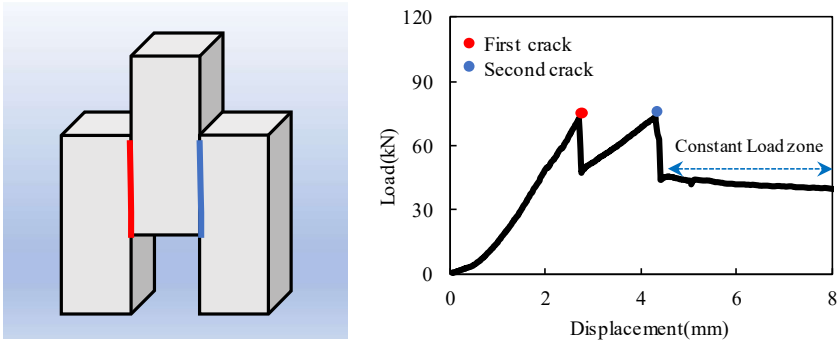

Figure 4-10 Typical Load-Displacement Patterns of shear bond strength test

4.3.3.1 Shear bond strength

To evaluate the shear bond strength of ALC mortar, SB(0.35)-UU and SB (0.5)-UU specimens without glass-fiber reinforcement were compared with the predicted strength as shown in Fig 4-11. The horizontal axis of the graph represents the compressive strength of the ALC block, and the vertical axis represents the shear bond strength. Test results of 0.35 (Ton/m^3) and 0.5 (Ton/m^3) were shown as yellow triangles and gray circles, respectively. The predicted strength (Eq. 4-4) in ACI.523.4R (Argudo 2003; Demboski; Snow 1999) was represented by a black dotted line.

$$f_{SB} = 0.08 f_{ALC}' + 0.17 \quad (4\text{-}4)$$

The average shear bond strength of 0.35 specimen was 0.46 MPa, which was higher than expected strength of 0.42 MPa, while the shear bond strength of 0.5 (Ton/m^3) specimen was 0.15 MPa, which was 31% of the expected strength of 0.48 MPa. 0.35 (Ton/m^3) specimens were broken in the block while 0.5 (Ton/m^3) specimens were fractured in the mortar. The fracture surface in figure 4-12

showed that the attaching condition of the mortar of 0.5 specimen was not good. Therefore, the results of 0.5 specimens were excluded from the comparison.

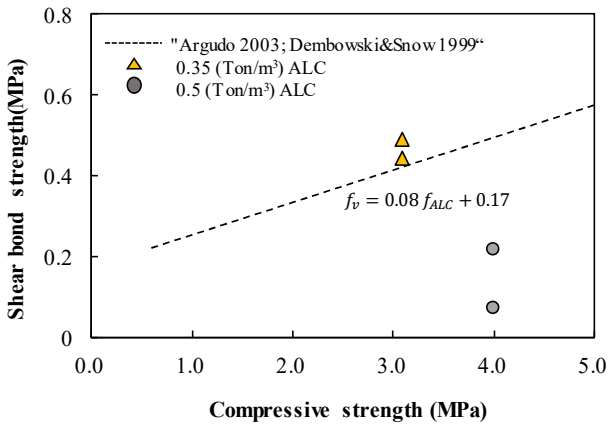

Figure 4-11 Shear bond strength with compressive strength

(a) 0.35(Ton/m³) ALC block **(b) 0.5(Ton/m³) ALC block**

Figure 4-12 The fractured surface of specimens

4.3.3.2 Shear bond strength with failure modes

In the test of shear bond strength, fracture occured at two joints simultaneously or continuouly. To confirm the difference in shear bond strength with the types of failure, shear bond strength with failure types were compared as shown in Table 4-4.

In the three variables, different failures occurred in the same variable. Comparing the shear bond strengths of these specimens, the shear bond strength of specimens with continuous fracture was lower than that of simultaneous fracture by 60% ~ 70%. Therefore, the shear bond strength was analyzed considering the fracture types.

Table 4-4 Shear bond strength(different fracture occured in the same variable)

Specimen	Shear bond strength(MPa)		A/B
	Continuous failure (A)	Simultaneous failure(B)	
SB(0.35)-UU(10)	0.41	0.66	0.62
SB(0.35)-FF(0)	0.36	0.60	0.60
SB(0.35)-FF(10)	0.49	0.71	0.69

4.3.3.3 Shear bond strength with glass-fiber reinforcement

The shear bond strength with glass-fiber reinforcement was verified as shown in Fig. 4-13. The vertical axis of the graph represents the shear bond strength when clamping force was not applied, and the horizontal axis represents the group of the test specimen. The group A, B, C and D are unreinforced specimens, specimens reinforced with glass-fiber at bed-joint, specimens reinforced with glass-fiber on the sides, and specimens reinforced with at bed-joint and on the sides, respectively. When the fracture in the specimen occured simultaneously on both bed-joints, it is indicated by a yellow triangle, and when a failure occured continuously, it is indicated by a yellow circle. The predicted shear bond strength of the specimen was indicated by blue dashed line and it was calculated by Eq.3-4 proposed by Argudo(2003). That equation is also suggested in ACI 523.4R.

The average shear bond strength of group B reinforced with glass-fiber at the bed-joint was 0.31 MPa, which was 33% lower than the shear bond strength of (unreinforced) group A. The shear bond strength of the C group reinforced with glass-fiber on the sides and at the bed-joints were 29% higher than the shear bond strength of the A group. The shear bond strengths of specimens in group D were significantly different because fracture shapes of specimens were different. Therefore, the glass-fiber reinforced at the bed-joint reduced the shear bond strength and the glass-fiber reinforced on the sides increased the shear bond strength.

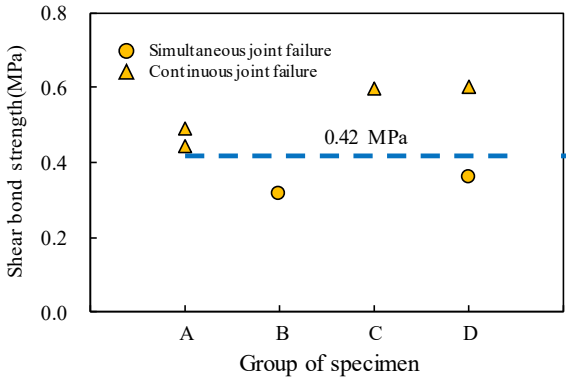

Figure 4-13 The shear bond strength with glass-fiber reinforcement

Table 4-5 Test results of shear bond strength with with different reinforcing method

0.35 Density ALC block			
Specimen	Load at first crack (kN)	Shear bond strength (MPa)	Fracture mode
SB(0.35)-UU(0)	79.61kN	0.44MPa	sliding
SB(0.35)-UU(0)	88.42kN	0.49MPa	sliding
SB(0.35)-FU(0)	56.2kN	0.31MPa	sliding
SB(0.35)-UF(0)	107.6kN	0.60MPa	sliding, compression
SB(0.35)-FF(0)	108.56kN	0.60MPa	sliding
SB(0.35)-FF(0)	65.16kN	0.36MPa	sliding
0.5 Density ALC block			
Specimen	Load at first crack (kN)	Shear bond strength (MPa)	Fracture mode
SB(0.5)-UU	13.3kN	0.07MPa	sliding
SB(0.5)-UU	39.21kN	0.22MPa	sliding
SB(0.5)-FU	20.36kN	0.11MPa	sliding
SB(0.5)-UF	59.38kN	0.33MPa	sliding
SB(0.5)-FF	60.81kN	0.34MPa	sliding, compression
SB(0.5)-FF	49.19kN	0.27MPa	sliding

4.3.3.4 Shear bond strength with Re-bar

As shown in Fig. 4-14, the relationships between load and displacement were compared to confirm the shear bond strength with Re-bar. The vertical axis of the graph represents the load, and the vertical axis represents the displacement of the head. The point at which the initial crack occurred was indicated by a yellow circle.

In the SB(0.35)-UU(0) specimen without reinforcement, failured at the joint at same time, and the maximum load was 88.4 kN. The SB(0.35)-UF(0) specimen reinforced with glass-fiber on the outer wall was broken at both joints simultaneously at a displacement of 5.83 mm and a maximum load of 107 kN. And SB(0.35)-UF(0) showed a ductility until 7.01 mm due to the tensile strength of the glass-fiber. SB(0.35)-SU(0) specimen reinforced with reinforcing bars was continuously fractured at joints, when displacement of 5.1 mm and a load of 93.5 kN. And the displacement continued to increase until compressive failure of the specimen.

The final failure of SB(0.35)-SU(0) and SB(0.35)-UF(0) are shown in Fig. 4-15. In SB(0.35)-UF(0), glass-fibers and blocks were separated and slip occurred after the fractures of both joints. On the other hand, in SB(0.35) - SU(0), the reinforcing bars prevented sliding deformation and caused compression and shear failure in the block. Although the vertical reinforcement did not have much effect on shear bond strength, but increased ductility greatly.

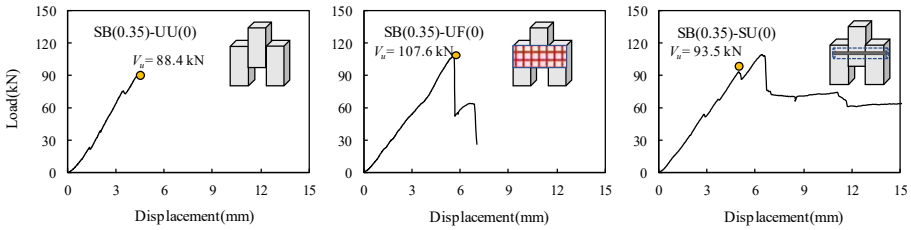

(a) SB(0.35)-UU(0) **(b) SB(0.35)-UF(0)** **(c) SB(0.35)-SU(0)**

Figure 4-14 The shear bond strength with glass-fiber reinforcement

Figure 4-15 Final failure in SB(0.35)-UF and SB(0.35)-SU(0)

4.3.3.5 Shear bond strength with axial force

The shear bond strength results of ALC mortar with axial force are shown in Fig. 4-16. The vertical axis of the graph represents the shear bond strength, and the horizontal axis of the graph represents the axial force. The yellow circle is the shear bond strength when the joint surfaces were broken simultaneously, and the yellow triangle is the shear bond strength when the joint surfaces were broken continuously.

Shear bond strength with axial force is shown in Table 4-6. In all specimens, shear bond strength increased with increasing axial force. As the axial forece increased by 10%, the shear bond strength increased by an average of 0.2 MPa.

The shear bond strength Eq. 4-4 proposed by ACI 523.4R is prediction in the absence of axial load and it does not reflect the tendency of shear bond strength with axial force. Therefore, it is desirable to design the shear bond strength with the axial load in the actual wall.

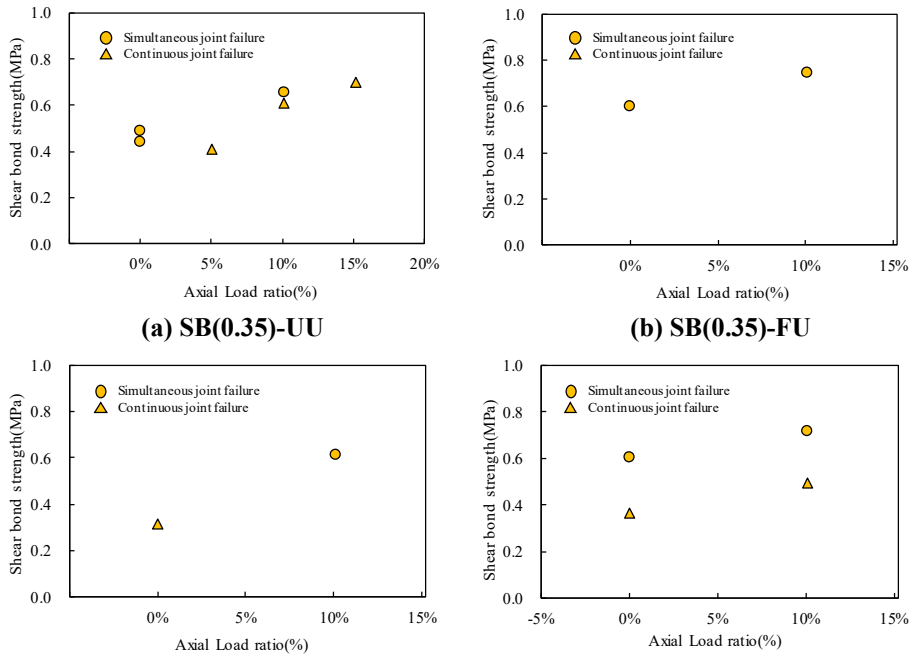

Figure 4-16 The shear bond strength with axial force

Table 4-6 Shear bond strength with axial force

Specimen	Shear bond strength(MPa)				Failure mode
	0 %[1)]	5 %	10 %	15%	
SB(0.35)-UU	-	0.41	0.61	0.70	continuous
	0.47	-	0.66	-	simultaneous
SB(0.35)-FU	0.31	-	-	-	continuous
	-	-	0.61	-	simultaneous
SB(0.35)-UF	0.60	-	0.74	-	simultaneous
SB(0.35)-FF	0.36	-	0.49	-	continuous
	0.49	-	0.71	-	simultaneous

1) Axial load ratio

4.3.3.6 Coefficient of friction of ALC mortar

The friction coefficient of ALC mortar was confirmed by shear bond strength test of non - reinforced specimen (SB(0.35/0.5)-UU). The friction coefficient was calculated as shown in Eq. 4-3, and the results are shown in Fig. 4-17 and Table 4-7. The frictional force was average load in the constant load zone. The axial force was the average clamping force in the constant load zone. The horizontal axis of the graph is the axial force ratio, and the vertical axis is the coefficient of friction. The red dotted line is the coefficient of friction presented in ACI 523.4R. The horizontal axis of the graph represents the axial load ratio, and the vertical axis represents the coefficient of friction. The red dotted line is the coefficient of friction between the ALC blocks with ALC mortar proposed in ACI523.4R.

The reason for using the load in the constant load zone was as follows. When slding cracks occured on both joints of the specimen, only frictional force acts on both bonded surfaces. This frictional force can be expressed as the product of the clamping force and the coefficient of friction which is the property of the surface. Since the clamping force is constant, the friction force after the slding crack also becomes constant. Therefore, the coefficient of friction was calculated in the load constant zone where friction force as kept constant after the slip occurred at both joints.

Experimental results showed that the friction coefficient does not increase or decrease with axial force. The coefficient of friction (mean = 1.69, SD = 0.27) was higher than the coefficient of friction 1.0 in ACI.523.4R. The coefficient of friction of the 0.35(ton/m^3) specimens was mean=1.87, SD = 0.20 and the

coefficient of friction of the 0.5(ton/m^3) was mean=1.51, SD = 0.33. Therefore, the axial force does not affect the coefficient of friction, and the coefficient of friction 1.0 between the ALC blocks in ACI 523.4R is conservative.

The coefficient of friction (mean = 1.87, SD = 0.20) of 0.35 (Ton/m^3) specimens was higher than that (mean = 1.51, SD = 0.33) of 0.5(Ton/m^3) specimens. This was because the surface of the 0.35 (Ton/m^3) specimens were roughly destroyed than 0.5 (Ton/m^3) specimens as shown in Fig. 4-12.

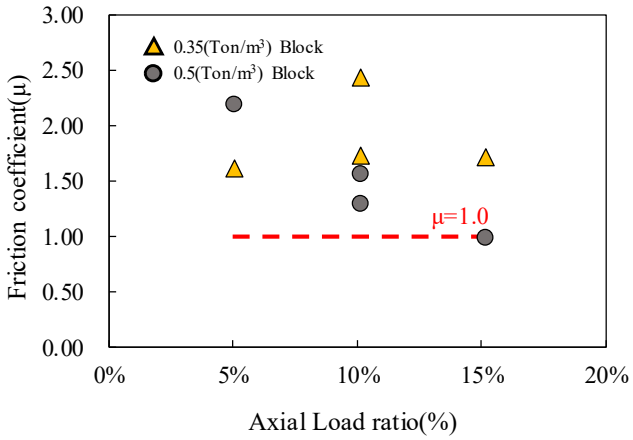

Figure 4-17 Coefficent of friction with axial load ratio

Table 4-7 Test results of the coefficient of friction

0.35(Ton/m^3) specimens				
Specimen	Axial(clamped) load(kN)		Average load in constant zone(P, kN)	Coeffcient of friction(*P/2N*)
	Initail	Average load in constant zone (*C*)		
SB(0.35)-UU(5)	15	11.98	38.66	1.61
SB(0.35)-UU(10)	30	15.59	75.91	2.43
SB(0.35)-UU(10)	30	24.36	84.11	1.73
SB(0.35)-UU(15)	45	18.20	62.36	1.71
0.5(Ton/m^3) specimens				
Specimen	Axial(clamped) load(kN)		Average load in constant zone(P)	Coeffcient of friction(*P/2N*)
	Initail	Average load in constant zone (*C*)		
SB(0.5)-UU(5)	15	12.80	55.98	2.19
SB(0.5)-UU(10)	30	25.55	77.38	1.52
SB(0.5)-UU(10)	30	26.12	67.90	1.30
SB(0.5)-UU(15)	45	32.44	64.46	0.99

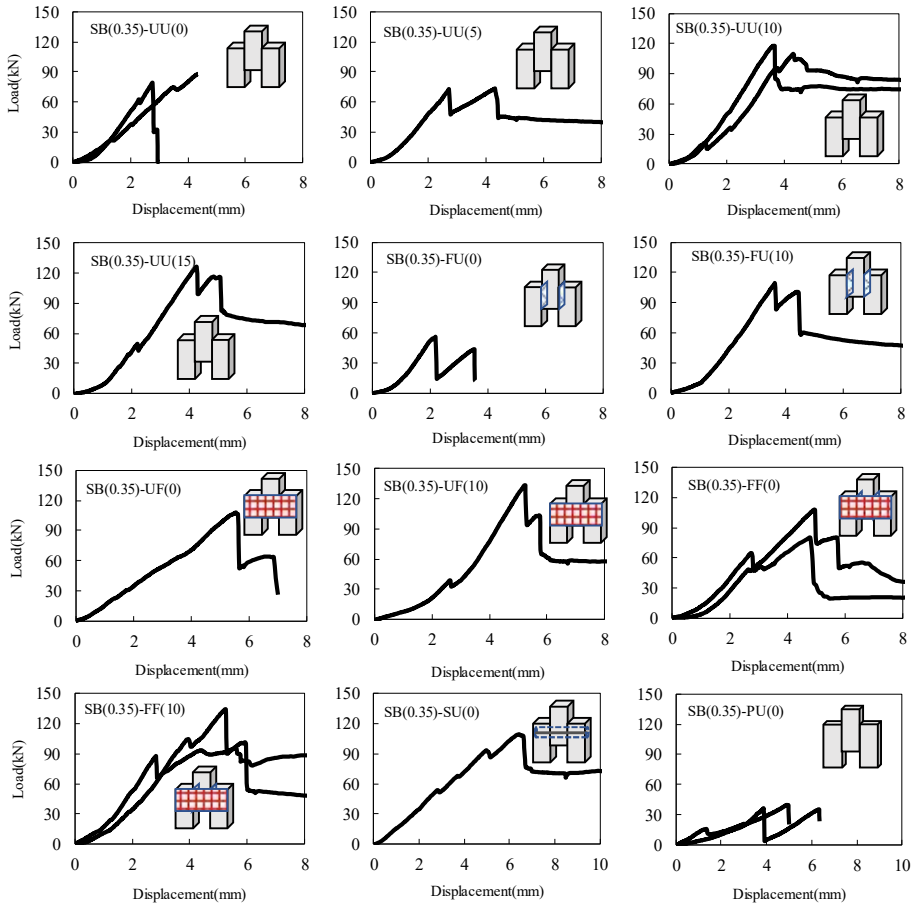

Figure 4-18 Relationships of Load-Displacement in shear bond strength tests (0.35(Ton/m^3) Block)

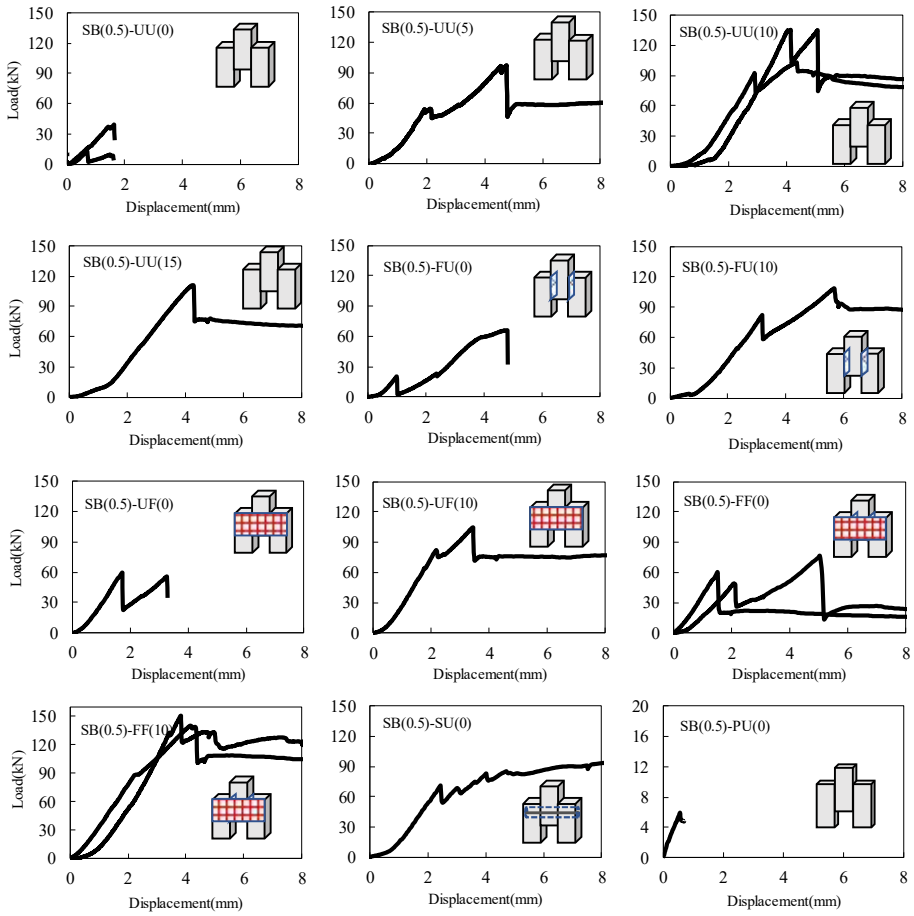

Figure 4-19 Relationships of Load-Displacement in shear bond strength tests (0.5 (Ton/m^3) Block)

4.4 Compressive strength of ALC prism

4.4.1 Variables

Compressive strength tests of ALC prism were performed to confirm the compressive strength of the ALC block wall. The variables are the density of the ALC block and glass-fiber reinforcement as shown in Table 4-8. Glass-fiber were used between the ALC blocks and on the out sides of the ALC prism. A-type glass-fiber as shown in Fig. 3-15 (a) was used for glass-fiber for the sides of wall and C-type glass-fiber was used for the glass-fiber used for bed-joint. The thickness of mortar at bed-joint and on wall was 2mm (± 1mm).

Table 4-8 Variables of compressive strength of ALC prism

Specimen	Glass-fiber reinforcement		Quantity
	Bedjoint	Sides of the wall	
CS(0.35)-UU	-	-	2
CS(0.35)-UF	-	A-Type	1
CS(0.35)-FF	C-Type	A-Type	2
CS(0.5)-UU	-	-	2
CS(0.5)-UF	-	A-Type	1
CS(0.5)-FF	C-Type	A-Type	2

Notes: CS (0.5)-FF, CS=Compressive strength test of ALC prism, 0.5=density, F-= fiber glass reinforcement at bedjoint, -F=fiber glass reinforcement on the sides of wall

4.4.2 Test set-up

The size of prism specimen was 800 mm × 300 mm × 800 mm (width × thickness × height) as shown in Fig. 4-20. The non-reinforced specimens were made of only ALC block and ALC mortar. The reinforced specimens were reinforced with glass-fiber at bedjoint and on the sides of wall.

The compressive strength of ALC prism tests were performed using a 1,000 kN actuator as shown in Fig. 4-21 according to ASTM C 1314-06.

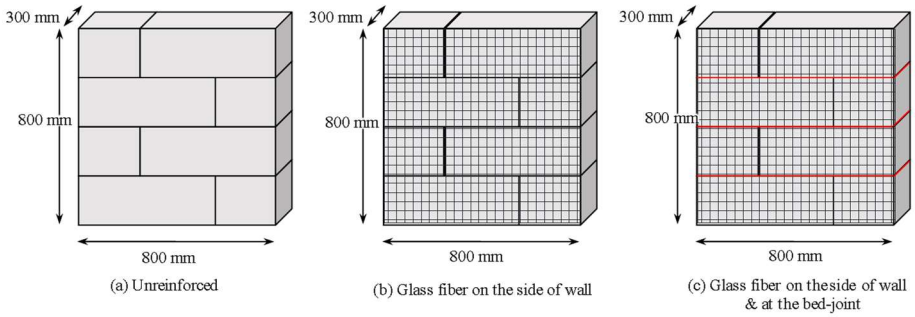

Figure 4-20 Test specimens of the compressive strength of ALC prism

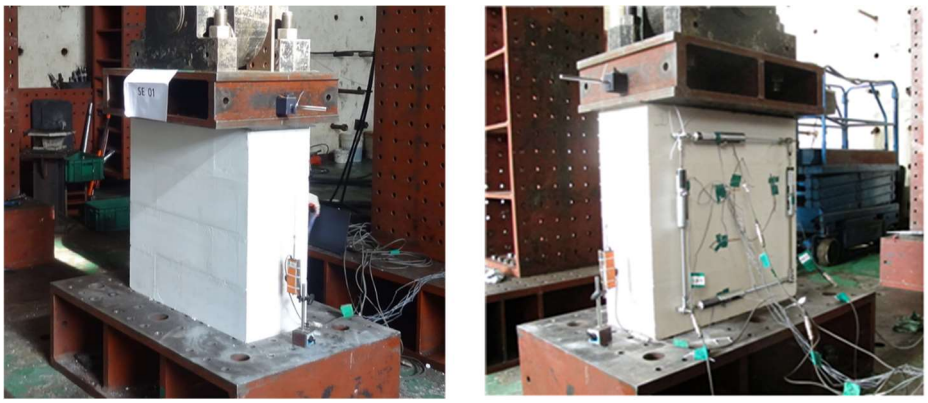

Figure 4-21 Test set-up for the compressive strength of ALC prism

4.4.3 Test results

4.4.3.1 Comparison of ALC prism compressive strength with compressive strength of ALC block

The relationships between the compressive strength of the ALC prism and the compressive strength of the ALC block was shown in Fig. 4-22. The horizontal axis of the graph represents the compressive strength of the ALC block, and the vertical axis represents the compressive strength of the prism specimens. The yellow triangle indicates test results of 0.35(Ton/m^3) ALC prism specimens, the gray circle indicates test results of 0.5(Ton/m^3) ALC prism specimens. The expected prism strength proposed by Eurocode 6 was shown in Eq. 4-5 and it was indicated by a black dotted line.

$$f_K = 0.8 f_{ALC}^{0.85} \quad (4\text{-}5)$$

Where f_k is the compressive strength of the prism, and f_{ALC} is the compressive strength of the ALC block.

Experimental results showed that the compressive strength of the ALC prism increases as the strength of the ALC block compressive strength increases. The prism compressive strength of 0.5(Ton/m^3) ALC block (mean=3.35MPa) showed higher than that of 0.35(Ton/m^3) ALC block (mean=1.88MPa). Comparing the prediction in Eurocode 6 with the test results, the prism compressive strength of 0.35(Ton/m^3) ALC was overestimated and that of 0.5(Ton/m^3) ALC was underestimated. The prism compression strength (1.88 MPa) of 0.35(Ton/m^3) ALC was 10.0% lower than the expected strength (2.09 MPa) and the prism compression strength (3.35 MPa) of 0.5(Ton/m^3) ALC was

higher than the expected strength (2.65 MPa) by 26.4%.

The ratio of average test results divided by predicted strength was 1.03(C.O.V 4.7%) and the predicted strength proposed by Eurocode 6 was relatively well matched with compressive strength of prism specimens.

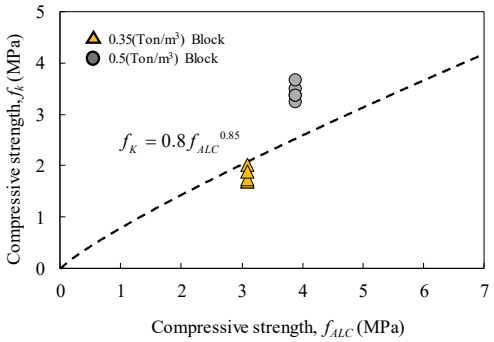

Figure 4-22 Compressive strength of ALC prism with compressive strength of ALC block

Table 4-9 Test results of the compressive strength of ALC prism

0.35(Ton/m³) specimens					
Specimen	Tested f_k(MPa)	Predicted f_k(MPa)	$\frac{\text{Tested } f_k}{\text{Predicted } f_k}$	Modulus of Elasticity	Poisson's ratio
CS(0.35)-UU	1.63	2.09	0.77	1,753	0.22
CS(0.35)-UU	1.63		0.77	1,741	0.21
CS(0.35)-UF	1.66		0.79	1,608	0.30
CS(0.35)-FF	1.94		0.92	1,372	0.25
CS(0.35)-FF	1.81		0.86	1,598	0.23
0.5(Ton/m³) specimens					
Specimen	Tested f_k(MPa)	Predicted f_k(MPa)	$\frac{\text{Tested } f_k}{\text{Predicted } f_k}$	Modulus of Elasticity	Poisson's ratio
CS(0.5)-UU	3.10	2.65	1.16	2,505	0.16
CS(0.5)-UU	3.21		1.21	2,803	0.29
CS(035)-UF	3.34		1.26	2,549	0.21
CS(0.5)-FF	3.50		1.32	2,747	0.29
CS(0.5)-FF	3.21		1.21	3,162	0.21

4.4.3.2 Comparison of prism compressive strength with glass-fiber reinforcement

The prism compressive strength with glass-fiber reinforcement were shown in Table 4-10. Test results showed that glass-fiber reinforcement has no significant effect on compressive strength of prism. The compressive strength of specimens reinforced with glass-fiber on the sides of wall increased more than unreinforced prism specimens by 2% ~ 6%. The compressive strength of specimens reinforced with glass-fiber at bed-joint and on the sides of wall increased more than unreinforced prism specimens by 6% ~ 15%. This is because the glass-fiber is a material subjected to a tensile force, so that it did not have a great influence on the compressive strength.

Table 4-10 Test results of the compressive strength of ALC prism with reinforcement

Glass-fiber reinforcement	Mean compressive strength (MPa)	
	0.35(Ton/m^3)	0.5(Ton/m^3)
Uureinforced	1.63	3.16
On the sides of wall	1.66	3.34
Reinforcred on the sides of wall & At bed-joint	1.88	3.35

4.4.3.3 Failure mode

In the failure modes of ALC prism at maximum load, cracks occurred around the bed-joints.On the other hand, cracks in the ALC block occurred in either vertical or diagonal shapes in the material tests.

"Failure mechanism of masonry prism loaded in axial compression: computational aspects" (L.Berto et al. 2004) explained that the failure mode of a prism is affected by the different deformation between the mortar and the block. If the strain of the block is larger than the strain of the mortar, the fracture occurs around the bedjoint. In these conditions, the block is compressed in triaxises, and the mortar receives compressive force in the direction of load and tensile force in the other axises as shown in Fig. 4-23(a).

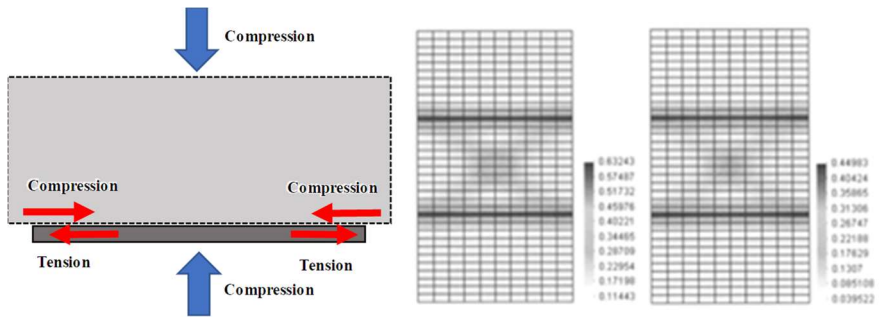

(a) Force equilibrium **(b) 2D analysis (L Berto et al, 2004)**

Figure 4-23 Anaysis of prism compressive specimen

The elastic modulus of the ALC block is about 3,000 MPa (Poisson's ratio = 0.25), and the elastic modulus of the mortar is about 15,000 MPa (Poisson's ratio = 0.10). Due to the difference in modulus of elasticity, the deformation of the ALC block is larger than that of the mortar when subjected to the same compressive force. Therefore, the ALC prism specimen was fractured due to

the difference in the deformation of the ALC block and the mortar, not compressive failure of ALC block as shown in Fig. 4-24.

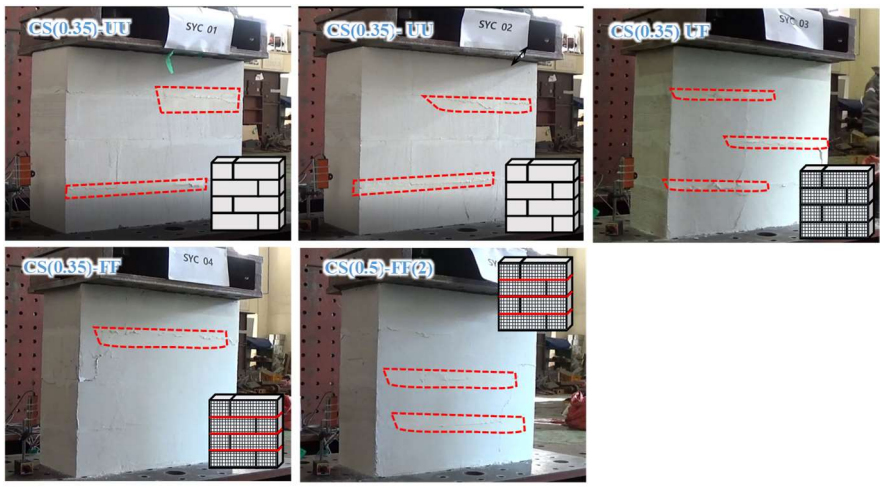

(a) 0.35(Ton/m^3) Block

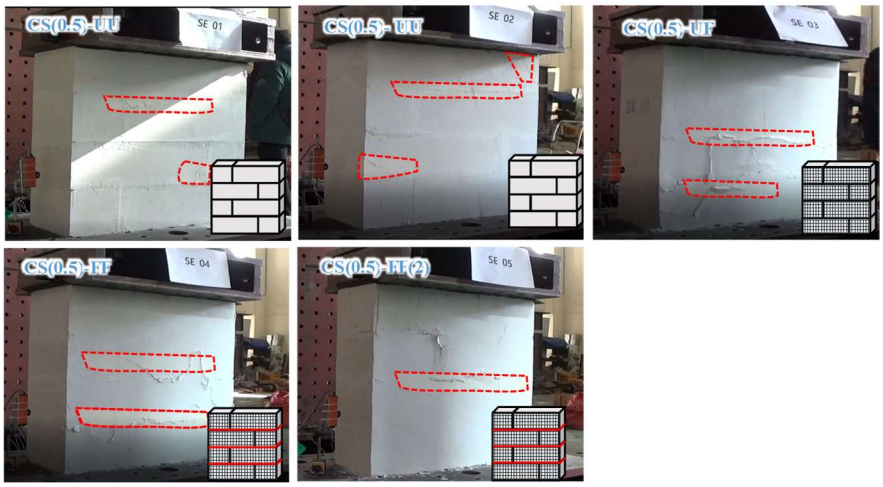

(b) 0.5(Ton/m^3) Block

Figure 4-24 Failure mode of specimens at peak load

4.5 Diagonal tensile strength (shear) of ALC prism

4.5.1 Variables

To verify the diagonal tensile (shear) strength of ALC prism with glass-fiber reinforcement method, the tests were performed with dry density of ALC block and glass-fiber reinforcement as shown in Table 4-11. DT (0.35/0.5)-UU were the specimens to investigate the diagonal tensile strength (shear) strength of the non-reinforced ALC wall. DT(0.35/0.5)-UM and DT(0.35/0.5) -UF were the specimens to examine the effect of mortar and fiber glass reinforced on the sides of wall. DT(0.35/0.5)-FU, DT(0.35/0.5)-FM and DT(0.35/0.5)–FF were the specimens to confirm the effect of fiber-glass reinforced on the side of wall. The thickness of mortar at the bedjoint and on the wall surface was 2 mm and 3 ~ 5 mm, respectively.

Table 4-11 Variables of Diagonal tensile strength(shear) of ALC prism test

Specimen	Fiber glass reinforcement		Qauntity
	Bed-joint	The side of wall	
DT(0.35)-UU	None	None	1
DT(0.35)-UM	None	Mortar	1
DT(0.35)-UF	None	C-Type	1
DT(0.35)-FU	C-Type	None	1
DT(0.35)-FM	C-Type	Mortar	1
DT(0.35)-FF	C-Type	C-Type	1
DT(0.5)-UU	None	None	1
DT(0.5)-UM	None	Mortar	1
DT(0.5)-UF	None	C-Type	1
DT(0.5)-FM	C-Type	None	1
DT(0.5)-FU	C-Type	Mortar	1
DT(0.5)-FF	C-Type	C-Type	1

Notes : DT(0.35)-FF, DT(Diagonal tension strength test), 0.35(dry density of ALC block), **F-**(Reinforcement at bedjoint), - F(Reinforcement on the sides of ALC block)

4.5.2 Test set-up

The size of test specimen was 800mm × 300mm × 800mm (width × length × height) as shown in Fig. 4-25, and Total 12 specimens were tested.

The prism specimens were rotated by 45 degrees and positioned to receive a concentrated loading at the corner as shown in Fig. 4-26. The diagonal tensile (shear) strength tests were performed according to ASTM E 519 using a 1,000 kN actuator. The diagonal tensile (shear) strength was the shear stress at which the shear crack occured at the center, and it was from Eq. 4-6.

$$f_v = \frac{0.707P}{A_n} \tag{4-6}$$

Where f_v is the diagonal tensile (shear) strength, P is the load at shear crack occured, and A_n is the net cross-sectional area of the prism specimen.

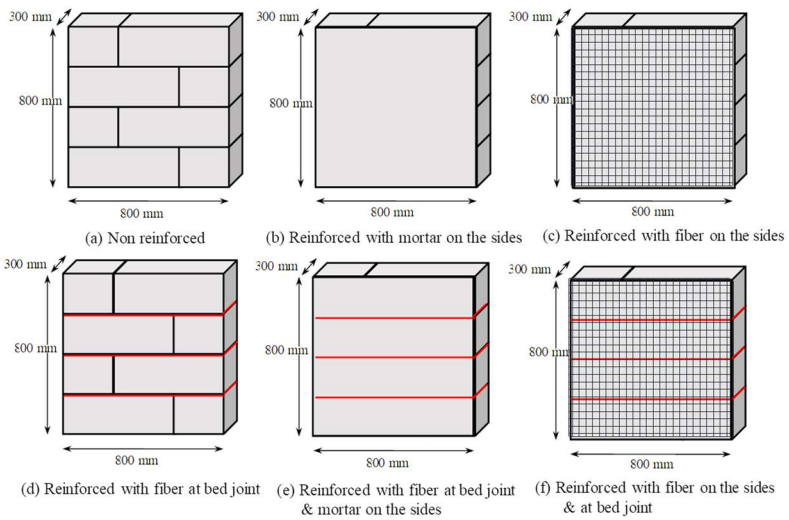

Figure 4-25 Types of specimen for diagonal tenile strength

(a) Test set-up (b) The front of specimen (c) The rear of specimen

Figure 4-26 Test set-up for for diagonal tenile strength of ALC prism

4.5.3 Test results

4.5.3.1 Diagonal Tension (Shear) Strength of unreinforced ALC prism

The prism diagonal tensile (shear) strengths of the unreinforced specimens were shown in Fig. 4-27. The horizontal axis of the graph is the compressive strength of the ALC block, and the vertical axis is the diagonal tensile strength of the specimen. The predicted strength (Eq. 4-7) in ACI-523.4R is the solid green line, the predicted strength (Eq. 4-8) in Eurocode 6 is the red dotted line, and the predicted strength (Eq. 4-9) in DIN is the red dashed line, respectively. The experimental results of the 0.35 (Ton/m^3) and of 0.5 (Ton/m^3) specimens are shown in yellow triangles and gray circles, respectively.

$$f_v = 0.133\sqrt{f_{ALC}} \tag{4-7}$$

$$f_v = f_{vo} + 0.4\sigma \tag{4-8}$$

$$f_v = 0.063\sqrt{f_{ALC}} \tag{4-9}$$

Where f_v is the shear strength, f_{vo} is the basic shear strength of the block (f_{vo} = 0.30 MPa), and σ is the axial stress.

The prism diagonal tensile strength (shear strength) of DT(0.35)-UU and DT (0.5)-UU were 0.24 Mpa. In DT(0.35)-UM and DT(0.5)-UM, the diagonal tensile strength was 0.26 MPa and 0.23 MPa, respectively. Therefore, DT (0.35)-UM and DT(0.5)-UM specimens were classified into non-reinforced specimens because the mortar reinforced on the sides wall had no effect. As shown in Fig. 4-27, Eq. 4-7 proposed by ACI 523.4R represented test results well, while predit of DIN and Eurocode 6 underestimates the experimental results.

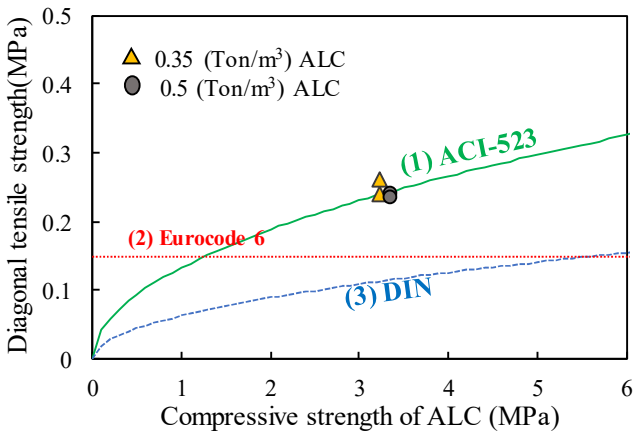

Figure 4-27 Diagonal tensile (shear) strength of unreinforced ALC prism

4.5.3.2 Diagonal tensile (shear) strength with glass-fiber reinforcement

Glass-fiber reinforcement increased diagonal tensile (shear) strength as shown in Table 4-12. The diagonal tensile strength of 0.35/0.5(Ton/m^3) ALC prism reinforced with glass-fiber at the bed-joints increased by 7% and 54%, respectively. When ALC prism specimens reinforced with the glass-fiber on the sides of wall, the diagonal tensile (shear) strength was increased by 13% and 38%, respectively. In 0.35/0.5(Ton/m^3) ALC prism specimens reinforced with glass-fiber on the sides of wall and at bed-joint, diagonal tensile (shear) strengths were increased by 17% and 75%, respectively. Therefore, the glass-fiber reinforcement increased the diagonal tensile (shear) strength.

To investigate difference in fiber glass reinforcement effect between 0.35 and 0.5(Ton/m^3) ALC prism specimens, material strength was examined as shown in table 4-13. In material test results, the strength of the mortar in the 0.35 (Ton/m^3) ALC specimen was 9.2 MPa, which was 40% lower than required compressive strength of S-Type mortar (14.5 MPa). Therefore, the low strength of mortar lowerd the adhesion of bed-joints and reduced the glass-fiber reinforcing effect.

Table 4-12 Test results of the diagonal tensile strength of ALC prism with reinforcement

Specimen	Digonal tensile strength (MPa)	
	0.35 (Ton/m^3) ALC	0.5 (Ton/m^3) ALC
DT(0.35/0.5)-UU	0.24	0.24
DT(0.35/0.5)-FU DT(0.35/0.5)-FM	0.26	0.37
DT(0.35/0.5)-UF	0.27	0.33
DT(0.35/0.5)-FF	0.28	0.42

Table 4-13 Compressive strength of materials in diagonal tensile strength test specimen

Compressive Strength (MPa)	ALC Block	Mortar at the bedjoint	Mortar on the sides of wall
0.35 (Ton/m^3) ALC	3.00	14.53	9.2
0.5 (Ton/m^3) ALC	3.91	16.72	15.17

4.5.3.3 Failure modes

ALC prism diagonal tensile (shear) specimens were fracurted in three shapes as shown in Fig. 4-28. The first was the shear failure. This type of fracture occured in unreinforced specimens and specimens reinforced with mortar on the sides of wall, resulting in brittle fracture. The second was a type that slides in the direction of the joint after shear cracking occurred. This was occurred in a 0.5(Ton/m^3) specimen with relatively high compressive strength. And the third was compressive failure after the shear crack around upper and lower part of specimem which received a testing loading. This failure mode was occurred in a 0.35(Ton/m^3) specimen with relatively low compressive strength.

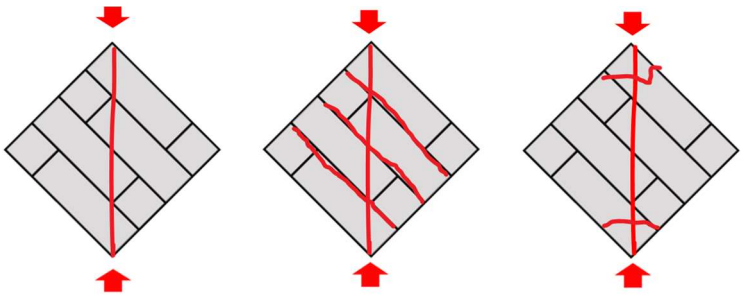

Figure 4-28 Failure modes of diagonal tensile strength test

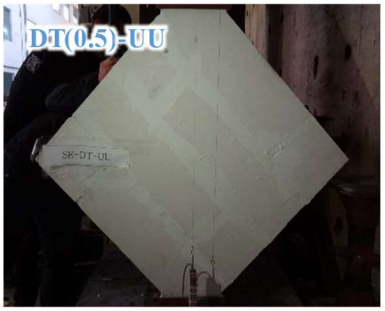

(a) Non reinforcement

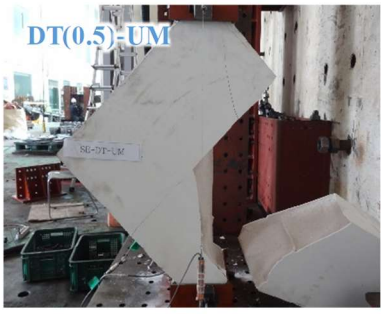

(b) Reinforced with mortar on the side of wall

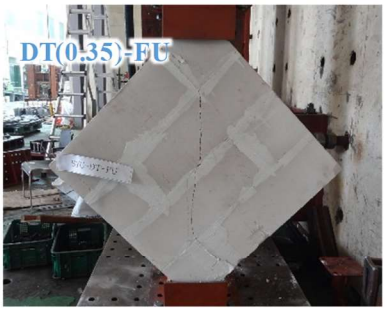

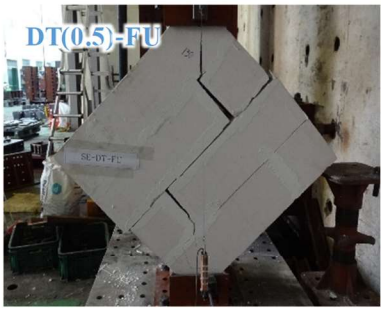

(c) Reinforced with glass fiber at the bedjoint

(d) Reinforced with glass fiber at the bedjoint
& mortar on the sides of wall

(e) Reinforced with glass fiber on the sides of wall

(f) Reinforced with glass fiber at the bedjoint
& on the sides of wall

Figure 4-29 Failure modes of diagonal tensile strength test

4.6 Disscussion

In the prism test, the flexural bond strength, shear bond strength, compressive strength and diagonal tension (shear) strength tests of the ALC prism specimens were performed before the ALC wall performance tests.

(1) Flexural bond strength of the mortar was confirmed by the flexural bond strength test. The flexural bond strength of the ALC mortar used in 0.35 and 0.5 (Ton/m^3) specimens was 0.552 MPa or more, as proposed in ACI 523.4R. Therefore, the ALC mortar used in 0.35 and 0.5 products had enough flexural bond strength.

(2) The Eq. 4-4 proposed by ACI 523.4R reflected the shear bond strength well with the compressive strength of the ALC block. However, in case the mortar was not bonded well as in the case of 0.5 (Ton/m^3) specimen, it was easily broken at lower strength than expected strength.

(3) In the shear bond strength test, glass-fiber reinforcement on the sides of wall and Re-bar in the wall increased the shear bond strength while glass-fiber reinforcement at the bed-joint reduced shear bond strength. Therefore, to reinforce the sliding shear strength of the wall, it is recommended to use glass-fiber at the bed-joint and on the sides of wall.

(4) In the prism compressive strength test, the compressive strength of prism specimen was smaller than that of the ALC block and increased with increasing compressive strength of the block. The Eq. 4-5 proposed in Eurocode 6 showed those tendency well. And the glass-fiber reinforcement did not affect the compressive strength of prism.

(5) In prism diagonal tensile strength test, Eq. 4-7 proposed in ACI 523.4R reflected the test results well. Glass-fiber reinforcement was effective in increasing diagonal tensile strength and its effect was the highest when reinforcing the glass-fibers simultaneously at the bed-joints and on the outer walls. In the prism diagonal tensile test, the glass-fiber reinforcing effect was not significant when the strength of the mortar was low.

In the all prism test, test reusults showed that the performance was improved with glass-fiber reinforcement. However, some specimens with low strength and poor construction conditions showed lower than required strength. Mortar strength and construction were the most important factors affecting the integrity of ALC wall, so thorough management is required.

Chapter 5. Cyclic tests of the ALC shear wall

5.1 Introduction

The load bearing walls resist axial and lateral loads in Low-rise building. Therefore, it is most important to analyze the seismic performance of the wall to confirm the performance of the ALC buildings. To verify the shear performance of the wall, cyclic tests of the ALC masonry wall were performed based on the previous material tests and prism tests.

When an ALC wall receive axial load and lateral load, four types of cracks occure in the wall. They are flexural tensile cracks, sliding cracks, diagonal tensile cracks, and diagonal strut' cracks as shown in Fig. 5-1. The test results of each stength were evaluated by comparing with the predictions in ACI 523.4R (The current US standard for ALC).

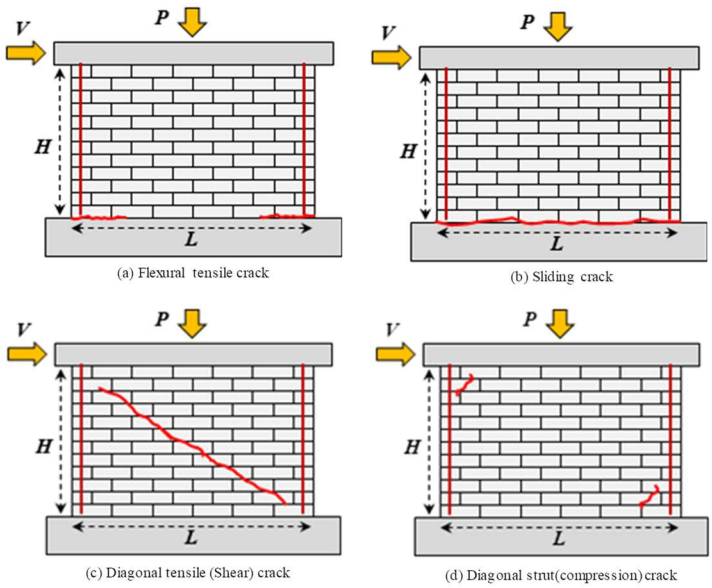

Figure 5-1 Classficaition of the crack in ALC wall

5.2 Test plan

5.2.1 Variables

The major variables of the ALC wall test were classified with wall type, section area of Re-bar, and glass-fiber reinforcement as shown in Table 5-1 and Fig. 5-2. Because the glass-fiber applied to bed-joint showed a great effect on diagonal tensile (shear) strength in section 4.5, the glass-fiber was reinforced at the bedjoint of the 1~ 7 specimens. 8 ~ 11 specimens were reinforced with 2 D 16 bars at the side of wall to confirm the shear strength of ALC the wall with glass-fiber reinforcement.

Each specimen had a width of 3,600 mm and a height of 2,400 mm, and the thickness of the specimen was 300 mm. The base was 4,800 mm wide, 800 mm thick, and 450 mm high. Details of each specimen are given in **Appendix 1**.

Table 5-1 Variables of the cyclic tests of wall

Specimen	Glass-fiber		Reinforced column		Wall thickness
	Bed-joint	Sides of wall	Qty	Re-bar in columm	
1. UW(FU)-0.5	○	×	-	-	300
2. UW(FU)-0.35	○	×	-	-	350
3. RW(FU)-0.5	○	×	2	1-D 16	300
4. RW(FF)-0.5	○	○	2	1-D 16	300
5. ROW(FU)-0.5	○	×	4	1-D 16	300
6. UOW(FU)-0.5	○	×	2	1-D 16	300
7. UOW(FF)-0.5	○	○	2	1-D 16	300
8. R_2W(UU)-0.5	×	×	2	2-D 16	300
9.R_2W(FU)-0.5	○	×	2	2-D 16	300
10. R_2W(UF)-0.5	×	○	2	2-D 16	300
11. R_2W(FF)-0.5	○	○	2	2-D 16	300

Note : R(U)W=(un)reinforced with 1-D16 at the sides of wall, R(U)OW= (un)reinforced with 1-D16 at sides of opening, R_2W=reinforced with 2-D16 at the sides of wall, (F-)=fiber glass at the bed joint, (-F)=fiber glass on the sides of wall.,

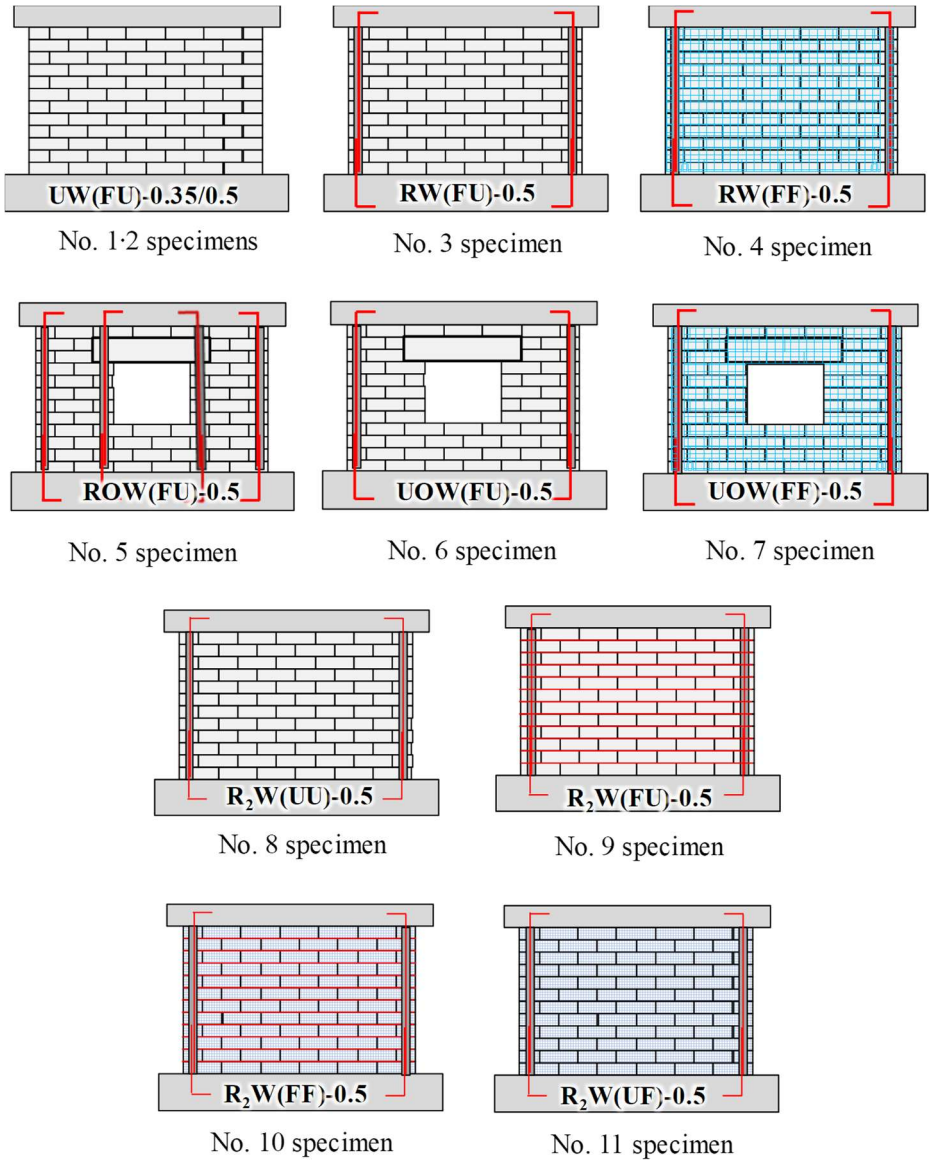

Figure 5-2 Specimens of test

5.2.2 Test set-up

The test set-up was shown in Fig. 5-3. The hydraulic appliances applied two points load to the steal beam at the top of the wall. Both hydraulic systems could apply a compressive force up to a total of 2,000 kN with a capacity of 1,000 kN each. The upper steel beam received the lateral force generated by the actuator (2,000 kN capacity) and it delivered the load to the wall.

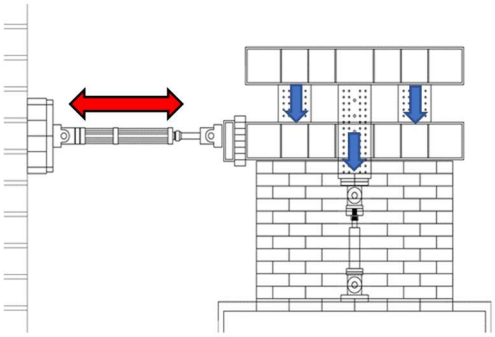

(a) Front view

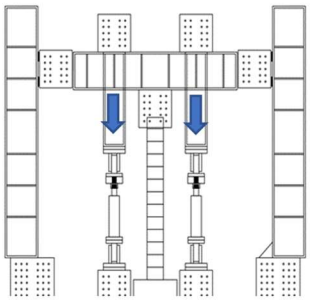

(b) Side view

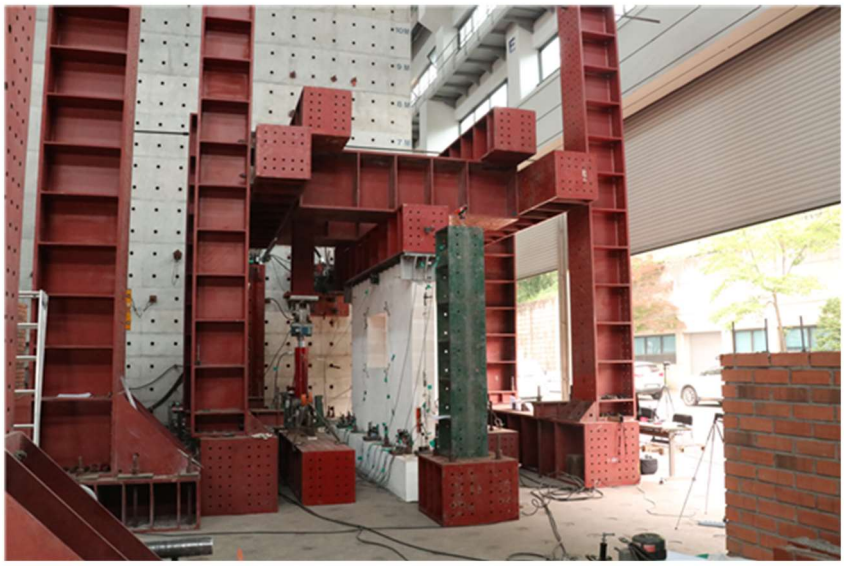

(c) Test view

Figure 5-3 Test set-up for the Wall test

5.2.3 Loading Protocol

As shown in Fig. 5-4, the load protocol of the test was planned to have 2 cycles per step (Total 13 step). The displacement ratio was planned from 0.05% to 3.0%. The cracks were recorded after the first cycle per step. The cracks were indicated by blue in the positive direction and red in the negative direction on the specimen. Two cycles of 30 kN in forward (+) and negative (-) load were applied before the experiment to set the initial point of load and displacement. The test was terminated at the load less than 80% of the maximum strength. Otherwise, the test was terminated with the fracture shape.

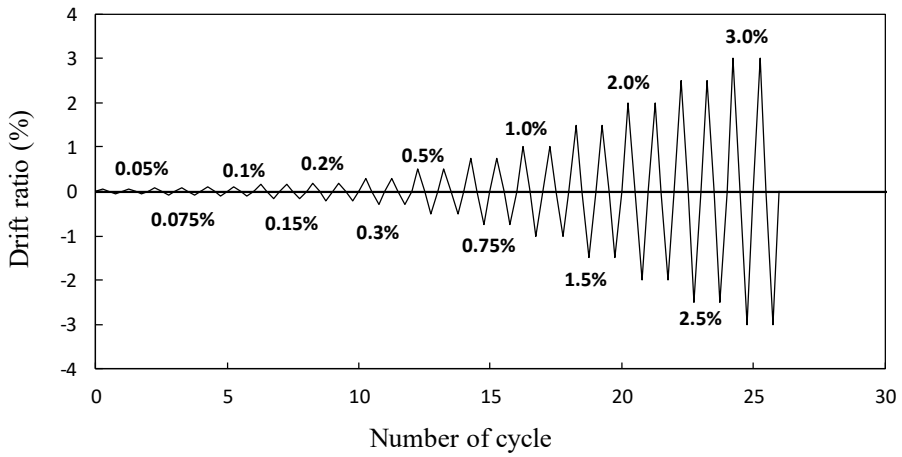

Figure 5-4 Loading protocol

5.2.4 Set-up for LVDT and Strain gage

5.2.4.1 LVDT

The LVDTs were installed as shown in Fig. 5-5 to check the load-displacement relationship, sliding, shear, flexural and rocking deformation of the specimen. The load-displacement relationships were measured by the ① LVDT, rocking deformations were measured by ⑫,⑬,⑱,⑲ LVDTs, sliding deformations were measured by ⑩,⑪,⑭,⑮ LVDTs, the shear deformations were measured by ②,③ LVDTs, flexural deformations were measured by ④,⑤,⑥,⑦,⑧,⑨,⑯,⑰ LVDTs. The ⑳,㉒,㉓ LVDTs were installed to check the slip occurring at the foundation. The LVDTs were installed in the same mathod for all specimens.

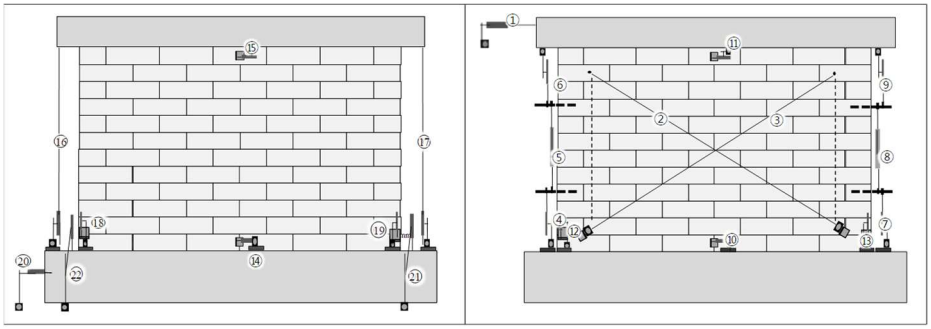

Figure 5-5 LVDT Set-up

5.2.4.2 Local Deformation

As shown in Fig. 5-6, total deformations in wall consists of local deformations such as shear deformation (Δ_{shear}), rocking deformation (Δ_{rock}), flexural deformation ($\Delta_{flexure}$) and sliding deformation ($\Delta_{sliding}$). In general, the wall has a smaller aspect ratio than the other vertical members such as columns. But each deformation are different with the the shape of the wall and the reinforcement method. Therefore, participations of local deformation at the maximum drift ratio were compared to see which local deformation was dominant for each specimen.

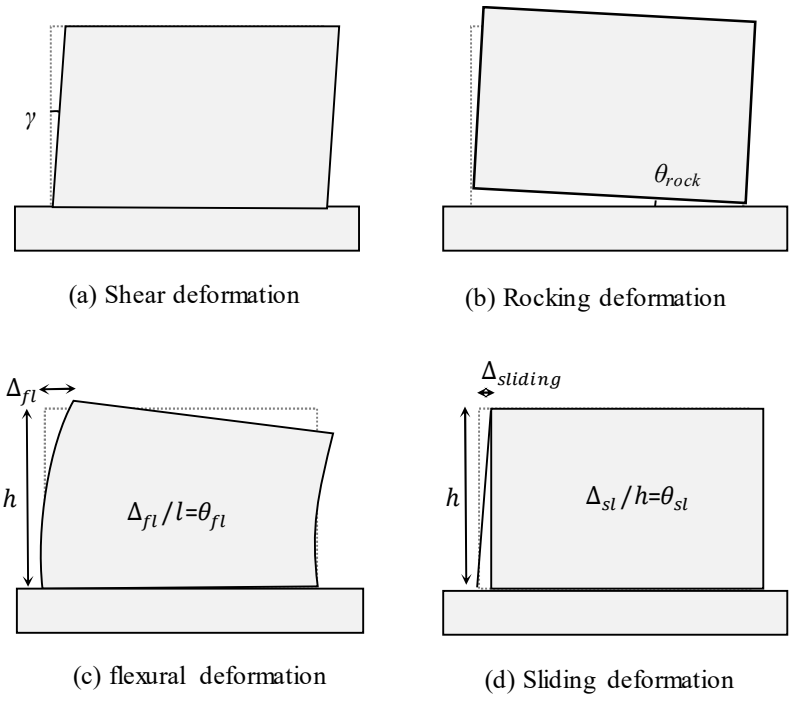

(a) Shear deformation (b) Rocking deformation

(c) flexural deformation (d) Sliding deformation

Figure 5-6 Local deformation occurred in a wall

(1) Shear deformation

To measure the shear deformation of the wall, two line-LVDTs were installed in the diagonal direction as shown in Fig. 5-7 (a). Based on the diagonal deformation values (δ_1 and δ_2) and the measured positions (a and b), the shear deformation value (γ) was calculated as shown in Fig. 5-7 (b).

$$\gamma = \frac{\sqrt{a^2 + b^2}}{2ab}(\delta_1 - \delta_2) \tag{5-1}$$

Where a and b are the horizontal distance and the vertical distance of the diagonal measurement distance, and δ_1 and δ_2 are the measured deformation of the diagonal line displacement meter.

(2) Rocking and Flexural deformation

To measure the rocking and flexural deformation of the wall, LVDTs were installed to the side wall as shown in Fig. 5-8 (a). Rocking deformation was masured by the vertical deformation ($\delta`_{OA}$ and $\delta_{OA}$) of the left and right ends of the wall and the horizontal distance ($h_p$). The pure flexural deformation of the wall was measured by the vertical deformation ($\delta`_{AB}$ and δ_{AB}) of the side of the wall and the horizontal distance (h_p).

$$\theta_A = \frac{\delta_{OA} - \delta`_{OA}}{h_p} \tag{5-2}$$

$$\theta_{BA} = \theta_B - \theta_A = \frac{\delta_{AB} - \delta`_{AB}}{h_p} \tag{5-3}$$

Where h_p is the horizontal distance between the displacement meters, $\delta`_{OA}$ and $\delta_{OA}$ are the vertical deformation between the bottom of the wall and the base, $\delta`_{AB}$ and δ_{AB} vertical deformation between A and B points.

(3) Sliding deformation

To measure the sliding deformation, the horizontal deformation between the center of the lower part of the wall and the base was measured. The slip deformation ($\Delta_{sliding}$) was divided by the wall height (h), to compare the other defomations.

(4) Total deformation

The sum of shear deformation, flexural deformation, and slip deformation in the wall were compared with the lateral displacement measured at the top of the wall.

(a) Measurement

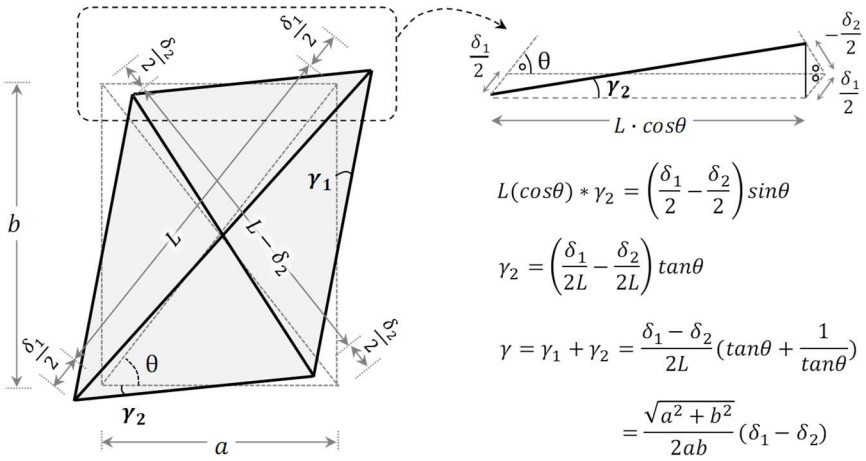

(b) Calcuation

Figure 5-7 Measurement and calculation of shear deformation

(a) Measurement

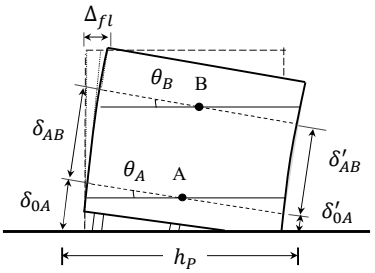

Rocking deformation $\theta_A = \dfrac{\delta_{0A} - \delta'_{0A}}{h_P}$

flexural deformation $\theta_{BA} = \theta_B - \theta_A = \dfrac{\delta_{AB} - \delta'_{AB}}{h_P}$

(b) Calcuation

Figure 5-8 Measurement and calculation of Rocking and Flexural deformation

5.2.4.3 Strain gage

To check the deformation of reinforced bars in the specimens, the strain gauges were attached at vertical Re-bar as shown in Fig. 5-9. The first type was a specimen without vertical bars sides of the opening, and a gauge was attached to only two Re-bars on the side of the wall. The second type was a specimen with vertical bars sides of the opening and attached gauges to the four internal reinforcing columns. No gauges were attached to the non-reinforced specimens.

The gauge was attached to the lower part of the Re-bar because the yielding of the reinforcing bar occurs at the lower part of the reinforcing column which receives the most moment. Therefore, two strain gauges were installed at the bottom of each column, and two additional gauges were installed at intervals of 200 mm.

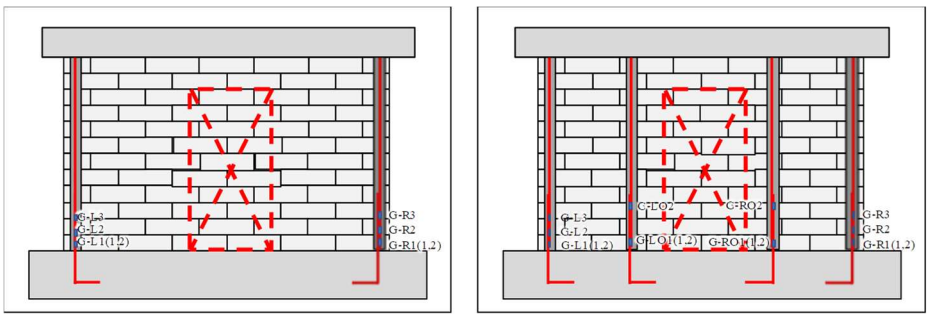

(a) Type 1 (b) Type 2

Figure 5-9 The Strain gage Set-up

5.2.5 Fabrication process of the specimen

The ALC wall specimens were fabricated as shown in Fig. 5-10. The base of the specimen was 4,800 mm wide, 800 mm thick, 450 mm high, and the wall was 3,600 mm x 2,400mm x 300mm (width x height x thickness).

The wall was made as follows. First, to lay the first row of the block, a leveling mortar with 2 cm thickness was applied on the base. After that, ALC blocks were stacked by using ALC mortar, and steel pins were installed between the blocks for wall integrity. When there was a column, high strength mortar was poured into a hole. Finally, the exterior of the specimen was finished with ALC mortar. The tests were carried out after the curing period of 3 weeks or more.

Figure 5-10 Making process of the specimen

5.3 Materal test

5.3.1 ALC block and mortar

Compressive strength of ALC block and mortar were shown as Table 5-2. To test the compressive strength of the ALC block and the mortar, three block specimens (size : 100 mm × 100 mm × 100 mm) were randomly picked from the blocks of the wall specimen and three mortar specimens (size : 50 mm × 50 mm × 50) were made.

The strength of the joint mortar used in 1st (specimen No. 1~7) and 2nd (specimen No. 8~11) walls showed 93% and 84% of the required strength (14.5 MPa) of S-Type mortar, respectively. Particularly, in the 2nd wall specimens showing 84% of the required strength, cracks occurred in the bed-joints in the tests. Therefore, the mortar used for the wall joint should satisfy the compressive strength of 14.5 MPa or more.

Table 5-2 Material strength

Classfication	ALC Block (MPa)	ALC Mortar (MPa)	Bed Mortar (MPa)	Exterior Mortar (MPa)	Grouting Mortar (MPa)
1st Test	4.83	17.5	**13.6**	15.9	33.3
2nd test	4.70	14.4	**12.2**	16.4	68.7

5.3.2 Re-bar

The results of the tensile strength tests of vertical Re-bar in the specimens were shown in Table 5-3 and Fig.5-11. The yield strength (f_y) and tensile strength (f_u) of the D16 Re-bars used in the 1~7 specimens were 456.0 MPa and 657.8 MPa, respectively. The yield strength and tensile strength of reinforcing bars used in the 8~11 specimens were 460.0 MPa and 663.8 MPa, respectively. The yield strength and tensile strength of reinforcing bars were obtained by averaging the tensile strength test results of three Re-bar specimens.

Table 5-3 Properties of Re-bar

SD 400 D16	Dia. (mm)	f_y (MPa)	f_u (MPa)	Elastic modulus (GPa)	Yield strain (mm/mm)
1st Test	15.9	456.0	657.8	198.8	0.0023
2nd test	15.9	460.0	663.8	189.1	0.0024

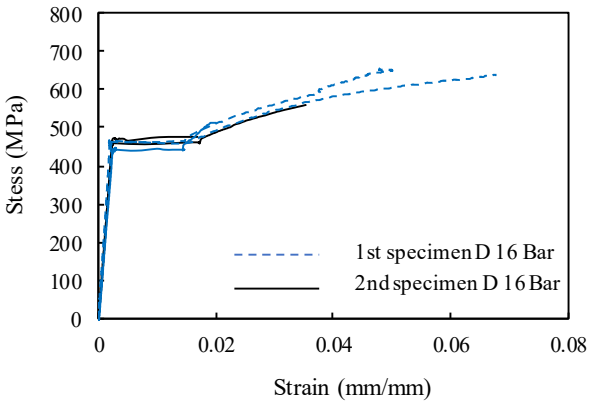

Figure 5-11 Stress-strain relationship of Re-bar specimens

5.4 Test Results

5.4.1 Shear wall (A) : No Re-bar

As shown in Fig. 5-12, cyclic tests were performed on two walls without vertical Re-bar. The major variables of the specimens were density of ALC Block.

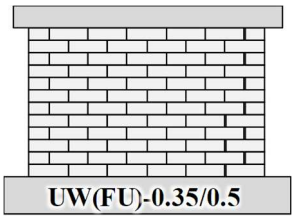

Figure 5-12 Shear wall specimens without vertical Re-bar

5.4.1.1 Lateral Load-Displacement Relationship

UW(FU)-0.35/0.5 are specimens reinforced with glass-fibers only in the bed-joints without vertical Re-bar in the sides of the wall. Fig. 5-13 (a) ~ (c) show the lateral load-displacement (lateral drift ratio) relationships of the unreinforced shear wall. The horizontal axis is the ratio of lateral displacement, which is obtained by dividing the lateral displacement (Δ) to the wall height (H= 2400 mm). The vertical axis represents the lateral load, which represents the actuator load at the displacement ratio. The maximum load in both positive and negative directions is indicated by a yellow circle. The predicted strengths are shown together to compare with the test results. The flexural crack strength (V_f) is indicated by a short dashed line, the sliding strength (V_{sl}) with a friction coefficient of 0.6 is indicated by a dashed line and the shear strength (V_{sh}) is indicated by a long-dashed line. The maximum load and maximum

displacement ratio of each cycle are shown in Table 5-4~5.

Tests were carried out at the same axial force (= 370 kN) in the two specimens. The axial load ratios of UW(FU)-0.35 and UW(FU)-0.5 were 7.1% and 10.5%, respectively. The axial force of the UW(FU)-0.5 specimen was 370 kN (axial load ratio 7.1%) until the displacement ratio 0.75%, and that was increased to 570 kN (axial load ratio 11.2%) after the displacement ratio 0.75%. That was because as shown in Fig. 5-13 (b), the load was kept constant without any cracks other than the sliding cracks from drift ratio 0.3% to drift ratio 0.75%. Therefore, to confirm the failure mode change with increasing axial force, the axial load ratio was increased to 11.2% after the displacement ratio of 0.75%. The graph with the axial load ratio of 7.1% are shown in Fig. 5-13 (b) and that with the axial load ratio of 11.2% are shown in Fig. 5-13 (c).

In UW(FU)-0.35 (Fig. 5-13(a)), The maximum load of the specimen was 272 kN in the positivie direction and 230 kN in the negative direction. The maximum load was more than the flexural crack strength (201kN) and the slidng strength (223kN) but it did not reach the shear strength (386kN).

In UW(FU)-0.5 (Fig. 5-13(b),(c)),The maximum load of the UW(FU)-0.5 specimen was 270.6 kN in the positive direction and 226.7 kN in the negative direction when the axial ratio was 7.1%. Which is 21.9% and 2.1% higher than the sliding strength (V_{sl} = 222 kN), respectively. After reaching the maximum load, only the deformation increased without a decrease in the load. After increasing the axial force ratio to 11.2%, the maximum load was 357.2 kN in the positive direction and 312.8 kN in the negative direction. As the axial load increased, the maximum load increased to the expected slding strength (V_{sl} =

350.4 kN) in positive direction (the negative maximum load showed a strength of 89.3% of V_{sl}).

Therefore, the strength of the unreinforced ALC wall was determined by the sliding strength regardless of the block density and axial force.

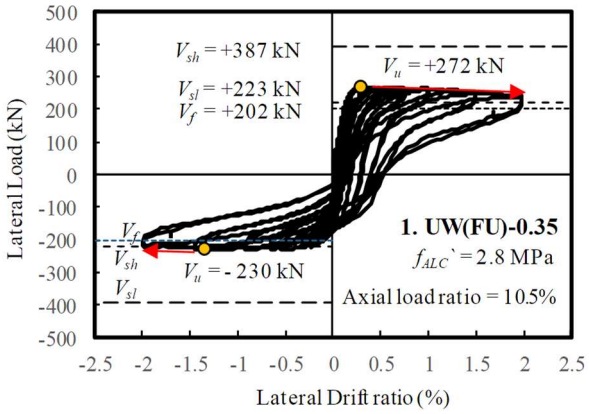

(a) UW(FU)-0.35(Axial load ratio =10.5%)

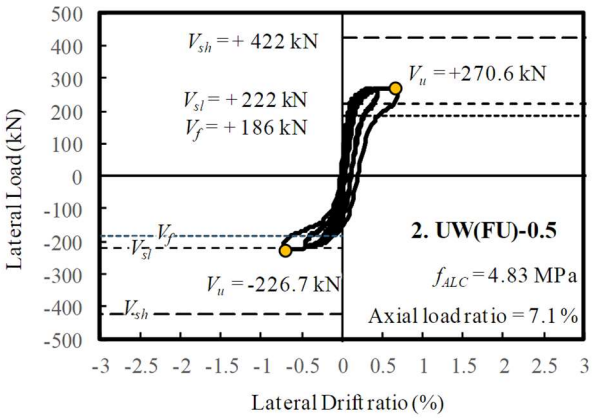

(b) UW(FU)-0.5(Axial load ratio =7.1%)

Figure 5-13 Lateral Load-Displacement Relationship of 1, 2 specimens

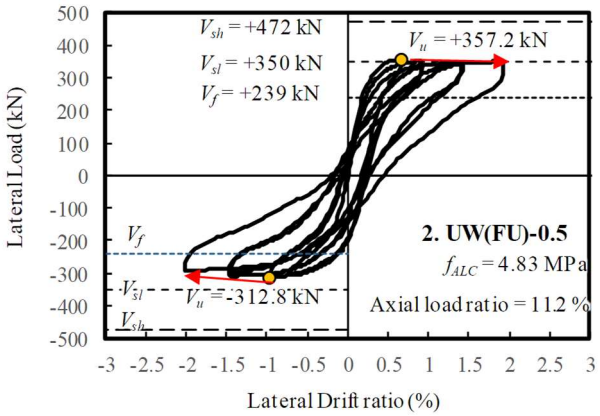

(c) UW(FU)-0.5(Axial load ratio =11.2%)

Figure 5-13 Lateral Load-Displacement Relationship of 1,2 specimens

Table 5-4 Maximum load and displacement ratio at each cycle in UW(FU)-0.5

Drift ratio	Cycle	Maximum load (kN)	Maximum Drift ratio (%)	Cycle	Maximum load (kN)	Maximum Drift ratio (%)
0.05 %	1a[1)]	71.88	0.023	1b[2)]	-90.04	-0.023
	2a	61.90	0.017	2b	-91.1	-0.024
0.075%	3a	118.32	0.038	3b	-125.86	-0.042
	4a	117.44	0.039	4b	-125.84	-0.043
0.1%	5a	157.76	0.058	5b	-147.16	-0.063
	6a	160.18	0.059	6b	-146.62	-0.063
0.15%	7a	216.56	0.100	7b	-175.82	-0.106
	8a	219.58	0.100	8b	-169.42	-0.108
0.2%	9a	239.14	0.148	9b	-186.16	-0.157
	10a	236.76	0.148	10b	-183.72	-0.156
0.3%	11a	258.94	0.240	11b	-204.72	-0.251
	12a	260.70	0.240	12b	-202.34	-0.251
0.5%	13a	266.54	0.356	13b	-214.76	-0.455
	14a	268.20	0.440	14b	-218.44	-0.458
0.75%	15a	270.64	0.69	15b	-226.66	-0.723
	Axial load was increased: 370kN →570kN					
	16a	357.16	0.66	16b	-306.14	-0.67
1%	17a	351.24	0.91	17b	-312.76	-0.95
	18a	339.84	0.90	18b	-303.44	-0.95
1.5%	19a	348.12	1.24	19b	-309.14	-1.45
	20a	344.32	1.40	20b	-298.32	-1.45
2.0%	21a	349.32	1.81	21b	-292.54	-1.99

1) a : Positive direction
2) b : Negative direction

Table 5-5 Maximum load and displacement ratio at each cycle UW(FU)-0.35

Drift ratio	Cycle	Maximum load (kN)	Maximum Drift ratio (%)	Cycle	Maximum load (kN)	Maximum Drift ratio (%)
0.05 %	1a	76.12	0.023	1b	-85.22	0.016
	2a	77.08	0.038	2b	-87.74	0.018
0.075%	3a	122.02	0.059	3b	-125.76	0.004
	4a	123.68	0.063	4b	-122.98	0.006
0.1%	5a	161.96	0.084	5b	-149.66	-0.012
	6a	164.12	0.088	6b	-144.42	-0.008
0.15%	7a	220.38	0.131	7b	-171.4	-0.049
	8a	221.1	0.134	8b	-169.56	-0.048
0.2%	9a	248.14	0.183	9b	-186.42	-0.092
	10a	249.88	0.184	10b	-186.94	-0.095
0.3%	11a	271.1	0.280	11b	-208.98	-0.187
	12a	272.32	0.284	12b	-207.74	-0.191
0.5%	13a	271.72	0.300	13b	-225.12	-0.383
	14a	265.1	0.482	14b	-223.44	-0.387
0.75%	15a	267.18	0.743	15b	-229.26	-0.514
	16a	265.3	0.735	16b	-224.28	-0.653
1%	17a	264.08	0.743	17b	-228.9	-0.883
	18a	261.64	0.998	18b	-226.74	-0.906
1.5%	19a	260.88	1.108	19b	-230.26	-1.352
	20a	247.68	1.593	20b	-226.86	-1.683
2.0%	21a	236.52	1.937	21b	-216.22	-1.982

5.4.1.2 Failure Modes

The failure modes of the UW(FU)-0.35 specimen are shown in Fig. 5-14(a). The first cracks were occurred at leveling mortar between wall and base at the drift ratio of 0.15%. At the drift ratio of 0.2%, sliding crack occurred due with rocking at the bottom of the wall. Shear cracking occurred from 0.3% drift ratio to 1.0% drift ratio. After 1.0% of drift ratio, flexural compressive cracks occurred at the lower side of the wall due to the rocking. The test was terminated at a displacement ratio of 2.0% due to only rocking and sliding deformation up without increasing the load.

The failure modes of UW(FU)-0.5 specimen are shown in Fig 5-14(b). In the axial ratio of 7.1%, flexural cracks and diagonal cracks occurred at a drift ratio of 0.15%. At drift ratios of 0.2%, sliding crack occurred between the wall and the base with rocking. To prevent sliding, brackets were installed at both ends to suppress the slip, but the load did not increase due to the increase in the rocking effect rather than the slip as the drift ratio increased. The axial load ratio was increased to 11.2%, and further test was carried out after the drift ratio of 0.75%.

In axial force ratio 11.2%, the rocking was relatively reduced than that at axial force ratio 7.1%, but additional diagonal cracks occurred. But after drift ratio 1.0%, the rocking deformation became worse without increasing the load and diagonal cracks were additionally generated. Although a load did not decrease significantly until the drift ratio of 2.0%, but the experiment was terminated at a displacement ratio of 2.0% for the safety of the test

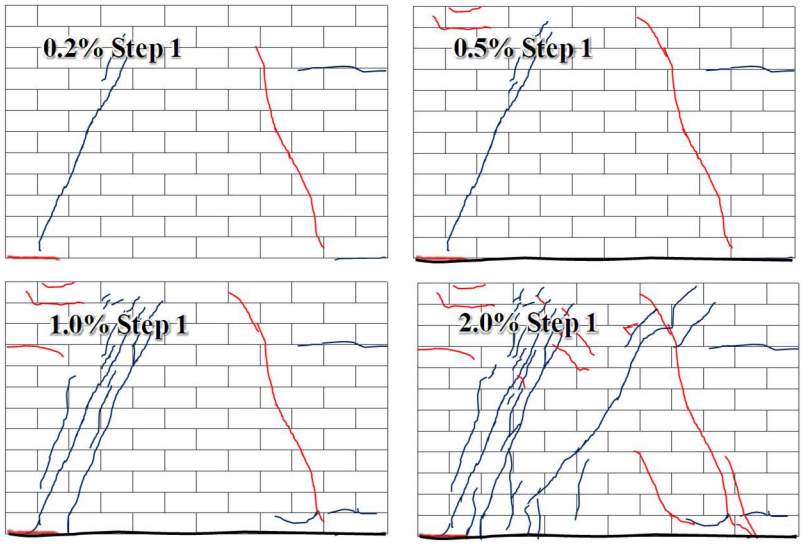

(a) UW(FU)-0.35

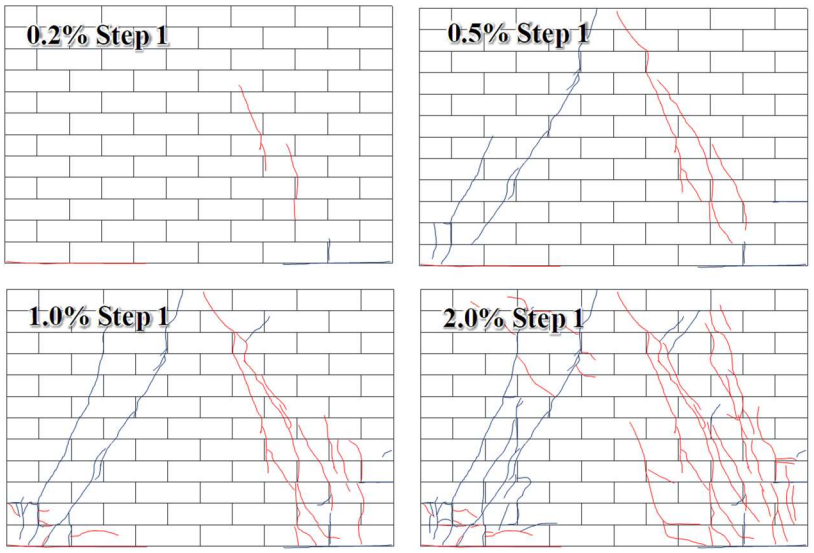

(b) UW(FU)-0.5

Figure 5-14 Crack propagation of UW(FU)-0.35/0.5

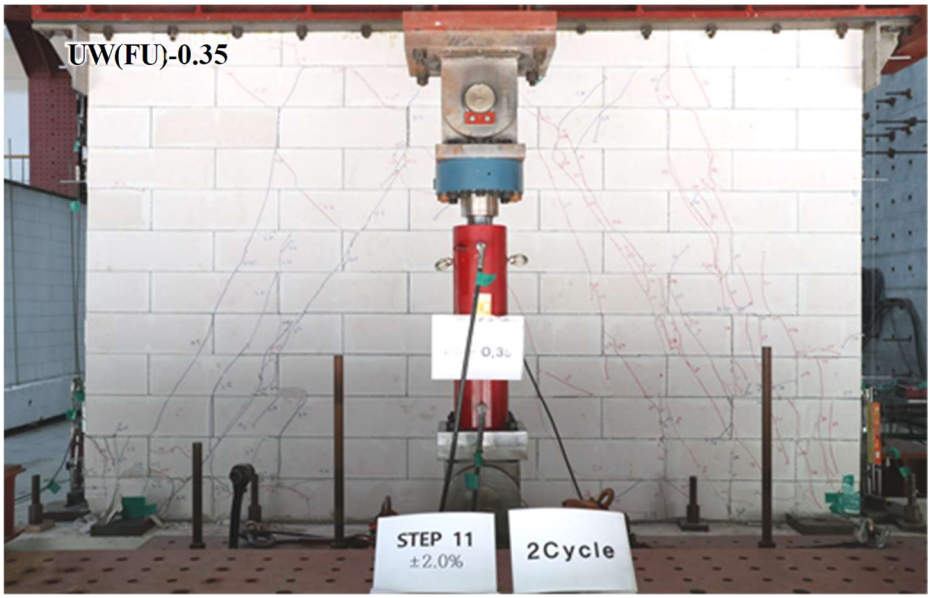

(a) UW(FU)-0.35

(b) UW(FU)-0.5

Figure 5-15 Failure modes of 1,2 specimens at the end of test

5.4.1.3 Deformation Contribution

The sum of shear deformation, the rocking deformation, the flexural deformation, and the slding deformation in the wall were compared with total diformations measured at the top of the wall. In Fig. 5-16, the solid line represents the sum of the shear deformation, rocking deformation, flexural deformation, and local deformation, and the dotted line represents the total lateral deformation measured at the top of the wall deformation.

In UW(FU)-0.35 sepecimen, The sum of the local deformation and the total lateral deformations were almost the same until 1.0% in the positive direction, but the sum of the local deformation was larger than the sum of the total deformation after the displacement ratio of 1.0%. This is because rocking deformation initiated flexural compressvie cracks in the left corner of the specimen at drift ratio 1.0%. In UW(FU)-0.5 sepecimen, the sum of the local deformation and the total lateral deformations were almost the same in the both axial load ratio of 7.1% and 11.2%.

As shown in Fig. 5-17, the contribution of each local deformation to the total lateral deformation of the specimens at the maximum drift atio was confirmed. Ih UW(FU)-0.35 and UW(FU)-0.35 specimens, the rocking deformation accounted for the largest deformation.This rocking deformation caused flexural compressive failure of the end of the wall, but did not significantly reduce the strength of the wall. In UW(FU) -0.5 specimen, the shear deformation was 27% of the total deformation, but shear deformation did not affect on brittle failure. Therefore, considering the relationship of load-displacement, failure mode, and local deformation, sliding deformation and strength were predominant in the

unreinfoced ALC walls.

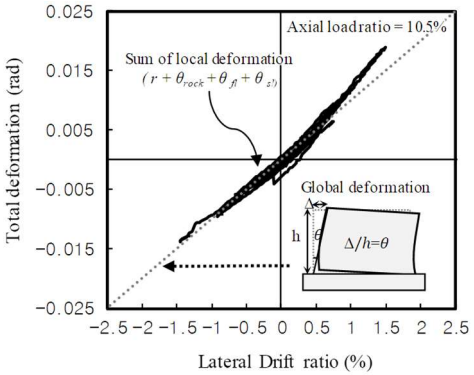

(a) UW(FU)-0.35

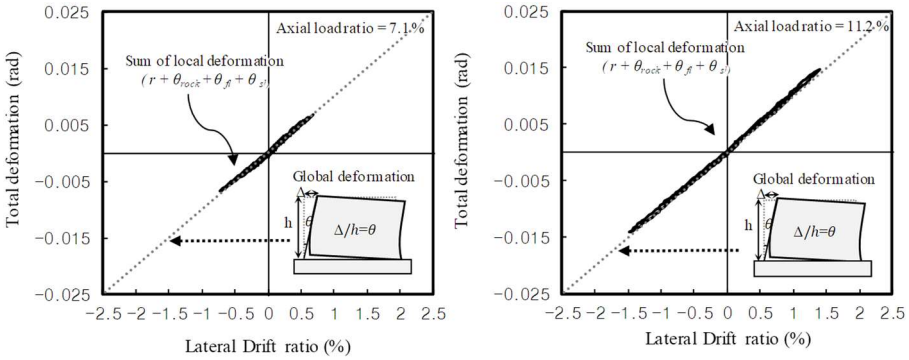

(b) UW(FU)-0.35

Figure 5-16 Comparison of sum of the local deformation and the total deformation (1, 2 specimen)

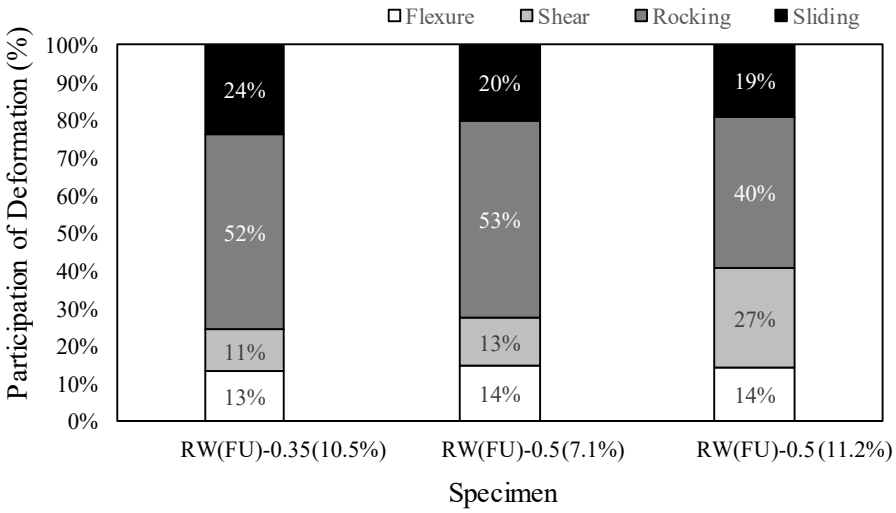

Figure 5-17 Deformation contribution of 1, 2 specimens at the maximum drift ratio

5.4.1.4 Comparison of Siding shear strength prediction

In ACI 523.4R, the coefficient of friction between the ALC wall and base is 1.0. To compare the coefficient of friction of the test specimen with the coefficient of friction proposed in ACI 523.4R, the friction coefficient was calculated by dividing the maximum load in positive and negative directions of each specimen by axial force as shown in Fig 5-18 and Table 5-6. The horizontal axis of the graph represents the axial force ratio, and the vertical axis represents the coefficient of friction. The coefficient of friction was calculated by dividing the lateral force by the axial force after the slip

In UW-0.35 (FU) specimen, two values were obtained with the directions of loading. And in UW-0.5 (FU) specimen, four values were obtained with axial force and direction of loading. From the six conditions with the directions of force and axial force, the average coefficient of friction was calculated as 0.63 (C.O.V=7%). Therefore, the coefficient of friction 1.0 proposed in ACI 523.4 overestimated the friction coefficient of the ALC walls.

Since the coefficient of friction of the ALC wall in ACI 523.4R was derived from the test results of only one specimen, the coefficient of friction was confirmed in ACI 318-14, which was more reliable. ACI 318-14 proposes a coefficient of friction of 0.6 under the condition of concrete placed against hardened concrete not intentionally roughened. Therefore, the coefficient of friction in ACI 318-14 better estimated test results than that in ACI 523.4R.

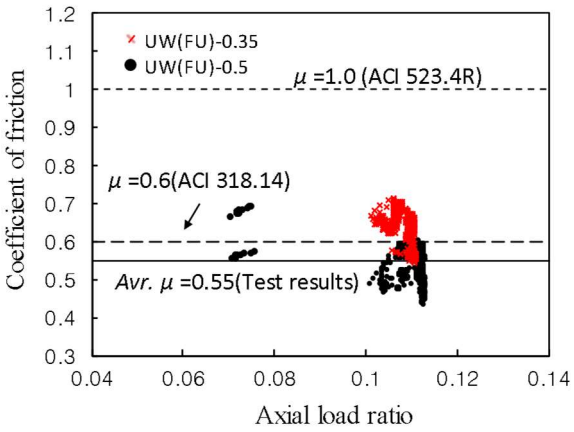

Figure 5-18 Coefficient of friction with an axial load ratio

Table 5-6 Coefficient of frction in 1,2 specimens

Specimen	Axial load (P,kN)	Peak Load (kN)		Coefficient of friction	
		Positive	Negative	Positive	Negative
UW(FU)-0.35	370	264	227	0.71	0.61
UW(FU)-0.5	370	270	227	0.73	0.61
UW(FU)-0.5	580	351	312	0.61	0.54
				Mean(C.O.V)	0.63(7%)
		10% lower Friction coefficient = 0.54			

5.4.2 Shear wall (B) reinforced with 1-D 16 Re-bar

As shown in Fig. 5-19, cyclic tests were performed on two walls with verticlal 1-D16 Re-bar at the side of the specimen. The major variable of the wall specimen was glass-fiber at the bed-joint. RW(FU)-0.5 was a specimen reinforced with glass-fiber at each bed-joint, and RW(FF)-0.5 was a specimen reinforced with glass-fiber at each bed-joint and on the sides of the wall.

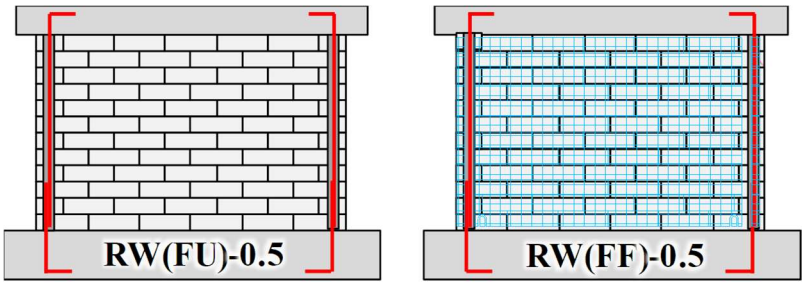

Figure 5-19 Shear wall specimens without vertical Re-bar

5.4.2.1 Lateral Load-Displacement Relationship

Fig. 5-20 (a) ~ (b) showed the relationships of lateral load and displacement in RW(FU)-0.5 and RW(FF)-0.5. The horizontal axis is the ratio of lateral displacement, which is obtained by dividing the lateral displacement (Δ) to the wall height (H= 2400 mm). The vertical axis represents the lateral load, which represents the actuator load at the displacement ratio. The maximum load in both positive and negative directions is indicated by a yellow circle. The predicted strengths are shown together to compare with the test results. The flexural crack strength (V_f) is indicated by a short dashed line, the sliding strength (V_{sl}) with a friction coefficient of 0.6 by a dashed line and the shear

strength (V_{sh}) by a long-dashed line and the nominal flexural strength (V_m) is indicated by the solid line. The flexural strength is a value obtained by dividing the nominal moment strength (M_n) by the height (H) of the wall. The maximum load and maximum displacement ratio per cycle in each specimen is shown in Table 5-7 ~ 8.

The relationship of load and displacement in RW(FU)-0.5 is shown in Fig. 5-20 (a). The load increased linearly up to the drift ratio 0.3% and reached the maximum load at the drift ratio 0.75%. After that, the load was kept constant until the drift ratio 1.0%. After the drift ratio 1.5%, the load decreased sharply. At the final drift ratio 2.0%, it decreased to 237.1kN which was 62% of maximum load in positive direction and decreased to 205.6kN which was 64% of maximum load in negative direction. The maximum load of the specimen in the positive was 372.4kN, which is similar to the flexural strength (V_m = 376kN) direction, and that in negative drection was 317.1kN, which is 90.4% of the slidng strength (V_{sl} = 336kN).

The relationship of load and displacement in RW(FF)-0.5 is shown in Fig. 5-20 (b). The load increased linearly up to the drift ratio 0.3% and reached the maximum load at the drift ratio 0.75%. After that, the load was kept constant until the drift ratio 1.0%. After the drift ratio 1.0%, the load in the positive direction was gradually decreased and the load in the negative direction was abruptly decreased. At the final drift ratio 2.5%, the load decreased to 193.1kN in the positive direction, which was 49.2% of the maximum load in positive direction, and 166.3kN in the negative direcion, which was 48.5% of the maximum load in negative direction. The maximum load in positive diriection

was higher than the flexural strength (V_m = 376kN) and 93% of the shear strength (V_{sh} = 422kN). RW (FF) -0.5 was superior to RW(FU)-0.5 in strength and deformation capacity by glass-fiber reinforcement on the sides of wall. In both specimens, the load in positive drection was higher than that in negative drection, because the flexural cracks, diagonal cracks, and sliding cracks occurred earlier in positive than in negative direction.

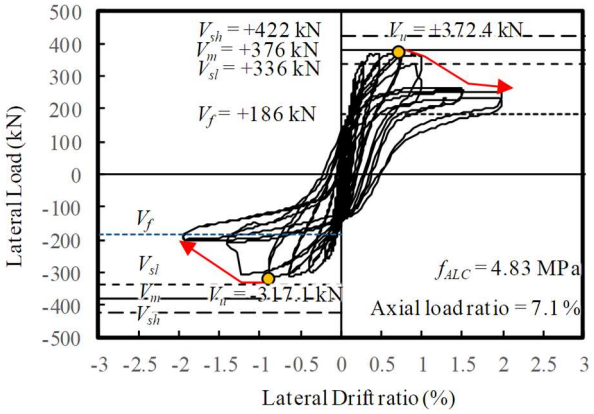

(a) RW(FU)-0.5

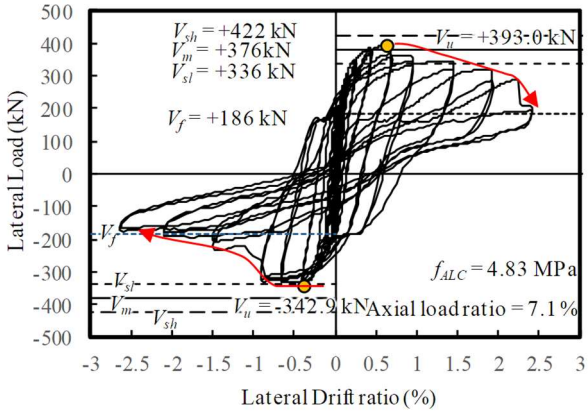

(b) RW(FF)-0.5

Figure 5-20 Lateral Load-Displacement Relationship of 3,4 specimens

Table 5-7 Maximum load and drift ratio at each cycle in RW(FU)-0.5

Drift ratio	Cycle	Maximum load (kN)	Maximum Drift ratio (%)	Cycle	Maximum load (kN)	Maximum Drift ratio (%)
0.05 %	1a	93.68	0.03	1b	-97.48	-0.01
	2a	102.82	0.03	2b	-87.64	-0.01
0.075%	3a	151.40	0.06	3b	-135.76	-0.02
	4a	154.38	0.06	4b	-133.28	-0.02
0.1%	5a	165.40	0.08	5b	-165.26	-0.04
	6a	168.60	0.09	6b	-160.16	-0.04
0.15%	7a	223.06	0.13	7b	-208.48	-0.07
	8a	230.12	0.13	8b	-205.02	-0.07
0.2%	9a	296.56	0.17	9b	-233.20	-0.10
	10a	294.08	0.18	10b	-225.58	-0.11
0.3%	11a	346.34	0.27	11b	-264.20	-0.20
	12a	331.18	0.28	12b	-254.60	-0.20
0.5%	13a	368.28	0.37	13b	-300.22	-0.38
	14a	352.28	0.48	14b	-289.62	-0.39
0.75%	15a	372.36	0.73	15b	-314.70	-0.63
	16a	365.84	0.72	16b	-306.20	-0.63
1%	17a	366.06	1.00	17b	-317.06	-0.88
	18a	338.94	0.91	18b	-295.32	-0.88
1.5%	19a	266.42	1.50	19b	-307.02	-1.19
	20a	257.78	1.48	20b	-211.56	-1.40
2.0%	21a	251.56	2.00	21b	-205.64	-1.94
	22a	231.70	1.92	22b		

Table 5-8 Maximum load and drift ratio at each cycle in RW(FF)-0.5

Drift ratio	Cycle	Maximum load (kN)	Maximum Drift ratio (%)	Cycle	Maximum load (kN)	Maximum Drift ratio (%)
0.05 %	1a	93.26	0.02	1b	-105.40	-0.02
	2a	100.26	0.02	2b	-105.48	-0.02
0.075%	3a	157.58	0.04	3b	-152.92	-0.03
	4a	161.60	0.04	4b	-150.84	-0.03
0.1%	5a	206.90	0.06	5b	-192.48	-0.04
	6a	210.36	0.06	6b	-186.48	-0.04
0.15%	7a	273.88	0.11	7b	-220.48	-0.08
	8a	275.28	0.11	8b	-217.74	-0.08
0.2%	9a	309.34	0.15	9b	-240.12	-0.12
	10a	310.76	0.15	10b	-236.22	-0.12
0.3%	11a	352.30	0.24	11b	-292.32	-0.21
	12a	345.18	0.25	12b	-284.90	-0.21
0.5%	13a	386.30	0.44	13b	-342.92	-0.40
	14a	382.24	0.44	14b	-336.64	-0.39
0.75%	15a	392.34	0.66	15b	-331.94	-0.52
	16a	366.58	0.69	16b	-322.82	-0.63
1%	17a	364.10	0.81	17b	-328.84	-0.86
	18a	344.84	0.94	18b	-323.22	-0.90
1.5%	19a	345.52	1.46	19b	-312.40	-1.48
	20a	321.32	1.45	20b	-206.40	-1.48
2.0%	21a	320.16	1.92	21b	-194.70	-1.78
	22a	287.42	1.93	22b	-180.50	-2.05
2.5%	23a	195.82	2.41	23b	-175.54	-2.60
	24a	193.14	2.39	24b	-166.32	-2.59

5.4.2.2 Failure Modes

The failure mode of the RW(FU)-0.5 specimen is shown in Fig. 5-21(a). At the drift ratio 0.15%, flexural bond cracks occurred at the leveling mortar. At the drift ratio 0.3%, horizontal cracks occurred due to roking and sliding at leveling joint. Shear cracks occurred throughout the wall until drift ratio 1.0%. This cracking behavior was due to the Re-bar at the sides of wall, which increased the maximum load more than UW(FU)-0.5 by 35% . At the drift ratio 1.5, the flexural compressive failure due to the occurred with the abrupt decrease of the load. At the final drift ratio 2.0%, the coner of the wall collapsed due to the flexural compressive failure at the sides of wall (Fig. 5-22(a)).

The failure mode of the RW(FF)-0.5 specimen is shown in Fig. 5-21(b). At the drift ratio 0.15%, flexural bond cracks occurred the leveling mortar and the sides of wall. At the drift ratio 0.3%, horizontal cracks occurred due to roking and sliding at leveling joint. The flexural cracks generated on the side of the wall were developed as flexural shear cracks. At the drift ratio 0.5%, the shear cracks occurred both in the positive and negative directions. Afterward, shear cracks and flexural shear cracks proceeded without any other cracks until the displacement ratio of 1.0%. Shear cracks were smaller than RW(FU)-0.5 specimens, and flexural shear cracks occurred more. This was because the glass- fiber on the wall increases the shear strength of the wall to suppress the occurrence of shear cracks, and the increased load caused the flexural shear cracks. The test was terminated at at the drift ratio 2.5% with the failure mode such as shown in Fig. 5-22(b).

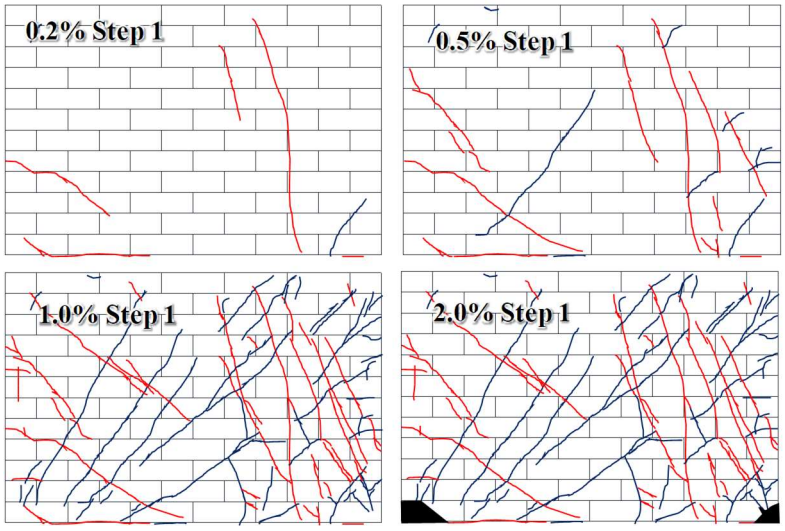

(a) RW(FU)-0.5

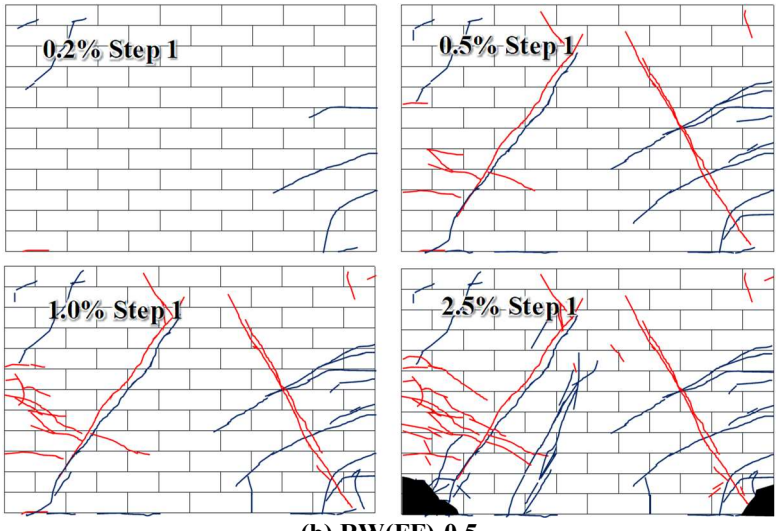

(b) RW(FF)-0.5

Figure 5-21 Crack propagation of 3, 4 Specimen

(a) RW(FU)-0.5

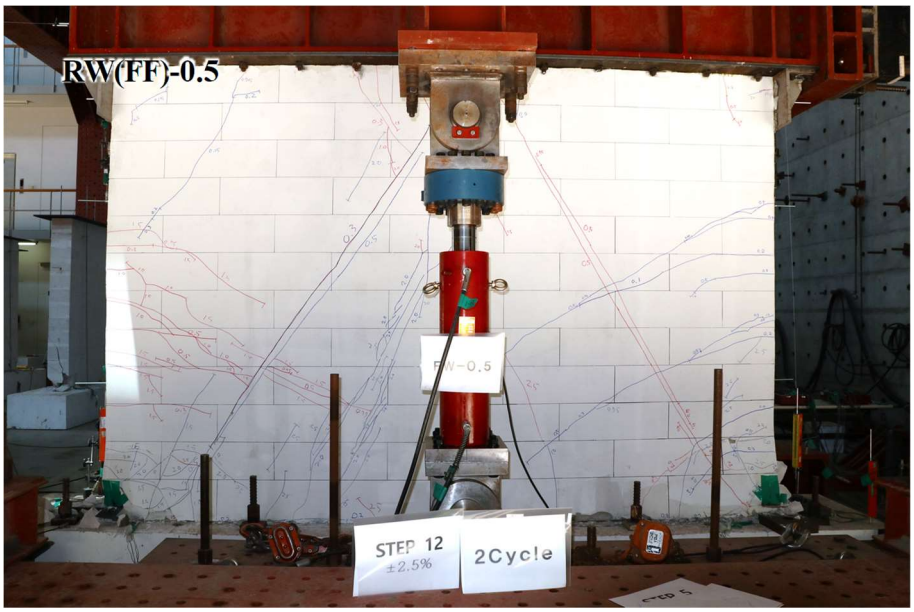

(b) RW(FF)-0.5

Figure 5-22 Failure modes of 3,4 specimens at the end of test

5.4.2.3 Strains of reinforcing bars

To check the deformation of the reinforcing bars located at sides of the wall, the strain was measured as shown in Fig. 5-23. The horizontal axis of the graph is the lateral displacement ratio, and the vertical axis is the strain (mm / mm) of the Re-bars. The yield strain of reinforcing bars is indicated by the dotted line (= 0.0023).

The strain of the Re-bar showed higher strain than the yield strain at around drift ratio 0.3 % in the both specimens. Therefore, the maximum strength of two specimens can be estimated as the flexural strength of the wall. To evaluate the shear strength of the ALC wall, shear fracture should be induced by increasing the amount of end reinforcement.

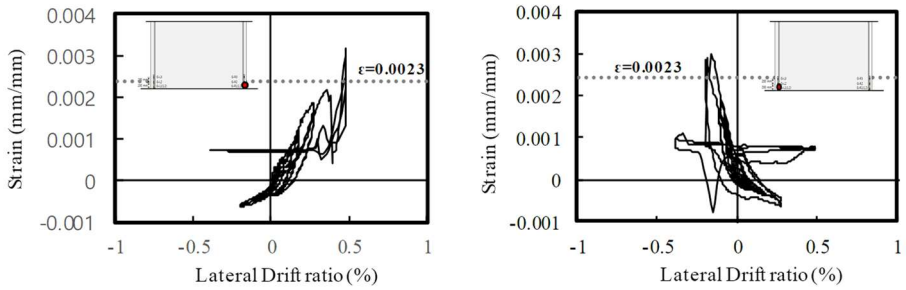

(a) RW(FU)-0.5

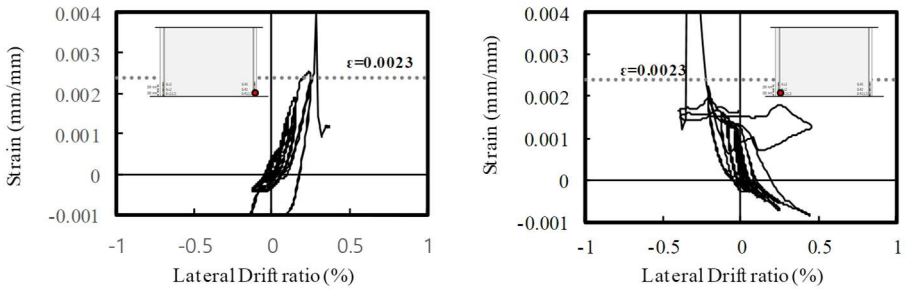

(b) RW(FF)-0.5

Figure 5-23 Measured strains in 3,4 specimens

5.4.2.4 Deformation Contribution

The sum of shear deformation, the rocking deformation, the flexural deformation, and the slding deformation in the wall were compared with the lateral displacement measured at the top of the wall. In Fig. 5-24, the solid line represents the sum of the shear deformation, rocking deformation, flexural deformation, and local deformation, and the dotted line represents the total lateral deformation measured at the top of the wall deformation.

The local deformation and the total deformation were almost identical, and it can be confirmed that no deformation other than the measured deformation had occurred.

As shown in Fig. 5-25, the ratio of rocking deformation was largest in total deformation. This was because the vertical reinforcement deformed more than the yield strain and then the rocking deformation between the wall and the base increased.

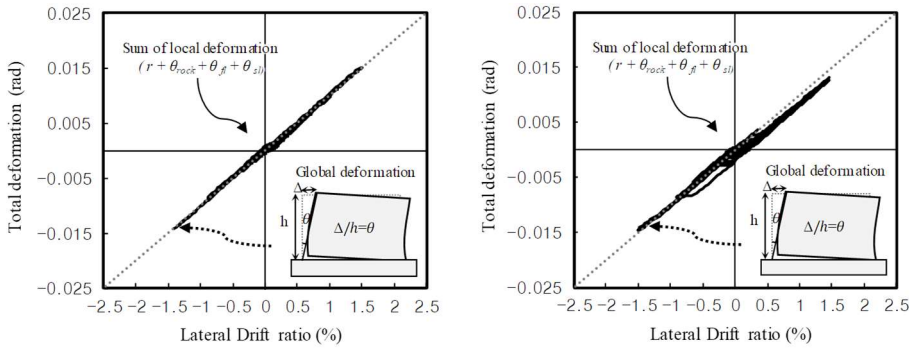

Figure 5-24 Comparison of sum of the local deformation and the total deformation (3,4 specimen)

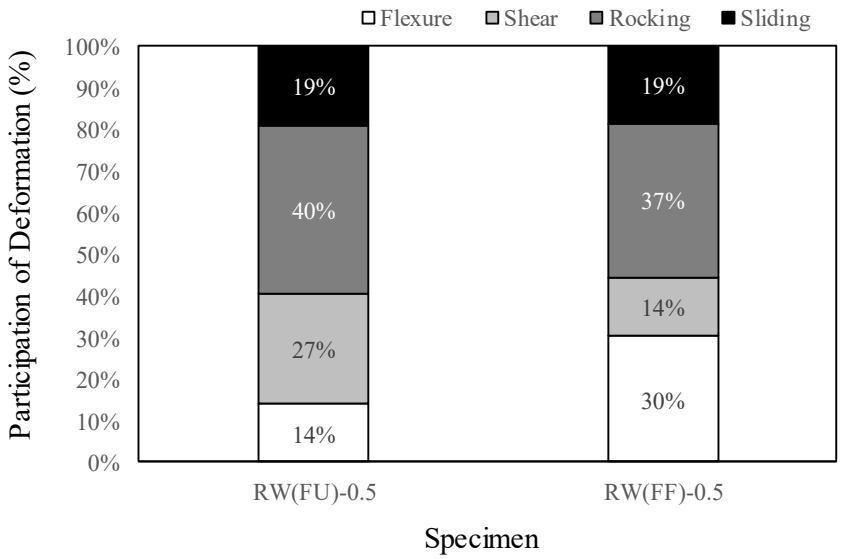

Figure 5-25 Deformation contribution of 3, 4 specimens at the maximum drift ratio

5.4.2.5 Energy dissipation

Figure 5-26 shows the envelop curves of RW(FU)-0.5 and RW(FU)-0.5. The envelop curve is the curve connecting the maximum load at the each drift ratio. The horizontal axis represents the displacement ratio and the vertical axis represents the load. RW(FF)-0.5 and RW(FU)-0.5 showed a similar shape of envelope curve, but the maximum drift ratio of RW(FF)-0.5 was 0.5% higher than that of RW(FU)-0.5.

To estimate the energy dissipation capacity of RW(FU)-0.5 and RW(FU)-0.5, the energy dissipation capacity with each drift was compared as shown in Fig. 5-27. The horizontal axis of the graph represents the drift ratio, and the vertical axis represents the accumulated energy dissipation. The energy dissipation capacity of RW(FF)-0.5 was higher than that of RW(FU)-0.5 at all drift ratios. The energy dissipation capacity of RW(FF)-0.5 at final drift ratio was 121.3 kNm, and it was 1.73 times that of RW(FU)-0.5. Therefore, reinforcement of fiberglass on the sides of wall increased the strength and ductility of the wall, which was effective for the lateral force.

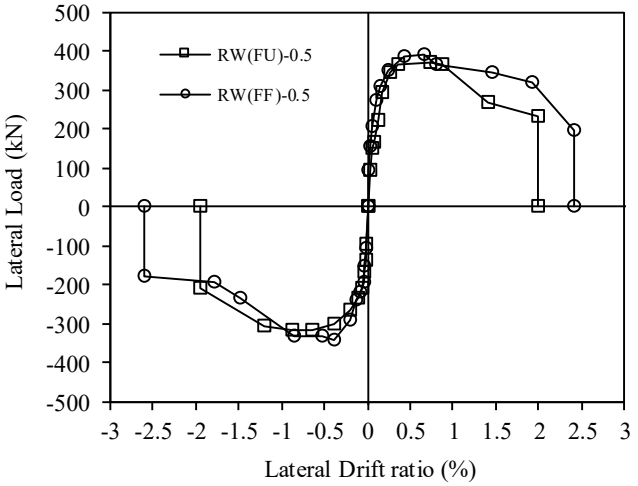

Figure 5-26 Envelope curves of 3, 4 specimens

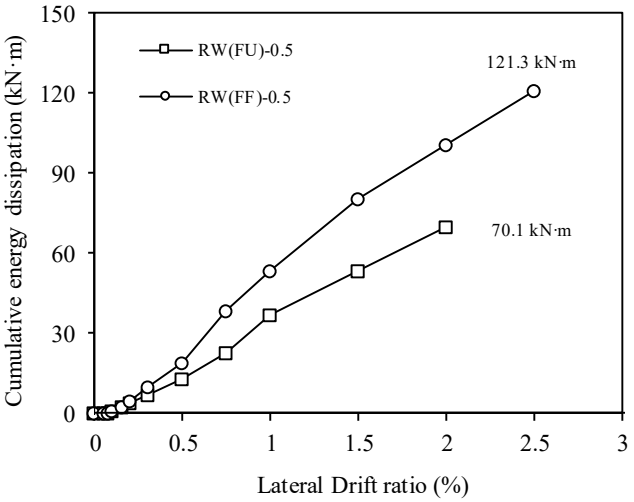

Figure 5-27 Cumulative energy dissipation of 3, 4specimens

5.4.2.6 Comparison of flexural strength prediction.

The P-M curve of the specimen is shown in Fig. 5-28 to compare the predicted flexural strength and test results. The horizontal axis of the graph represents the moment capacity, and the vertical axis represents the axial force. In the calculation, the maximum compressive strain of the ALC block was 0.003, the height of the compressive stress block was 0.85 f_{ALC}, and width of the compressive stress block was calculated as $\beta_1 c$. The moment capacity of the two specimens with an axial force of 370kN was 902kN·m. And the flexural strength was 376kN which was obtained by dividing moment capacity by wall height (2400mm).

The maximum strengths of RW(FU) -0.5 and RW(FF)-0.5 were 372 kN and 393 kN, respectively, which were similar to the predicted flexural strength (V_m=376 kN). Therefore, the flexural strength of the ALC wall could be predicted by using conventional flexural theory.

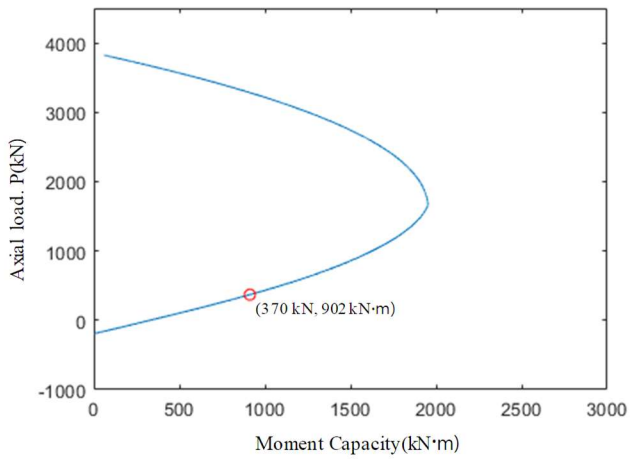

Figure 5-28 P-M curve (3,4 specimens)

5.4.3 Shear wall (C) with a opening

To verify the effect of vertical reinforcement and glass-fiber reinforcement on the wall, the wall specimens with openings were divided into three types as shown in Fig. 5-29. ROW(FU)-0.5 was the specimen reinforced with vertical reinforcement at the sides of the opening, and UOW(FU)-0.5 was the specimen without vertical reinforcement at the sides of the opening. UOW(FF)-0.5 was a wall reinforced with on the sides of wall instead of vertical reinforcements.

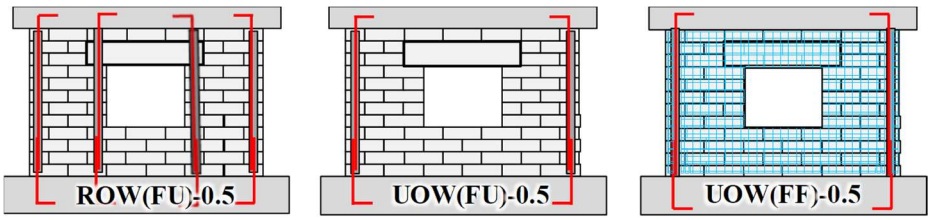

Figure 5-29 Shear wall 5,6,7 specimens with a opening

5.4.3.1 Lateral Load-Displacement Relationship

Fig. 5-30 (a) ~ (c) showed the relationships of lateral load and displacement in ROW(FU)-0.5, UOW(FU)-0.5 and UOW(FF)-0.5. The horizontal axis is the ratio of lateral displacement, which is obtained by dividing the lateral displacement (Δ) to the wall height (H= 2400 mm). The vertical axis represents the lateral load, which represents the actuator load at the displacement ratio. The maximum load in both positive and negative directions is indicated by a yellow circle. The predicted strengths are shown together to compare with the test results. The flexural crack strength (V_f) is indicated by a short dashed line, the sliding strength (V_{sl}) with a friction coefficient of 0.6 is indicated by a

dashed line and the shear strength (V_{sh}) is indicated by a long-dashed line and the nominal flexural strength (V_m) is indicated by a solid line. The flexural strength is a value obtained by dividing the nominal moment strength (M_n) by the height (H) of the wall. The maximum load and maximum displacement ratio per cycle are shown in Table 5-9 ~ 11.

The relationship of load and displacement in ROW(FU)-0.5 is shown in Fig. 5-30 (a). The load increased linearly up to the drift ratio 0.3% and reached the maximum load at the drift ratio 0.5%. The maximum load was 247.5kN in the positive direction and 219.6kN in the negative direction and showed 79% and 70% of the shear strength (V_{sh} = 311kN), respectively. After the drift ratio 0.5, the load decreased sharply in the positive direction and the load gradually decreased in the negative direction. At the final drift ratio 1.0%, it decreased to 56.2% of maximum load in positive direction.

The relationship of load and displacement in UOW(FU)-0.5 is shown in Fig. 5-30 (b). The load increased linearly up to the drift ratio 0.3% and reached the maximum load at the drift ratio 1.0% in positive drection and at drift ration 0.5 % in negative drection. The maximum load was 231.8kN in the positive direction and 223.8kN in the negative direction and showed 75% and 72% of the shear strength (V_{sh} = 311kN), respectively. After reacing the maximum load, the load decreased sharply. At the final drift ratio 1.5%, it decreased to 72.2% of maximum load in positive direction and 38.7% maximum load in negative direction.

The relationship of load and displacement in UOW(FF)-0.5 is shown in Fig. 5-30 (c). The load increased linearly up to the drift ratio 0.3% and reached the

maximum load at the drift ratio 0.75 %. The maximum load was 336.2 kN in the positive direction and 322.5kN in the negative direction and showed 108% and 104% of the shear strength (V_{sh} = 311kN), respectively. After reacing the maximum load, the load was kept constant until drift ratio 1.0%. At the final drift ratio 2.0%, load decreased to 69% (232.2 kN) of maximum load in positive direction and 40%(128.7 kN) maximum load in negative direction.

The initial stiffness of the ROW(FU)-0.5 specimens reinforced with vertical reinforcements at the side of opening was higher than UOW(FU) -0.5, but the strength was not different. Rather, UOW(FU)-0.5 without vertical reinforcement at the sides of opening showed a higher ductility capacity. Comparing the load-displacement relationships between ROW(FU)-0.5 and UOW(FU)-0.5, there was no difference in performance with vertical reinforcements at the side of opening.

UOW(FF)-0.5 reinforced with glass-fiber reinforced on the sides of wall instead of vertical reinforcement around the opening showed higher strength and ductility than ROW(FU)-0.5 and UOW(FU)-0.5. Therefore, reinforcing the sides of the wall with glass-fiber was more effective in strength and ductility than vertical reinforcement at the sides of opening.

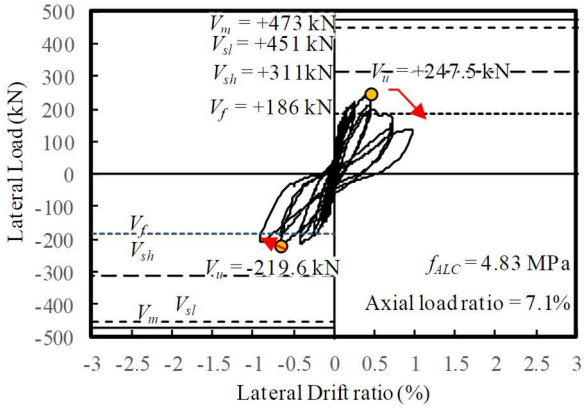

(a) ROW(FU)-0.5

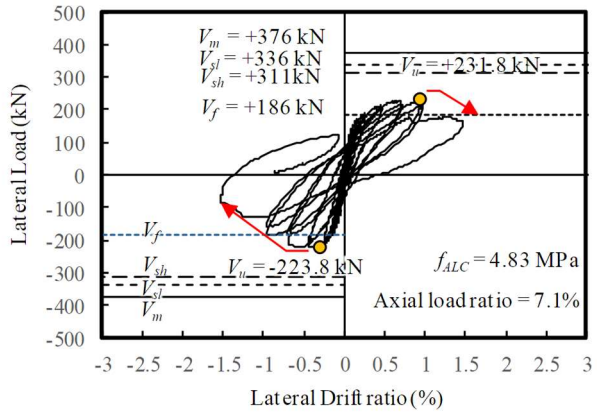

(b) UOW(FU)-0.5

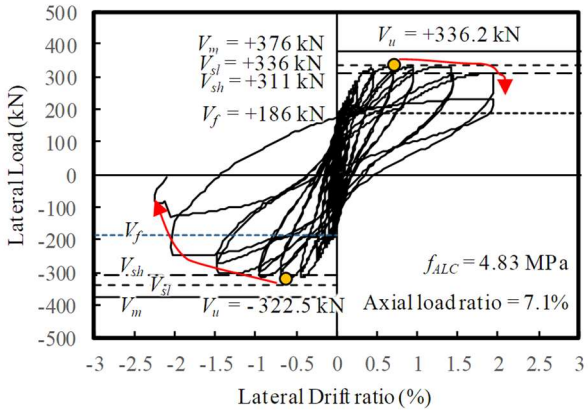

(c) UOW(FF)-0.5

Figure 5-30 Lateral Load-Displacement Relationship of the 5,6,7 specimens

Table 5-9 Maximum load and drift ratio at each cycle of ROW(FU)-0.5

Drift ratio	Cycle	Maximum load (kN)	Maximum Drift ratio (%)	Cycle	Maximum load (kN)	Maximum Drift ratio (%)
0.05 %	1a	63.10	0.02	1b	-70.44	-0.02
	2a	69.88	0.02	2b	-71.40	-0.02
0.075%	3a	108.44	0.04	3b	-104.92	-0.04
	4a	110.46	0.04	4b	-102.60	-0.04
0.1%	5a	145.40	0.06	5b	-128.36	-0.06
	6a	146.74	0.06	6b	-126.14	-0.06
0.15%	7a	167.58	0.11	7b	-145.60	-0.10
	8a	167.28	0.11	8b	-136.26	-0.10
0.2%	9a	201.50	0.16	9b	-159.74	-0.15
	10a	193.90	0.16	10b	-152.30	-0.15
0.3%	11a	221.40	0.26	11b	-192.02	-0.24
	12a	212.04	0.26	12b	-175.00	-0.24
0.5%	13a	247.48	0.45	13b	-212.96	-0.42
	14a	216.08	0.46	14b	-198.44	-0.42
0.75%	15a	176.68	0.71	15b	-219.58	-0.66
	16a	141.06	0.72	16b	-191.88	-0.66
1%	17a	139.02	0.98	17b	-208.02	-0.89

Table 5-10 Maximum load and drift ratio at each cycle of UOW(FF)-0.5

Drift ratio	Cycle	Maximum load (kN)	Maximum Drift ratio (%)	Cycle	Maximum load (kN)	Maximum Drift ratio (%)
0.05 %	1a	59.50	0.02	1b	-72.26	-0.02
	2a	63.82	0.02	2b	-70.48	-0.02
0.075%	3a	93.24	0.04	3b	-99.00	-0.04
	4a	95.32	0.04	4b	-97.22	-0.04
0.1%	5a	118.80	0.06	5b	-122.18	-0.06
	6a	122.92	0.07	6b	-120.60	-0.06
0.15%	7a	152.94	0.11	7b	-158.44	-0.10
	8a	148.00	0.11	8b	-152.98	-0.10
0.2%	9a	172.94	0.16	9b	-183.40	-0.14
	10a	159.90	0.16	10b	-177.30	-0.14
0.3%	11a	188.26	0.26	11b	-210.64	-0.24
	12a	184.88	0.26	12b	-201.24	-0.24
0.5%	13a	214.46	0.46	13b	-223.82	-0.30
	14a	209.50	0.46	14b	-212.84	-0.44
0.75%	15a	229.42	0.71	15b	-223.06	-0.52
	16a	217.28	0.71	16b	-184.70	-0.70
1%	17a	231.82	0.96	17b	-184.32	-0.96
	18a	213.02	0.96	18b	-157.78	-0.97
1.5%	19a	167.32	1.47	19b	-87.04	-1.52

Table 5-11 Maximum load and drift ratio at each cycle of UOW(FF)-0.5

Drift ratio	Cycle	Maximum load (kN)	Maximum Drift ratio (%)	Cycle	Maximum load (kN)	Maximum Drift ratio (%)
0.05 %	1a	81.84	0.01	1b	-97.44	-0.02
	2a	86.44	0.01	2b	-99.32	-0.02
0.075%	3a	131.12	0.03	3b	-139.70	-0.04
	4a	134.80	0.03	4b	-135.86	-0.04
0.1%	5a	169.52	0.05	5b	-171.90	-0.05
	6a	175.92	0.05	6b	-165.90	-0.05
0.15%	7a	216.40	0.09	7b	-208.06	-0.09
	8a	214.94	0.10	8b	-200.02	-0.09
0.2%	9a	238.40	0.14	9b	-222.74	-0.13
	10a	237.42	0.15	10b	-219.06	-0.14
0.3%	11a	286.08	0.24	11b	-266.04	-0.24
	12a	275.26	0.24	12b	-252.36	-0.24
0.5%	13a	326.82	0.44	13b	-316.08	-0.43
	14a	307.18	0.44	14b	-296.84	-0.43
0.75%	15a	336.24	0.69	15b	-322.54	-0.63
	16a	318.04	0.69	16b	-298.32	-0.69
1%	17a	332.76	0.93	17b	-317.82	-0.94
	18a	320.40	0.94	18b	-298.68	-0.95
1.5%	19a	331.30	1.42	19b	-300.44	-1.46
	20a	305.00	1.43	20b	-272.36	-1.47
2.0%	21a	232.20	1.93	21b	-245.72	-2.03
	22a	232.20	1.63	22b	-128.68	-2.04

5.4.3.2 Failure Modes

The failure mode of the specimens are shown in Fig. 5-31(a)~(c). In ROW(FU)-0.5 and UOW(FU)-0.5, shear cracks occurred on the right and left sides of the wall excluding the upper and lower parts of the opening. Thus, the two walls divided around the opening resisted lateral load. In Fig. 5-31(c), shear cracks occurred at the upper and lower part of the opening of UOW(FF)-0.5. This was because the glass-fiber integrated the wall with the opening, and the wall was entirely resistant to the lateral load.

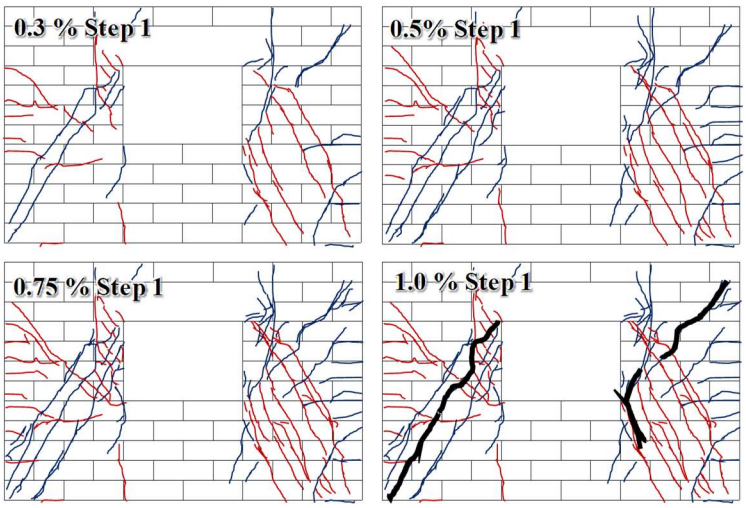

(a) ROW(FU)-0.5

Figure 5-31 Crack propagation of 5,6,7 specimens

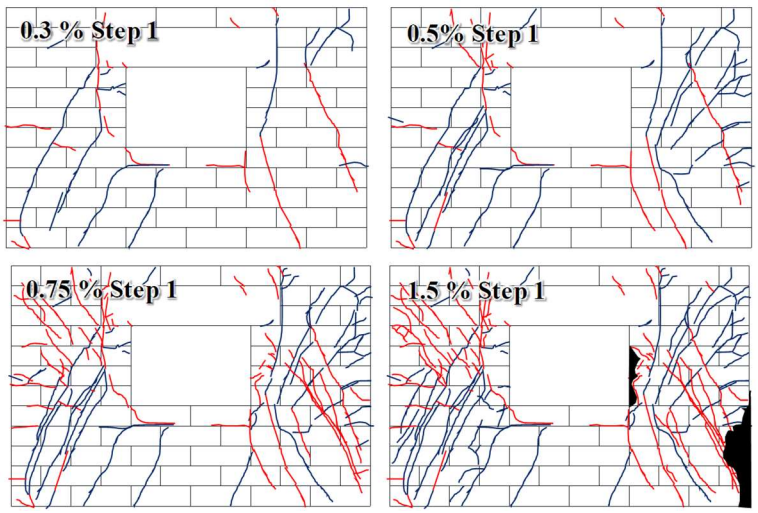

(b) UOW(FU)-0.5

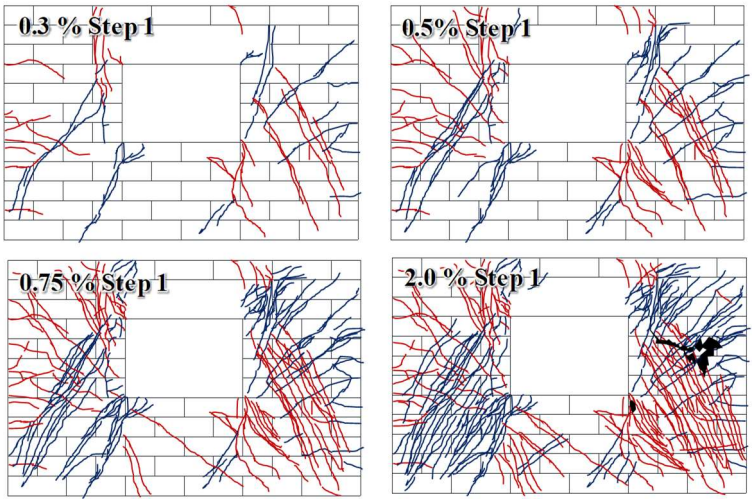

(c) UOW(FF)-0.5

Figure 5-31 Crack propagation of 5,6,7 specimens

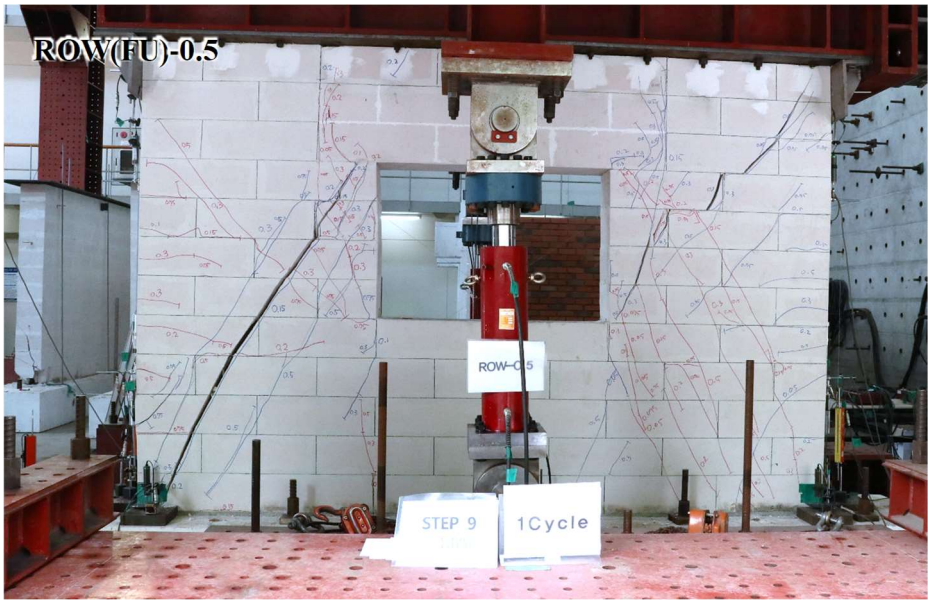

(a) ROW(FU)-0.5

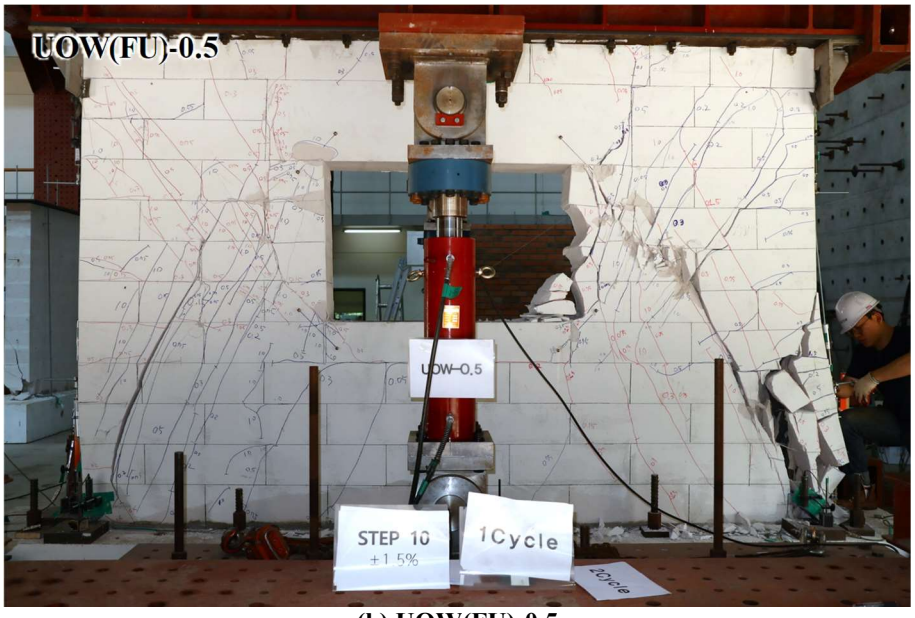

(b) UOW(FU)-0.5

Figure 5-32 Failure modes of 5,6,7 specimens at the end of test

(c) UOW(FF)-0.5

Figure 5-32 Failure modes of 5,6,7 specimens at the end of test

5.4.3.3 Strains of reinforcing bars

To check the deformation of the Re-bar located at sides of the wall, the strain of the reinforcing bar was measured as shown in Fig. 5-33. The horizontal axis of the graph is the lateral displacement ratio, and the vertical axis is the strain (mm / mm) of the Re-bar. The yield strain of reinforcing bars is indicated by the dotted line (= 0.0023).

In the ROW(FU)-0.5 specimens (Fig. 5-33(a)), the Re-bars at the left column reached the yield strain at the drift ratio 0.3% in negative direction, but Re-bar

at the right column exhibited lower deformation than the yield strain. This was because the shear crack concentrated at the lower right of the wall from drift ratio 0.3% to drift ratio 0.5% caused more deformation of the Re-bar at the left of wall. The strain of the vertical reinforcing bars near the opening showed a negative value in the total displacement ratio, which means that the vertical reinforcing bars were being compressed.

In the UOW(FU)-0.5 specimens (Fig. 5-33(b)), the Re-bars at the right column reached the yield strain at the drift ratio 0.3% in positive direction, but the left column exhibited lower deformation than the yield strain. This was because the shear cracks concentrated at the left conner between drift ratio 0.3% and 0.5%, which caused more deformation of the reinforcing bar in column on the right side.

In the UOW(FF)-0.5 specimens (Fig. 5-33(c)), The strain of the Re-bar reached the yield strain around drift ratio 0.3%, and the load was kept constant in the range of 0.5% ~ 1.0% of the drift ratio. This was because the Re-bar of UOW(FF)-0.5 specimen yielded and the flexural strength was kept constant. Therefore, unlike the other two specimens, UOW(FF) -0.5 exhibited flexural strength.

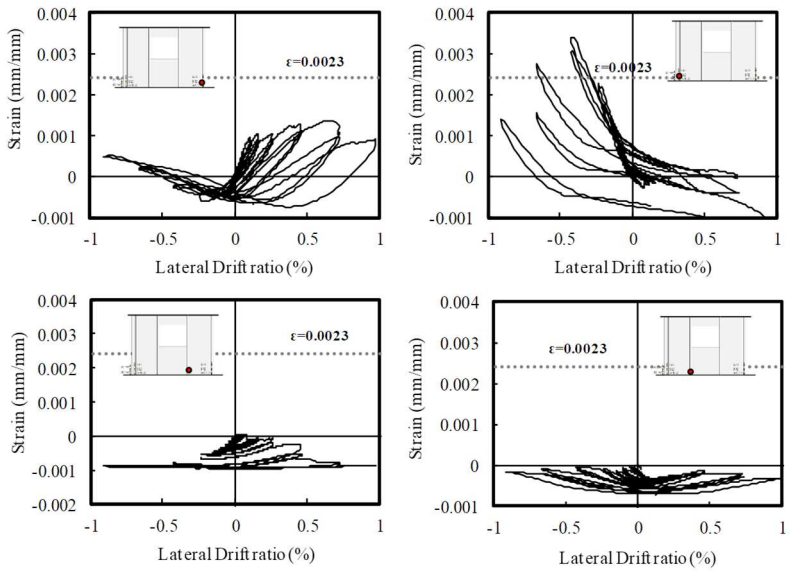

(a) ROW(FU)-0.5

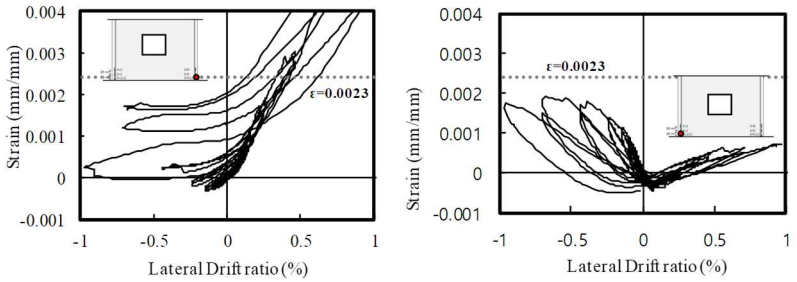

(b) UOW(FU)-0.5

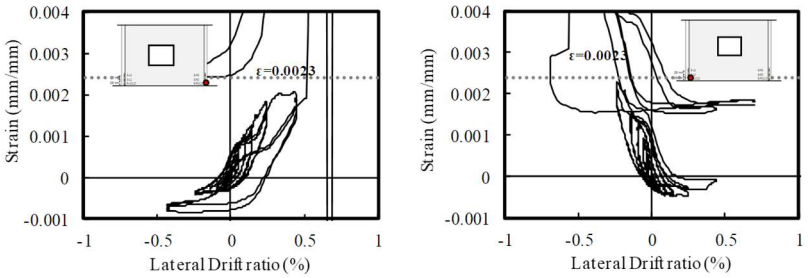

(c) UOW(FF)-0.5

Figure 5-33 Measured strains in 5,6,7 specimens

5.4.3.4 Deformation Contribution

The sum of shear deformation, the rocking deformation, the flexural deformation, and the slding deformation in the wall were compared with the lateral displacement measured at the top of the wall. In Fig. 5-34, the solid line represents the sum of the shear deformation, rocking deformation, flexural deformation, and local deformation, and the dotted line represents the total lateral deformation measured at the top of the wall deformation.

The local deformation and the total deformation were almost identical, and it could be confirmed that no deformation other than the measured deformation had occurred. In ROW(FU)-0.5 and UOW(FU)-0.5, the sum of the local deformation was slightly larger than the total deformation. The reason for this was that the shear deformation of the whole wall was measured instead of the shear deformation of each part.

As shown in Fig. 5-35, the ratio of the local deformation to the maximum deformation ratio of each specimen was confirmed, and the shear deformations were the largest. This was because the shear strength was lower than the fexural strength and shear failure occured.

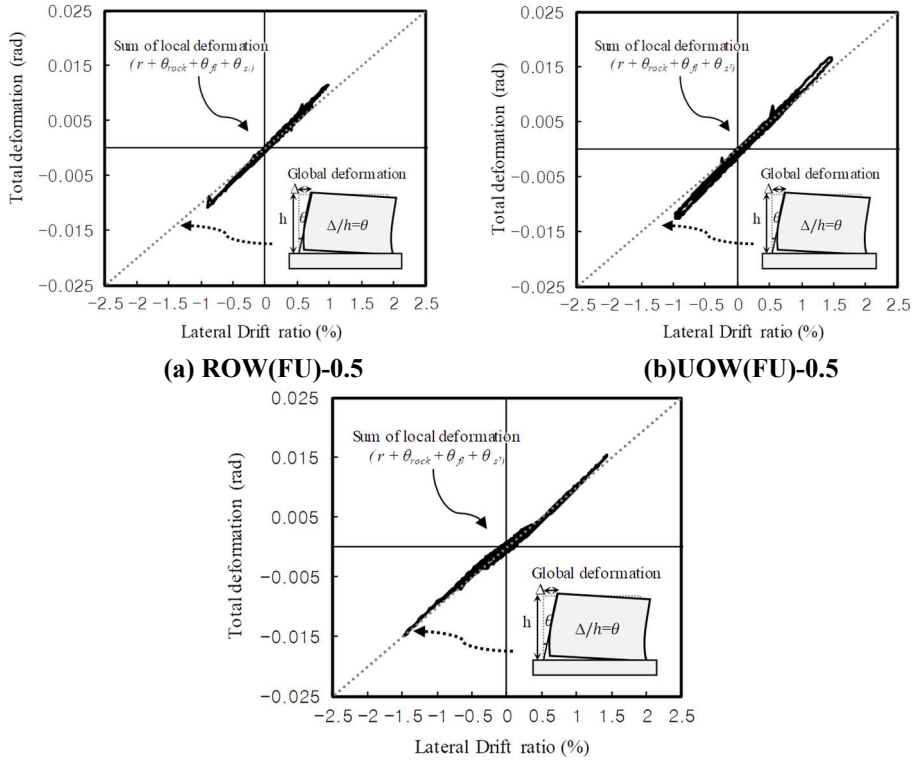

(a) ROW(FU)-0.5 **(b)UOW(FU)-0.5**

(c) UOW(FF)-0.5

Figure 5-34 Comparison of sum of the local and the total deformation

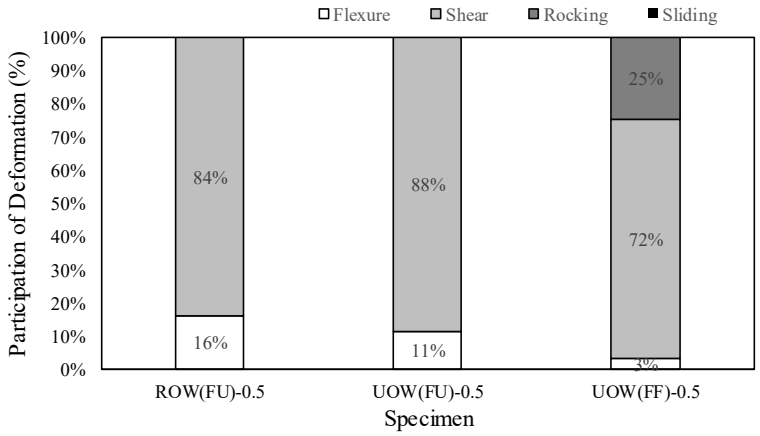

Figure 5-35 Deformation contribution of 5,6,7 specimen at the maximum drift ratio

5.4.3.5 Energy dissipation

Fig. 5-36 showed the envelop curves of ROW(FU)-0.5, UOW(FU)-0.5 and UOW(FF) -0.5. The envelop curve is the curve connecting the maximum load at each drift ratio. The horizontal axis represents the displacement ratio and the vertical axis represents the load. UOW(FU)-0.5 showed the highest maximum load and deformation capacity. ROW(FU) -0.5 and UOW (FU) -0.5 showed similar maximum load, but the maximum drift ratio of UOW(FU) was 0.5% higher than ROW(FU)-0.5. UOW(FF)-0.5 showed the highest performance in strength and ductility.

To estimate the energy dissipation capacity of each specimen, the energy dissipation capacity with each drift was compared as shown in Fig. 5-37. The horizontal axis of the graph represents the drift ratio, and the vertical axis represents the accumulated energy dissipation. The energy dissipation capacity of UOW(FF)-0.5 was 88.3 kNm, which was the highest among the three specimens. The energy dissipation capacities of ROW(FU)-0.5 and UOW(FU) -0.5 were 16.3kNm and 26.9kNm respectively. Therefore, glass-fiber reinforced on the sides of wall was most effective for the performance of the opening wall in the energy dissipation capacity.

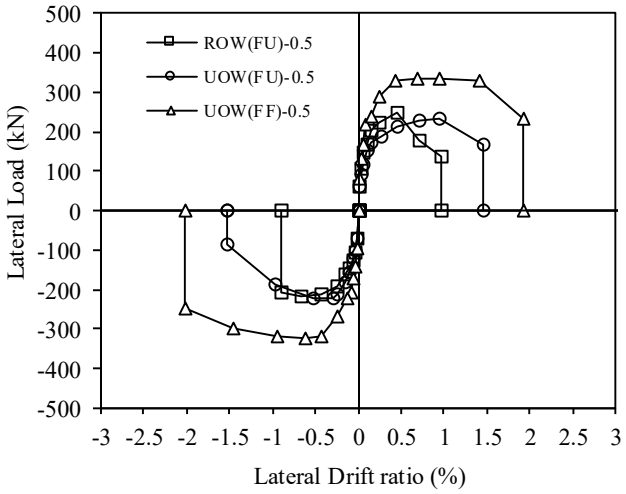

Figure 5-36 Envelope curves of 5,6,7 specimens

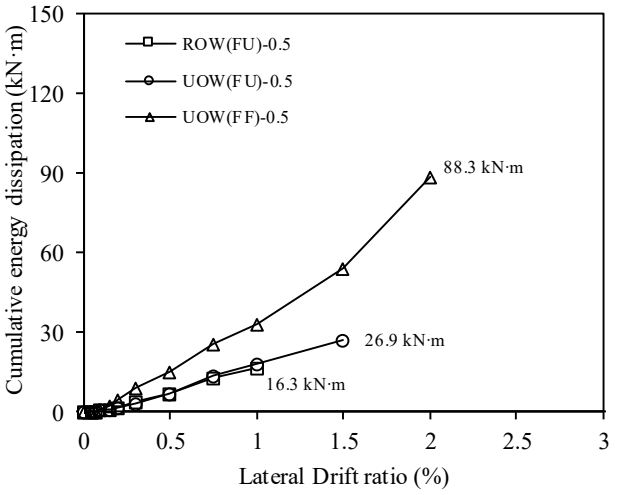

Figure 5-37 Cumulative energy dissipation of 5,6,7 specimens

5.4.3.6 Comparison of Shear strength prediction

Considering the failure modes and the local deformation, the walls with opening were destroyed by shear. And since the ratio of shear deformation is large, it can be confirmed that the relation between load and shear distortion was similar to the load-displacement relation as shown in Fig. 5-38.

Therefore, the strength of each specimen was compared with the expected shear strength of the wall. The predicted shear strength is predicted by multiplying the leading coefficient to Eq. 2-1 in Chapter 2. In ACI 523.4R, the leading factor is 0.59 or 0.38. The leading coefficient of 0.59 is applied to fully mortared walls constructed with mortar at vertical and bed-joints, and the leading coefficient of 0.38 applies to walls constructed with mortar only at bed-joints. Because all specimens were fully mortared, so that the predicted shear strength was evaluated by Eq. 5-1. In Section 3, the splitting tensile strength of the block was shown in Eq. 3-6 with the compressive strength of the block. Therefore, Eq.5-1 can be expressed by Eq.5-2 wih compressive strength of the block.

$$V_{sh} = 0.39 L t f_t \sqrt{1 + \frac{P}{f_t L t}} \tag{5-1}$$

$$V_{sh} = 0.78 L t \sqrt{f_{ALC}} \sqrt{1 + \frac{P}{0.2\sqrt{f_{ALC}} L t}} \tag{5-2}$$

The predicted shear strength and test results for the specimens are compared as shown in Table 5-12. The shear strengths of ROW(FU)-0.5 and UOW(FU)-0.5 were 28% and 24% higher than expected strength, respectively. This

indicates that the glass-fiber reinforcement at the bed-joint is effective in increasing the shear strength. Test results of UOW(FF) -0.5 showed 79% higher strength than predicted shear strength and showed that shear strength is most effective when glass-fiber is reinforced simultaneously on sides of wall and at bed-joints.

Table 5-12 Comparison of Test results and Shear strength prediction

Specimen	Shear strength V_{sh}(kN)	Test results			V_{test}/V_{sh}
		V_{posi} (kN)	V_{nega} (kN)	V_{test} (kN)	
ROW(FU)-0.5	183	247.5	219.6	233.55	1.28
UOW(FU)-0.5	183	231.8	223.8	227.8	1.24
UOW(FF)-0.5	183	336.2	322.5	329.35	1.79

1) V_{posi}, V_{nega}, and V_{test} = the Maxmum load in positive direction, the Maxmum load in negative direction, and average load (V_{posi} and V_{nega}), respectively.

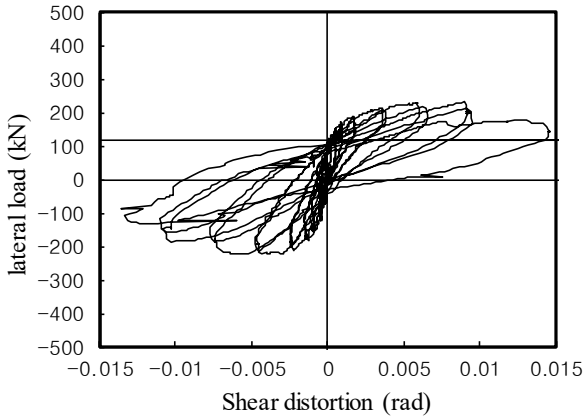

(a) ROW(FU)-0.5

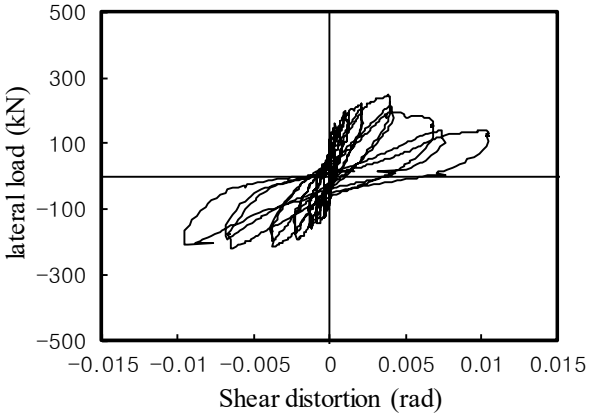

(b) UOW(FU)-0.5

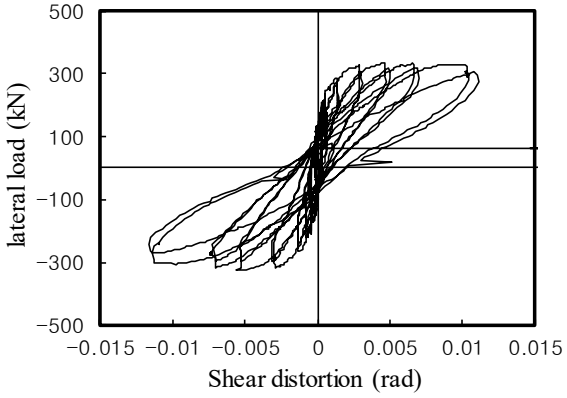

(c) UOW(FF)-0.5

Figure 5-38 Relationships of Lateral Load-Shear distortion

5.4.4 Shear wall (D) reinforced with 2-D 16 Re-bar

The walls with 2-D16 reinforcing bar at the sides of wall were tested to verify shear strength of ALC wall with different the glass-fiber method. To increase the flexural strength of the wall, 2-D16 Re-bars were reinforced at the sides of wall. Each specimen was classified as follows.

(1) $R_2W(UU)$-0.5: a specimen without reinforcement of glass-fiber

(2) $R_2W(FU)$-0.5: a spcimen reinforced with glass-fiber at the bed-joint

(3) $R_2W(UF)$-0.5: a spcimen reinforced with glass-fiber on the sides of wall

(4) $R_2W(FF)$-0.5: a spcimen reinforced with glass-fiber at the bed-jont and on the sides of wall

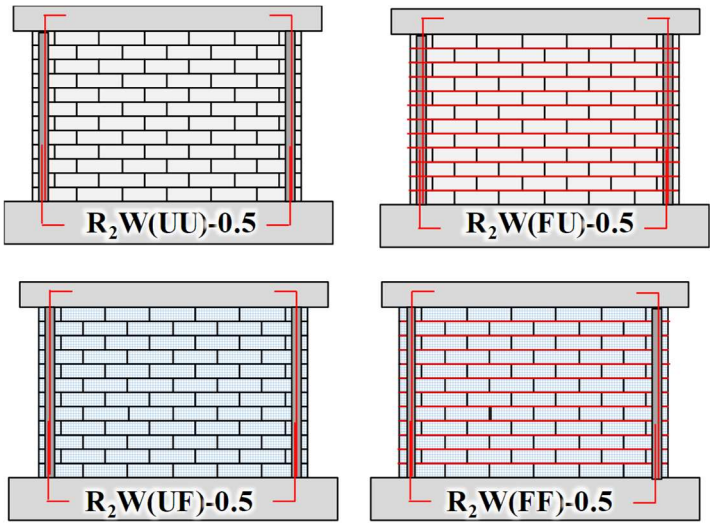

Figure 5-39 Shear wall 8,9,10,11 specimens with 2-D 16 Re-bar

5.4.4.1 Lateral Load-Displacement Relationship

Fig. 5-40 (a) ~ (d) showed relationships of the lateral load and displacement relationships in each specimen. The horizontal axis is the ratio of lateral displacement, which was obtained by dividing the lateral displacement (Δ) to the wall height (H= 2400 mm). The vertical axis represents the lateral load, which represents the actuator load at the displacement ratio. The maximum load in both positive and negative directions is indicated by a yellow circle. The predicted strengths are shown together to compare with the test results. The flexural crack strength (V_f) is indicated by a short dashed line, the sliding strength (V_{sl}) with a friction coefficient of 0.6 is indicated by a dashed line and the shear strength (V_{sh}) is indicated by a long-dashed line and the nominal flexural strength (V_m) is indicated by the solid line. The flexural strength is a value obtained by dividing the nominal moment strength (M_n) when the Re-bar reaches yielding in the section analysis of the wall by the height (H) of the wall. The maximum load and maximum displacement ratio per cycle are shown in Table 5-13~ 16.

The relationship of load and displacement in R_2W(UU)-0.5 is shown in Fig. 5-40(a). The maximum load was 218 kN in posotive direction and 217 kN in the negative direction. The maximum loads in each direction were 52 % and 52 % of the shear strength, respectively.

The relationship of load and displacement in R_2W(FU)-0.5 is shown in Fig. 5-40(b). The maximum load was 170 kN in posotive direction and 214 kN in the negative direction. The maximum loads in each direction were 41 % and 51 % of the shear strength, respectively. There was no increase in load with

glass-fiber reinforcede at the bed-joint.

The relationship of load and displacement in R_2W(UF)-0.5 is shown in Fig. 5-40 (c). The maximum load was 317 kN in posotive direction and 271 kN in the negative direction. The maximum loads in each direction were 76 % and 65 % of the shear strength, respectively. Glass-fiber reinforced on the sides of wall was effective in increasing load and ductility.

The relationship of load and displacement in R_2W(FF)-0.5 is shown in Fig. 5-40 (d). The maximum load was 333 kN in posotive direction and 293 kN in the negative direction. The maximum loads in each direction were 79 % and 70 % of the shear strength, respectively. Glass-fiber reinforced on the sides of wall and bed-joints had the highest effect on load and ductility.

The strengths of the specimens reinforced with 2-D16 ends were lower than those of the specimens reinforced with 1-D16 at the ends. The strength of mortar used in the specimens with 2-D16 was lower than the required strength and that influenced the strength of the specimen. The reason of low strength of specimens also could be confirmed through failure mode.

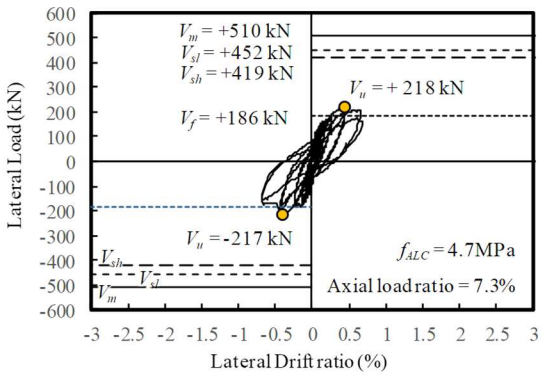

(a) R_2W(UU)-0.5

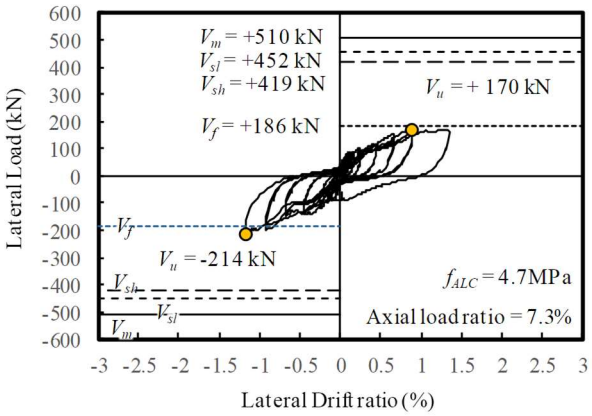

(b) R₂W(FU)-0.5

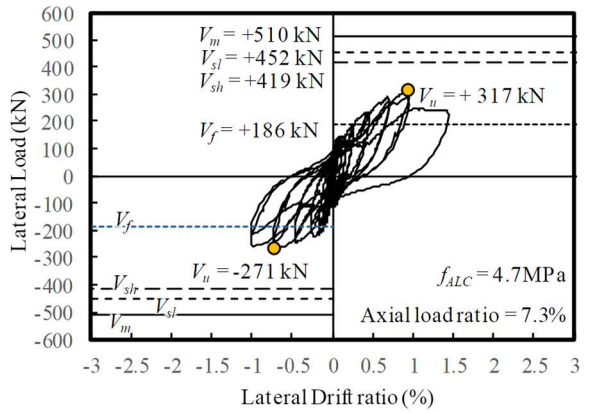

(c) R₂W(UF)-0.5

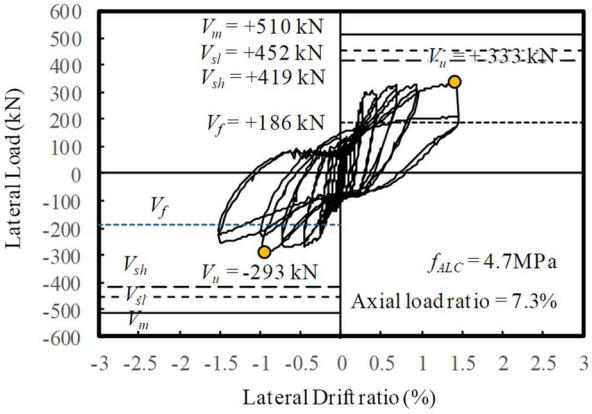

(d) R₂W(FF)-0.5

Figure 5-40 Lateral Load-Displacement Relationship of 8,9,10,11 specimens

Table 5-13 Maximum load and drift ratio at each cycle of $R_2W(UU)$-0.5

Drift ratio	Cycle	Maximum load (kN)	Maximum Drift ratio (%)	Cycle	Maximum load (kN)	Maximum Drift ratio (%)
0.05 %	1a	88.65	0.033	1b	-97.17	-0.005
	2a	92.09	0.038	2b	-95.27	-0.006
0.075%	3a	118.26	0.056	3b	-125.97	-0.025
	4a	118.62	0.056	4b	-122.99	-0.028
0.1%	5a	126	0.086	5b	-133.43	-0.051
	6a	132.04	0.086	6b	-128.24	-0.051
0.15%	7a	150.18	0.133	7b	-158.5	-0.098
	8a	154.99	0.133	8b	-149.34	-0.101
0.2%	9a	160.12	0.174	9b	-179.02	-0.147
	10a	154.43	0.180	10b	-174.3	-0.148
0.3%	11a	184.73	0.278	11b	-186.16	-0.161
	12a	184.08	0.274	12b	-174.84	-0.250
0.5%	13a	218.15	0.468	13b	-217.03	-0.428
	14a	196.58	0.473	14b	-203.81	-0.456
0.75%	15a	205.95	0.690	15b	-173.5	-0.722
	16a	174.23	0.657	16b	-155.12	-0.716

Table 5-14 Maximum load and drift ratio at each cycle of R_2W(FU)-0.5

Drift ratio	Cycle	Maximum load (kN)	Maximum Drift ratio (%)	Cycle	Maximum load (kN)	Maximum Drift ratio (%)
0.05 %	1a	53.36	0.025	1b	-56.2	-0.022
	2a	54.58	0.027	2b	-53.73	-0.023
0.075%	3a	66.76	0.046	3b	-69.74	-0.041
	4a	64.78	0.046	4b	-65.5	-0.041
0.1%	5a	74.51	0.065	5b	-81.39	-0.065
	6a	73.16	0.065	6b	-79.43	-0.065
0.15%	7a	87.46	0.109	7b	-86.38	-0.096
	8a	77.87	0.112	8b	-78.4	-0.112
0.2%	9a	88.6	0.158	9b	-96.36	-0.155
	10a	81.79	0.158	10b	-87.92	-0.158
0.3%	11a	104.71	0.238	11b	-118.88	-0.247
	12a	94.76	0.246	12b	-109.55	-0.249
0.5%	13a	110.76	0.426	13b	-140.96	-0.428
	14a	117.6	0.424	14b	-133.34	-0.434
0.75%	15a	154.06	0.654	15b	-151.47	-0.671
	16a	141.62	0.652	16b	-144.31	-0.677
1%	17a	170.14	0.879	17b	-198.92	-0.915
	18a	159.14	0.891	18b	-177.28	-0.919
1.5%	19a	165.67	1.332	19b	-213.91	-1.177

Table 5-15 Maximum load and drift ratio at each cycle of R_2W(UF)-0.5

Drift ratio	Cycle	Maximum load (kN)	Maximum Drift ratio (%)	Cycle	Maximum load (kN)	Maximum Drift ratio (%)
0.05 %	1a	96.57	0.018	1b	-103.44	-0.023
	2a	100.38	0.018	2b	-99.86	-0.026
0.075%	3a	130.82	0.040	3b	-141.9	-0.046
	4a	131.51	0.043	4b	-137.52	-0.048
0.1%	5a	139.16	0.058	5b	-161.08	-0.067
	6a	135.46	0.063	6b	-154.87	-0.068
0.15%	7a	144.87	0.092	7b	-200.09	-0.113
	8a	144.46	0.112	8b	-190.05	-0.115
0.2%	9a	149.57	0.159	9b	-214.41	-0.159
	10a	142.94	0.162	10b	-197.04	-0.164
0.3%	11a	191.7	0.253	11b	-222.89	-0.220
	12a	184.13	0.259	12b	-192.62	-0.269
0.5%	13a	235.81	0.448	13b	-248.6	-0.458
	14a	235.12	0.450	14b	-229.45	-0.471
0.75%	15a	291.16	0.689	15b	-271.2	-0.728
	16a	277.48	0.694	16b	-245.22	-0.732
1%	17a	312.01	0.941	17b	-256.88	-0.976
	18a	290.43	0.926	18b	-216.22	-0.996
1.5%	19a	246.86	1.442			

Table 5-16 Maximum load and drift ratio at each cycle of R_2W(FF)-0.5

Drift ratio	Cycle	Maximum load (kN)	Maximum Drift ratio (%)	Cycle	Maximum load (kN)	Maximum Drift ratio (%)
0.05 %	1a	94.47	0.026	1b	-82.75	-0.017
	2a	96.44	0.028	2b	-82.47	-0.017
0.075%	3a	124.82	0.043	3b	-121.73	-0.038
	4a	126.96	0.048	4b	-119.03	-0.037
0.1%	5a	133.33	0.062	5b	-132.64	-0.062
	6a	127.45	0.073	6b	-128.29	-0.063
0.15%	7a	130.48	0.119	7b	-134.69	-0.108
	8a	121.93	0.122	8b	-129.94	-0.114
0.2%	9a	144.17	0.163	9b	-142.34	-0.166
	10a	140.95	0.167	10b	-137.66	-0.168
0.3%	11a	263.16	0.253	11b	-218.63	-0.250
	12a	257.13	0.257	12b	-214.65	-0.252
0.5%	13a	303.07	0.385	13b	-265.9	-0.441
	14a	274.82	0.442	14b	-250.26	-0.448
0.75%	15a	325.96	0.678	15b	-270.45	-0.708
	16a	309.6	0.694	16b	-242.67	-0.728
1%	17a	328.9	0.940	17b	-293.66	-0.947
	18a	309.82	0.935	18b	-230.78	-0.983
1.5%	19a	333.8	1.405	19b	-254.77	-1.503
	20a	207.09	1.446	20b	-225.22	-1.498

5.4.4.2 Failure Modes

The failure mode of each specimen is shown in Fig. 5-41(a)~(d). The fracture shape of the specimen was divided into two types with glass-fiber reinforce ment on the sides of wall. The first is the fracture shape generated by concentrating diagonal cracks at several spots, and the second is the fracture shape generated by diagonal cracks dispersed throughout the wall. The reason of difference between these types of cracks was that the glass-fiber on the sides of wall prevented concentrated crack.

In the four specimens, cracks occurred in the bed-joints that did not occur in the previous specimens, because of the problems with the mortar applied to the lateral joints. Judging from the low strength of the specimen and cracks in the bed-joints, the strength of the low mortar caused cracks in the bed-joints and the performance of the specimens was lowered.

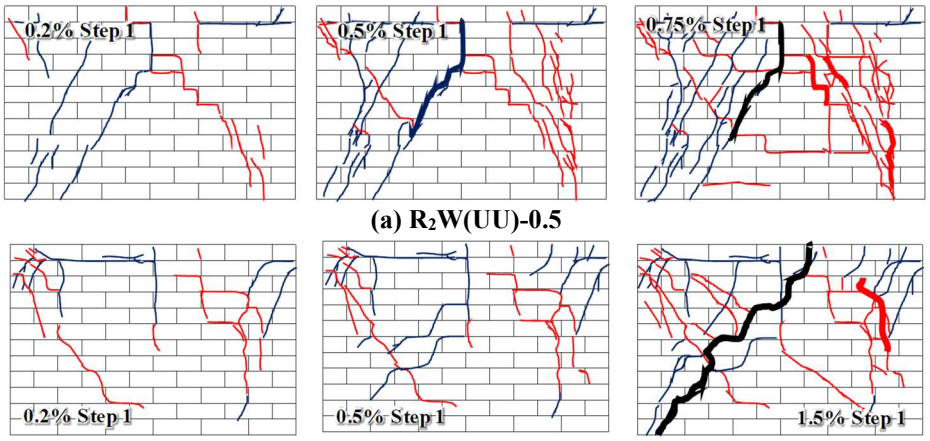

Figure 5-41 Crack propagation of the specimens

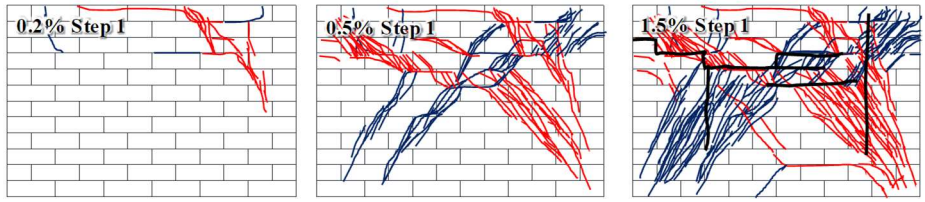

(c) $R_2W(UF)$-0.5

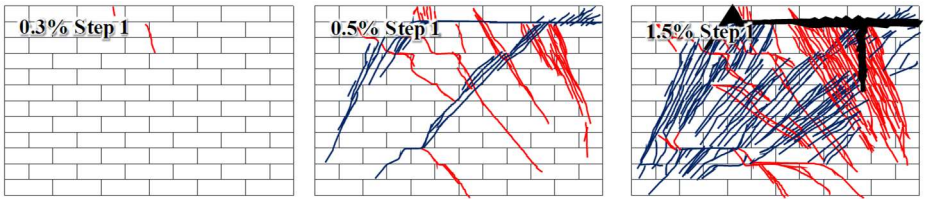

(d) $R_2W(FF)$-0.5

Figure 5-41 Crack propagation of the specimens

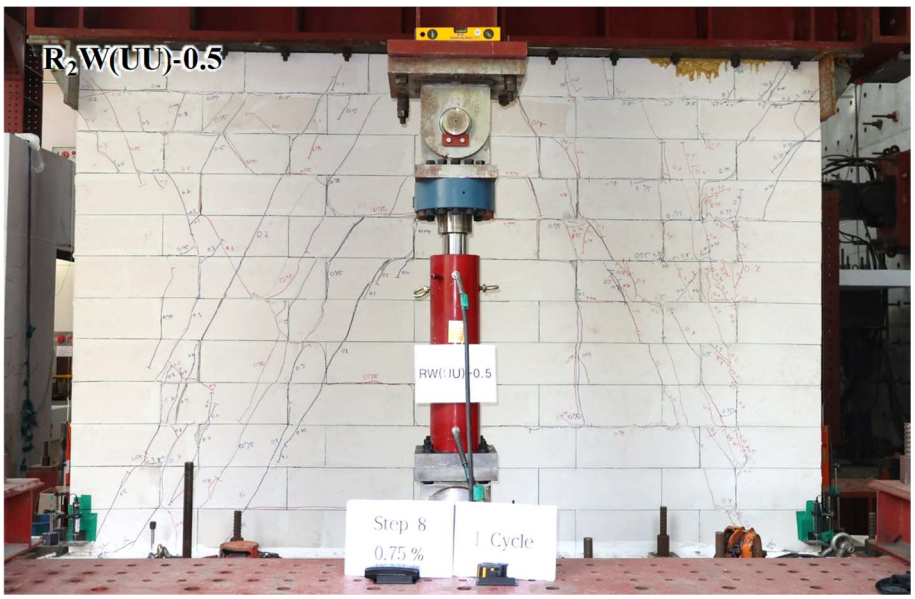

(a) $R_2W(UU)$-0.5

Figure 5-42 Failure modes of 8,9,10,11 specimens at the end of test

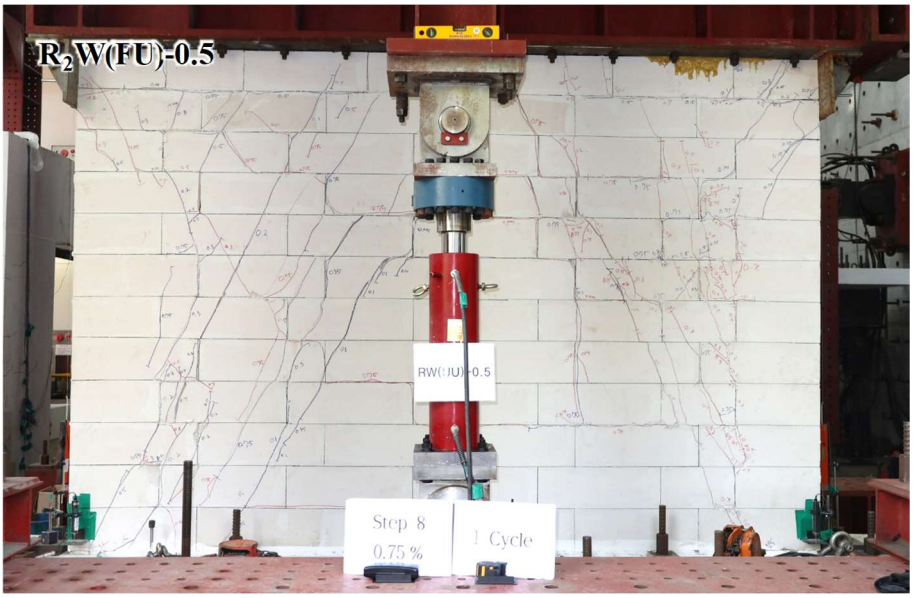

(b) $R_2W(FU)$-0.

(c) $R_2W(UF)$-0.5

Figure 5-42 Failure modes of 8,9,10,11 specimens at the end of test

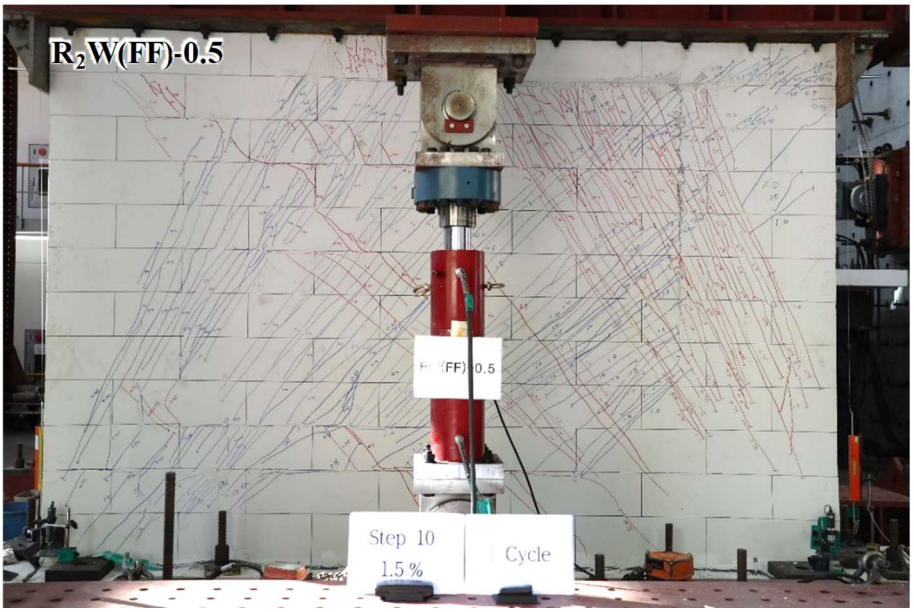

(d) $R_2W(FF)$-0.5

Figure 5-42 Failure modes of 8,9,10,11 specimens at the end of test

5.4.4.3 Strains of reinforcing bars

To check the yield of the reinforcing bar located at sides of the wall, the strain of the reinforcing bar was measured as shown in Fig. 5-43. The horizontal axis of the graph is the lateral displacement ratio, and the vertical axis is the strain (mm / mm) of the Re-bar. The yield strain of reinforcing bars is indicated by the dotted line (= 0.0023). In all four specimens, the reinforcing bars at the ends were deformed under the yield strain.

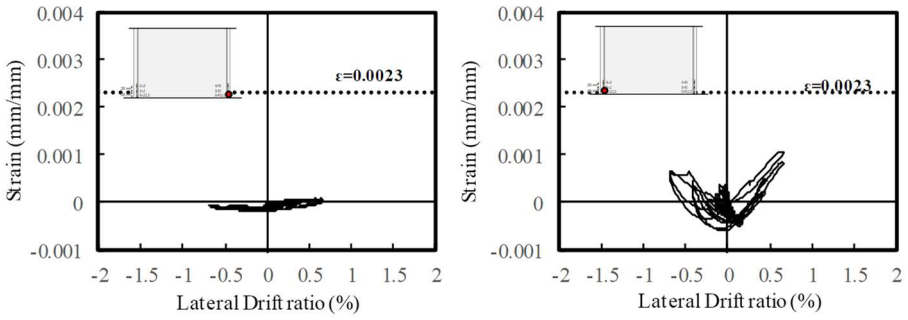

(a) R_2W(UU)-0.5

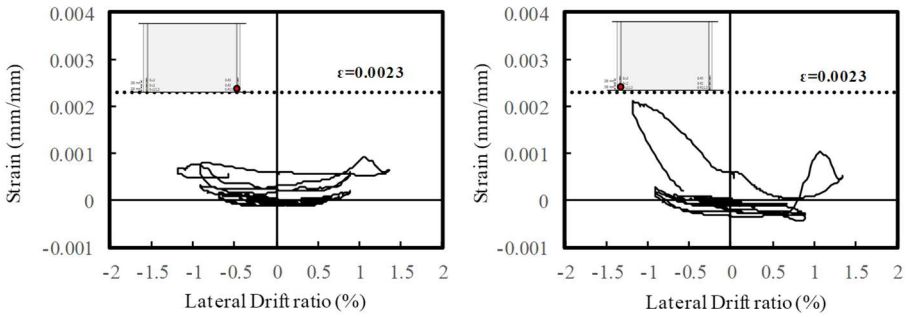

(b) R_2W(FU)-0.5

Figure 5-43 Measured strains in 8,9,10,11 specimens

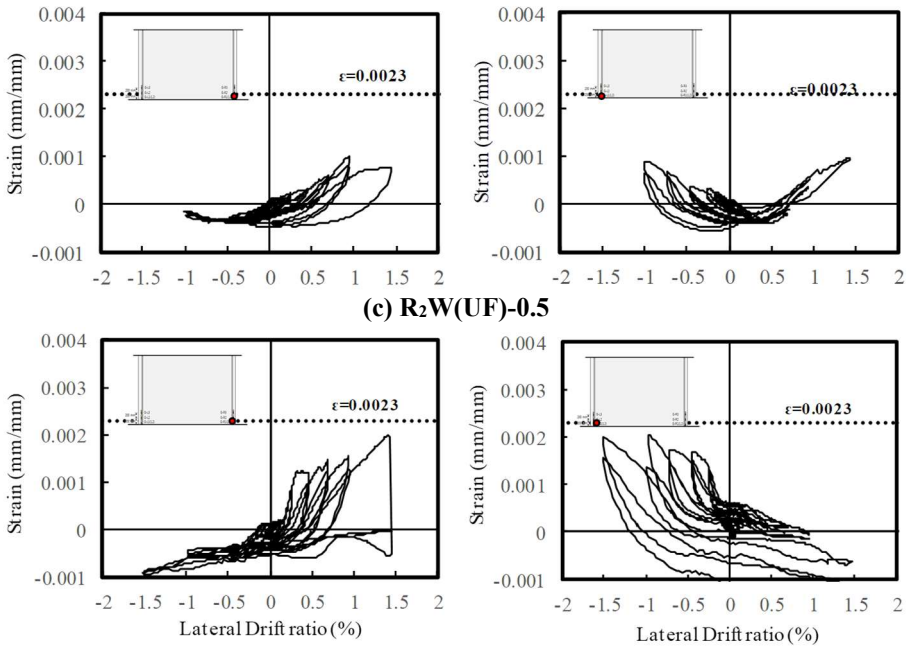

(c) R_2W(UF)-0.5

(d) R_2W(FF)-0.5

Figure 5-43 Measured strains in 8,9,10,11 specimens

5.4.4.4 Deformation Contribution

The sum of shear deformation, the rocking deformation, the flexural deformation, and the slding deformation in the wall were compared with the lateral displacement measured at the top of the wall. In Fig. 5-44, the solid line represents the sum of the shear deformation, rocking deformation, flexural deformation, and local deformation, and the dotted line represents the total lateral deformation measured at the top of the wall deformation.

In R_2W(UU)-0.5 and R_2W(UF)-0.5, sum of the local deformation almost coincided with the total deformation. However, in R_2W (FU) -0.5 and R_2W (FF) -0.5, sum of the local deformaion was smaller than the total deformation. This was because the glass-fibers reinforced at the bed-joints accelerated the sliding

cracks, resulting in additional lateral deformation.

As shown in Fig. 5-45, the ratio of the local deformation to the maximum deformation ratio of each specimen was confirmed, and the shear deformation was the largest. This is because the the fexural strength increased with 2-D16 Re-bar at the sides of wall.

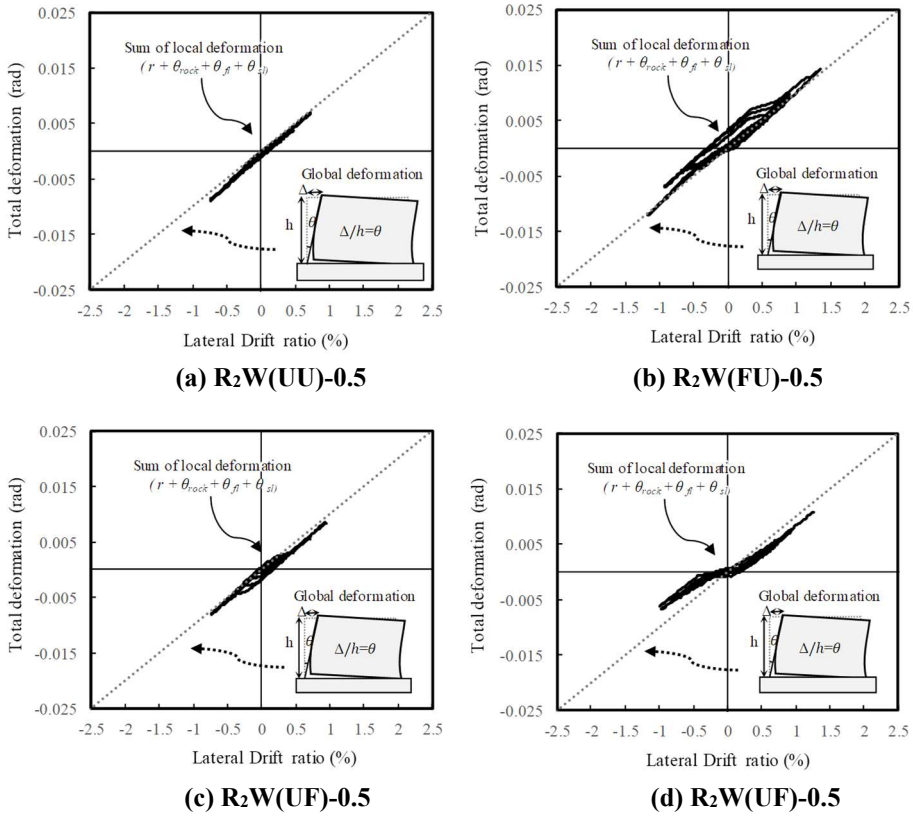

(a) R2W(UU)-0.5 **(b) R2W(FU)-0.5**

(c) R2W(UF)-0.5 **(d) R2W(UF)-0.5**

Figure 5-44 Comparison of sum of the local deformation and the total deformation

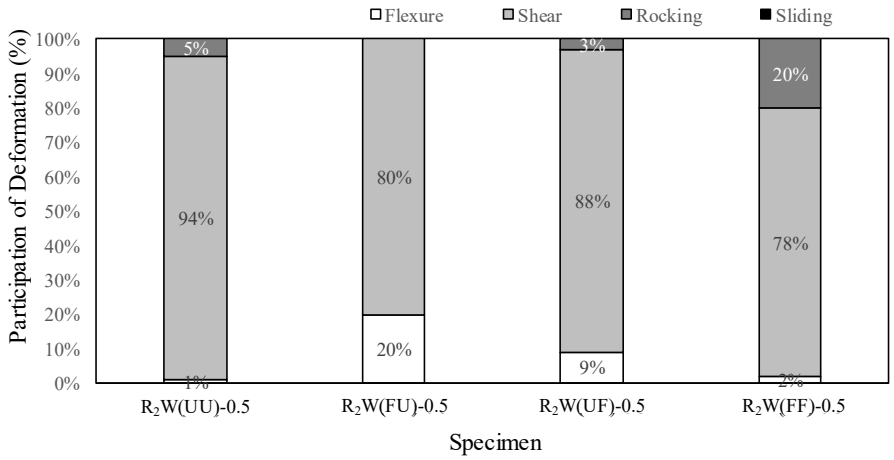

Figure 5-45 Deformation contribution of 8,9,10,11 specimen at the maximum drift ratio

5.4.4.5 Energy dissipation

Fig. 5-46 shows the envelop curves of each specimen. The envelop curve is the curve connecting the maximum load at each drift ratio. The horizontal axis represents the displacement ratio and the vertical axis represents the load. The strength of R_2W(FU) -0.5 was expected to be higher than that of R_2W(FU) -0.5 by reinforcing glass fiber in the bed-joint, but the strength of the specimen was similar to R_2W(UU)-0.5 due to unexpected bed-joint cracks. However, in ductility, R_2W(FU)-0.5 reinforced with glass fibers in the bed-joint showed higher performance than R_2W(UU)-0.5. The strength and ductility of R_2W(UF)-0.5 and R_2W(FF)-0.5, which were reinforced with glass fiber on the sides of wall, increased significantly more than R_2W(UU) -0.5. The strength of R_2W(FF) -0.5 was higher than that of R_2W(UF)-0.5, because the glass fiber on the outer wall prevented the slip between the bed-joints and made glass-fiber at the joint be resisted with shear deformation.

To estimate the energy dissipation capacity of each specimen, the energy dissipation capacity with each drift was compared as shown in Fig. 5-47. The energy dissipation capacity of the four specimens was highest in R_2W(FF)-0.5 reinforced with glass fiber at the bed-joints and on the sides of wall. In the case of R_2W(UU)-0.5 and R_2W(FU)-0.5 not reinforced with the glass fiber on the sides of wall, the strength of joint mortar was weak and there was no difference between R_2W(UU)-0.5 and R_2W(FU)-0.5 in energy dissipation capacity. On the other hand, the effect of glass fiber reinforced with bed-joints was greater in R_2W(UF)-0.5 and R_2W(FF) -0.5 reinforced with glass fiber on the outer wall, and the energy dissipation capacity of R_2W(FF) Which is 70% higher than the

energy dissipation capacity of RW(UF)-0.5. Therefore, when glass-fibers were reinforced simultaneously at the bed-joint and the sides of the wall, the seismic performance of the wall were increased stably.

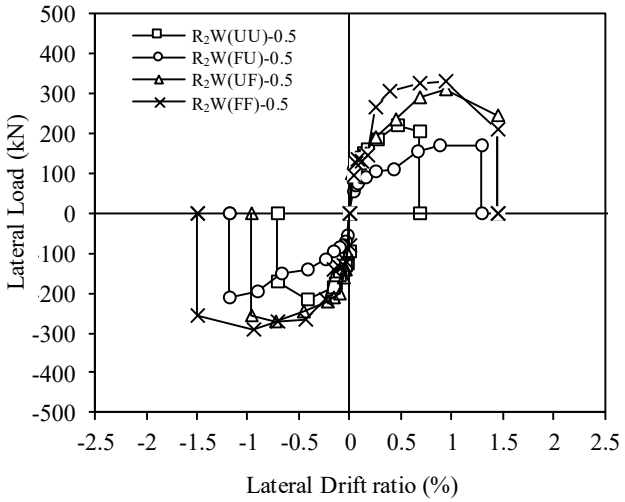

Figure 5-46 Envelope curves of 8,9,10,11 specimens

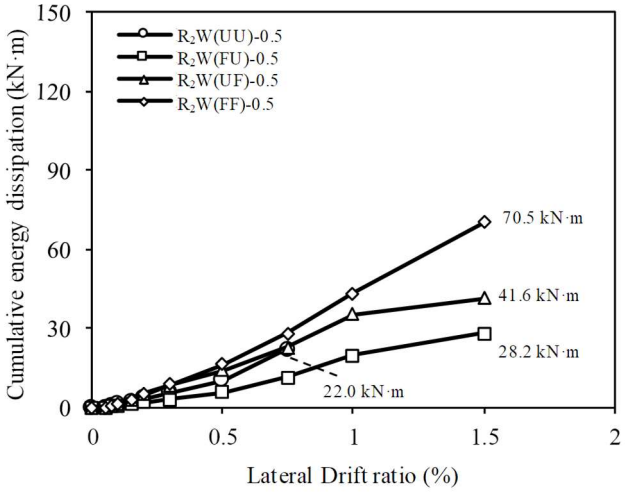

Figure 5-47 Cumulative energy dissipation of 8,9,10,11 specimens

5.5 Discussion

To verify the performance of the ALC wall, the wall cyclic tests were performed with several reinforcement methods. Tests were divided into four types with the reinforcement of the wall, and the performance of the wall with the glass-fiber reinforcement methods were verified for each type.

(1) In the case of walls without reinforcing bars at sides of wall, sliding failure occured at leveling mortar. Therefore, the strength of the wall without vertical Re-bar was determined by the sliding strength.

(2) The flexural strength of Walls reinforced with 1-D16 Re-bar at the sides of the wall were lower than the shear strength. Therefore, a rocking deformation mainly occurred at the sides of the wall, and both conners were destroyed by flexural compression. The flexural strength in these tests was calculated based on the conventional flexural theory, and it was well matched in the ALC wall. In addition, the specimen reinforced with glass-fiber on the sides of wall showed higher ductility and energy dissipation capacity. Therefore, it is possible to increase the seismic resistance of the ALC wall by reinforcing glass-fiber on the wall.

(3) In the wall with openings, the walls devided by an opening resisted lateral loads, and shear cracks occurred on both walls. Therefore, the strength of the opening wall was calculated by the shear strength of both walls. To reinforce the wall with opening, vertical reinforcement was reinforced to the left and right of the opening, or glass-fiber was reinforced on the sides of wall. The vertical reinforcing bars installed on the right and left sides of the opening had no effect,

but the glass-fibers on the outside of the wall increased the strength and ductility by more than 30% and the energy dissipation capacity by more than three times than other specimens. Therefore, it was more effective to reinforce wall with glass-fiber on the sides of wall than to reinforce vertical reinforcement the right and left sides of an opening.

(4) To examine shear strength of ALC wall with of the glass-fiber reinforcement, Walls reinforced with 2-D16 Re-bar at the sides of the wall were tested. However, in all the specimens, cracks occurred in the bed-joints and the expected strength could not be obtained. Especially, in specimen reinforced glass-fiber at bed-joint, cracks easily occured at the bed-joints and failed to perform enough shear strength. However, the glass-fibers on the sides of wall suppressed the sliding of the bed-joints, and made the glass-fibers at the bed-joints exhibit higher shear strength. Therefore, it is recommended to reinforce the glass-fiber on the sides of wall and bed-joints for the seismic reinforcement of the ALC wall.

Table 5-17 Test results of wall specimen

Specimen	Rebar at the end ofwall	Opening	Glass-fiber		Axial force (kN)	Peak Load (kN)	Maximum Drift ratio(%)	Failure Mode	Expected Strength (kN)	Peak Load / Expected strength
			Bed joint	Side of wall						
UW(FU)-0.35	×	×	○	×	370	251	2.0	Slding	222	1.13
UW(FU)-0.5			○	×	370→540	335	2.0	Slding	324	1.03
RW(FU)-0.5	1-D16	×	○	×	370	344.8	2.0	Flexure	376	0.92
RW(FF)-0.5			○	○	370	368	2.5	Flexure	376	0.98
ROW(FU)-0.5		○	○	×	370	233.5	1.0	Shear	311	0.75
UOW(FU)-0.5			○	×	370	227.8	1.5	Shear	311	0.73
UOW(FF)-0.5			○	○	370	329.4	2.5	Shear	311	1.06
R2W(UU)-0.5	2-D16	×	×	×	370	217.5	1.5	Shear	419	0.52
R2W(FU)-0.5			○	×	370	192	1.5	Shear	419	0.46
R2W(UF)-0.5			×	○	370	267	1.5	Shear	419	0.64
R2W(FF)-0.5			○	○	370	313	1.5	Shear	419	0.75

Chapter 6. Summary and conclusion

In this paper, the performance of ALC wall was verified through material tests, prism tests, and cyclic tests of wall. In the material tests, the characteristics of ALC block and mortar were confirmed and the glass-fiber construction method was determined. In the prism test, the effects of glass-fiber reinforcement on different crack modes were tested. In the cyclic tests of wall, the effect of glass-fiber reinforcement on shear performance was tested.

Glass-fiber reinforced ALC walls showed higher performance in terms of strength and ductility than conventional ALC walls. Therefore, seismic performance can be improved by simple reinforcement method with glass-fiber, and it is expected to be useful for seismic ALC building. However, some of the fiber-glass reinforced specimens were not effective due to the low performance of the mortar. Therefore, to exhibit the seismic performance of the ALC building, it is necessary to manage the strength of the mortar.

6.1 Material test

In chapter 3 (material tests), the characteristics of ALC block and mortar were confirmed and the glass-fiber reinforcement method was determined.

(1) The compressive strength of ALC block showed 3~5MPa compressive strength with dry density. The elastic modulus and flexural tensile strength of

ALC block increased with increasing compressive strength and dry density of ALC block. The predictions in ACI 523.4R matched well with test results. These predictions showed elastic modulus and flexural tensile strength of ALC block with compressive strength of ALC block. The compressive strength, elastic modulus and flexural tensile strength of the ALC block varied with the position of the block even if the block had the same dry density. Therefore, before the performance of the structure is evaluated, the compressive strength of the ALC block should be confirmed.

(2) An effective glass-fiber reinforcement method was verified by the flexural tensile strength test of ALC block reinforced with glass-fiber. When the thickness of mortar was 3 ~ 5mm and C-type glass-fiber (tensile strength = 2kN / 50mm, spacing between fibers = 9.5mm) were used, the flexural tensile strength and mortar adhesion of ALC block were the highest. In addition, when the glass-fiber was fixed with a tacker with an interval of 200 mm, adhesion of the glass-fiber was improved.

6.2 Prism test

In chapter 4, based on the test results in chapter 3, the perpormance of mortar and the effects of glass-fiber reinforcement were investigated through prism tests.

(1) Flexural bond strength of the mortar was confirmed by the flexural bond strength test. The flexural bond strength of the ALC mortar satisfied the strength of 0.552 MPa or more proposed by ACI 523.4R. And the glass fiber reinforced

on the sides of specimens increased flexural bond strength and ductility.

(2) The Eq. 4-4 proposed by ACI 523.4R reflected the shear bond strength well with the compressive strength of the ALC block. However, if the mortar was not bonded well, it was easily broken at lower shtrength than expected. And Fiber-glass reinforced at the bed-joints reduced the shear bond strength, whereas glass-fiber reinforced on the sides of specimen increased the shear bond strength and ductility.

(3) In the prism compressive strength test, the compressive strength of prism specimen was smaller than that of the ALC block and it increased with increasing compressive strength of the block. And the glass-fiber reinforcement did not affect the compressive strength of prism.

(4) In prism diagonal tensile strength test, Glass-fiber reinforcement was effective in increasing diagonal tensile strength and its effect was the highest when reinforcing the glass-fibers on the bed-joints and the sides of specimen. In the prism diagonal tensile test, the glass-fiber reinforcing effect was not significant when the strength of the mortar was low.

In the all prism test, test results showed that the performance was improved with glass-fiber reinforcement. However, when the strength of mortar was low and construction conditions was poor, all prisms showed lower strength than expected. Therefore, because mortar strength and conditions were the most important factors affecting the integrity of ALC wall, so that thorough management about mortar is required.

6.3 Cyclic tests of wall

In chapter 5 (cyclic test of wall), sliding shear strength, flexural strength of ALC shear wall and the effects of glass-fiber reinforcement on shear strength were investigated.

(1) In the case of walls without reinforcing bars at sides of wall, sliding failure occurs at leveling mortar. Therefore, the strength of the wall without vertical Re-bar was determined by the sliding shear strength.

(2) In the wall with openings, the vertical reinforcing bars installed at the right and left sides of the opening had no effect, but the reinforced glass-fibers on the outside of the wall increased the strength and deformation capacity by more than 30% and the energy dissipation capacity by more than three times than other specimens. Therefore, it was more effective to reinforce wall with glass-fiber on the sides of wall than to reinforce vertical reinforcement at the right and left sides of opening.

(3) To examine the effects of the glass-fiber reinforcement, Walls reinforced with 2-D16 Re-bar at the sides of the wall were tested. In all the specimens, cracks occurred in the bed-joints and the expected strength could not be obtained. Among them, the glass-fibers on the sides of wall suppressed the sliding cracks at the bed-joints, and made the glass-fibers at the bed- joints exhibit shearing performance. Therefore, it is recommended to reinforce the glass-fiber simultaneously on the sides of wall and at the bed-joints for the seismic reinforcement of the ALC wall.

Appendix A: Design Example

This is an example of the seismic load calculation procedure and method of ALC building according to the Korean building structure standard (KBC 2016) and the evaluation method of seismic performance of ALC masonry wall. The seismic load (Demand) was estimated according to the equivalent static analysis, and the capacity of the ALC wall was evaluated based on the strength equation and test results of ACI 523.4R. The load bearing walls were classified by applying the present low-rise building standard. Instead of considering the atypical of the building, the seismic load was increased by 1.2 times. The building is a two-story ALC house, as shown in Fig. A-1.

The examples are divided into three types with the reinforcement method as shown below.

(1) Case #1 : No Re-bar at both ends of the load bearing wall

(2) Case #2 : 1- D16 Re-bar at both ends of the load bearing wall

(3) Case #3 : 2- D16 Re-bar at both ends of the load bearing wall

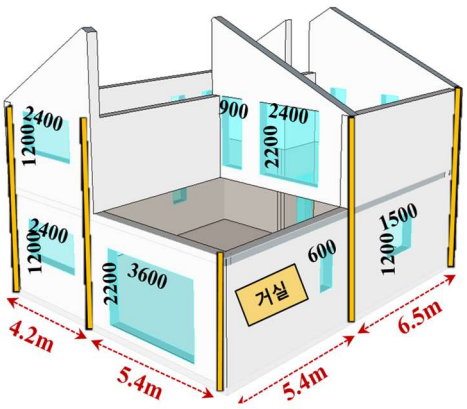

Location	Pohang
Structural type	Loading bearing wall
Usage	Living
Main material	ALC Block, ALC Pannel
Total Area	201.9 m^2
Floor Area	1st floor : 115.5 m^2 2nd floor : 86.4 m^2

Figure A-1 .Informations of example model

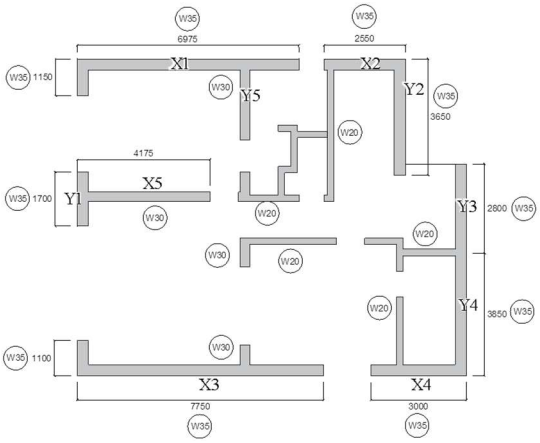

Classification	Thickness of wall
W20	200mm
W30	300mm
W35	350mm

Figure A-2 .Informations of example model

1. Seismic load(Equivalent static analysis)

(a) Effective ground acceleration : S=0.22g

(b) Design ground acceleration : 2/3S

(c) Classication of Ground : S_D

(d) Coefficient of Ground amplication in short period building (F_a) = 1.46

(e) Spectra acceleration

(1) $S_{DS} = S \times 2.5 \times F_a \times 2/3 = 0.22g \times 2.5 \times 1.46 \times 2/3 = 0.535g$

(2) $S_I = S \times F_v \times 2/3 = 0.22g \times 1.58 \times 2/3 = 0.232g$

* Because this building is a low-rise building, it is affected by the acceleration (S_{DS}) of the **short period** design spectrum below.

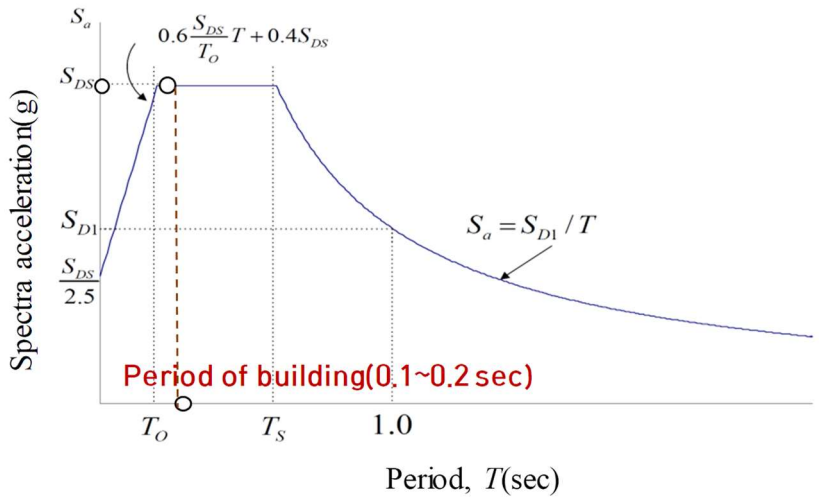

Figure A-3 .Relationships of Period of building and spetra acceleration

(f) Importance factor(I_E) : 1.0 (building for living below 5th floor)

(g) Seismic Category : *D*

(h) Period of building

(1) $T_S = 0.049h_n^{3/4}$=0.188 sec (Height of building : 3m)

(i) Response modification factor(*R*) =1.5

* *R* for Unreinforced masonry wall : 1.5

(j) Base shear (*V*) = 0.357*W* =389.2kN

$$V = C_S W = \frac{S_{D1} W}{[R / I_E]T} \le \frac{S_{DS} W}{[R / I_E]} = \frac{0.535W}{1.5 / 1} = 0.357W$$

(a) Weight of building : 908.6kN

* Floor aera of building×*DL* = 201.9×4.5=908.6 kN

(j) Demand Moment (M_u) = 5/3×389.2×6=1946 kN · m

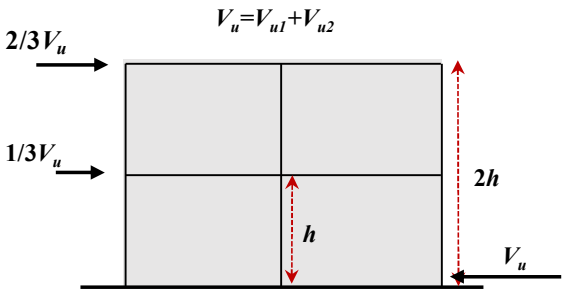

$$\phi M_n > V_{u1}h + V_{u2}2h > (1/3V_u)h + (2/3V_u)2h > (5/3V_u)h$$

Figure A-4 . Demand moment at the base

2. Seismic capacity of ALC walls

2.1 Requirements of ALC load bearing wall in low-rise building standard

(a) The sum of the lengths of the load-bearing walls in each direction shall be not less than 50% of the long-side length. The length of load-bearing wall shall be excluded length of the openings and walls less than 1 m.

(b) Vertical Rebar does not have to be reinforced in the following cases.

(1) Walls with a length of 1200 mm or less.

(2) Vertical reinforcement within 600 mm from wall intersection

(c) The minimum thickness of the bearing walls is to be in accordance with Table A-1.

(d) The minimum ratio of the bearing walls is to be in accordance with Table A-2.

Table A-1 Minimum thickness of bearing wall

Classification	f_{ALC}(MPa)	Inside wall(mm)	Outside wall(mm)
ALC-2	2.0	290	350
ALC-3	3.0	230	290
ALC-4	4.0	200	250
ALC-5	5.0	200	220
ALC-6	6.0	200	200

Table A-2 Minimum ratio of bearing wall

Classification	Floor area≤80m^2	Floor area≥80m^2
1st floor	0.070	0.060
2nd floor	0.063	0.054

(e) Area of bearing walls

The bearing wall of the example building is shown in Fig. A-5 according to low-rise building standard. The x-direction bearing wall is indicated by a blue hatch, and the y-direction bearing wall is indicated by a red hatch. The sectional area of the bearing walls was 8.35m^2 and 4.48m^2 respectively in the x and y directions, and the ratio of bearing wall was 11%, which satisfied the minimum ratio of bearing wall in low-rise building standard.

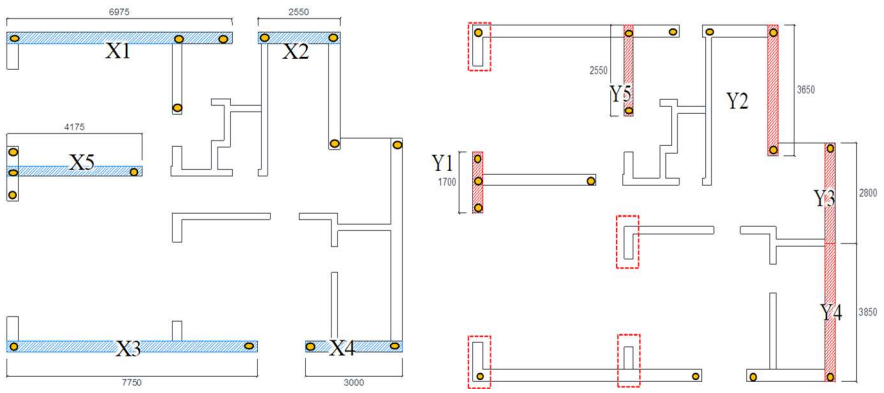

(a) x-drection(8.35m^2) **(b) y-drection(4.48m^2)**

Figure A-5 . Area of bearing walls about each direction

2.1 Capacity of ALC wall

(a) The strength-reduction factors in each code are shown in Table A-3. In this example, according to KBC 2016, the shear strength reduction factor is 0.6 and the flexural strength reduction factor is 0.85.

Table A-3 The strength-reduction factors in each code.

Classification	KBC 2016	ACI 523.4R	ACI 318.14	BCRSM
Shear	0.6[1)] 0.8[2)]	0.75	0.6[1)] 0.75[2)]	0.80
Flexure	0.85	0.9	0.9	0.90

1) shear dominated wall

2) flexural dominated wall

(b) Since the strength equations of the ALC bearing wall are not in the national standard, Eqations in ACI 523.4R were used to evaluate capacity of ALC walls. Explanations of each equation are more discussed follow sections.

(1) Sliding strength

Since there is no domestic standard for the coefficient of friction between the base and the ALC wall, a coefficient of friction of 0.6, which is lower than the coefficient of friction of 1.0 proposed by ACI 523.4R, is applied.

$$V_{sl} = \mu P + 0.6 f_y A_S$$

Where μ is friction coefficient, P is axial load, f_y is yield strength of Re-bar, A_s is sectional area of Re-bar.

· Case #1 : No Re-bar at both ends of the load bearing wall (x-direction)

$$\phi V_{sl} = 0.6(\mu P + 0.6 f_y A_S) = 0.6(0.6 \times 908.6 + 0.6 \times 400 \times 198.6 \times 0) = 327\text{kN}$$

· Case #2 : 1- D16 Re-bar at both ends of the load bearing wall (x-direction)

$$\phi V_{sl} = 0.6(\mu P + 0.6 f_y A_S) = 0.6(0.6 \times 908.6 + 0.6 \times 400 \times 198.6 \times 11) = 642\text{kN}$$

· Case #3 : 2- D16 Re-bar at both ends of the load bearing wall (x-direction)

$$\phi V_{sl} = 0.6(\mu P + 0.6 f_y A_S) = 0.6(0.6 \times 908.6 + 0.6 \times 400 \times 198.6 \times 22) = 956\text{kN}$$

Table A-4 Sliding strength in each case

Classification	Case #1		Case #2		Case #3	
	x[1)]	y[2)]	x	y	x	y
Number of Re-bar	0	0	11	9	22	18
Sliding Capacity (kN)	327	327	642	584	956	842
Sliding Demand (kN)	389.2					
Result	N·G	N·G	O·K	O·K	O·K	O·K

1) X = x-direction, 2)Y=y-drection

As a result of the elastic analysis on the sliding strength, sliding failure occurred in the building without vertical reinforcement. Therefore, to prevent fracture to the sliding, the end Re-bar must be reinforced to be higher than the demand strength.

(2) Shear strength

The shear strength of ALC wall in ACI 523.4R is 59% of the elastic shear strength of the ALC wall in which the ALC mortar is applied to both the horizontal and vertical joints, and the wall constructed only in the horizontal joint is calculated to be 38% of the elastic shear strength. The shear strength of the wall of the example is 59% of the elastic shear strength because the mortar is a wall constructed in both horizontal and vertical joints.

$$V_{sh} = \phi 0.59 \cdot \frac{2}{3} L t f_t \sqrt{1 + \frac{P}{f_t L t}}$$

Where L is length of wall, t is thickness of wall, f_t is split tensile strength of ALC block.

The shear strength of each model was calculated by summing the shear strengths of the walls in each direction. At this time, the compressive strength of ALC was assumed to be 3 MPa and the axial force ratio was assumed to be 2%, and relationships of the splitting tensile strength(f_t) and compressive strength(f_{ALC}) was used[$f_t = 0.2\sqrt{f_{ALC}}$]. The shear strength of the X1 wall is shown below, and the shear strength of the total strength wall is shown in Table 6-14

· Shear strength of X1 wall

$$V_{sh} = 0.6 \times 0.59 \times \frac{2}{3} Lt \times 0.2\sqrt{f_{ALC}} \times \sqrt{1 + \frac{f_{ALC} Lt \times \text{Axial load ratio}}{0.2\sqrt{f_{ALC}}\, Lt}}$$

$$= 0.6 \times 0.59 \times \frac{2}{3} \times 6975 \times 350 \times 0.2\sqrt{f_{ALC}} \times \sqrt{1 + \frac{\sqrt{3} \times 0.02}{0.2}} = 221 \text{ kN}$$

Table A-5 Shear strength of bearing walls

X -direction			Y -direction		
Wall	Length(mm)	Shear Strength(kN)	Wall	Length(mm)	Shear Strength(kN)
X1	6,975	221	Y1	1,700	54
X2	2,550	81	Y2	3,650	116
X3	7,750	246	Y3	2,800	89
X4	3,000	95	Y4	3,850	122
X5	4,175	114	Y5	2,550	67
$\sum V_{sh}$		757			448
Demand	389.2 kN				
Result	O·K				

(3) Flexural crack strength (unreinforced ALC wall)

In ACI 523.4R, flexural cracks occur when the tensile stress generated by the moment due to the lateral force in the leveling mortar where the foundation meets the wall is larger than the flexural bond strength of the leveling mortar. Therefore, wall without vertical reinforcing steel reinforcement, leveling mortar of wall recieve tensile stress greater than the flexural crack strength, fracture due to sliding occurs following the lower end flexural crack.

When there is no axial force, the stress due to moment is symmetrically distributed as shown in Fig. A-6 (a). However, when axial force acts, the tensile stress acts on the flexural bond strength of the leveing mortar as shown in Fig. A-6(c). And a wall could receive grater lateral load until mortar stress reaches the flexural bond strength.

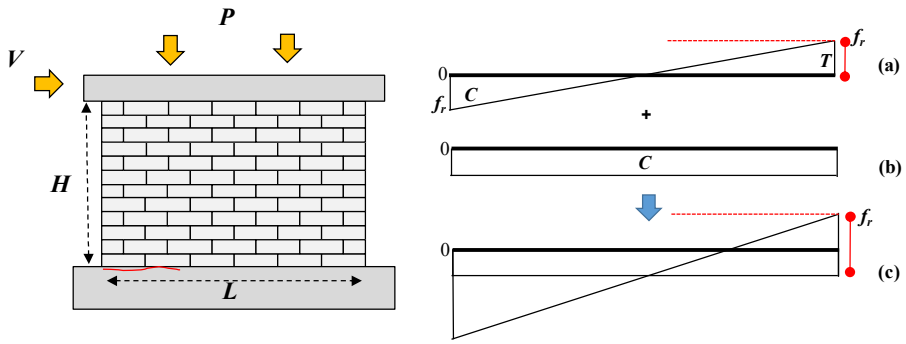

Figure A-6 . Forces in unreinforced ALC walls

Since the flexural crack strength is lower than the sliding strength and flexural strength associated with the wall strength, ACI 523.4R does not consider wall strength calculations. Therefore, in this example, the flexural crack strength was examined only for the purpose of confirming the magnitude of the flexural crack strength. The flexural bond strength (f_r) was proposed by

ACI 523.4R as 0.345 MPa. (The average of flexural bond strength (f_r) was 0.350 MPa, which was consistent with the flexural bond strength proposed by ACI 523.4R) Therefore, the flexural crack strength of the X1 wall is calculated as follows, and the flexural crack strength of the total load wall is shown in Table 6-15.

$$V_f = \left(f_r + \frac{P}{A} \right) \times \frac{tL^2}{6H} \rightarrow M_f = \left(f_r + \frac{P}{A} \right) \times \frac{tL^2}{6}$$

Where f_r is flexural tensile strengh of leveling (bed) mortar, H is height of wall.

· flexural crack strength of X1 wall

$$M_f = (0.345 + 3 \times 0.02) \times \frac{350 \times 6975^2}{6} \times 10^{-6} = 1{,}149 \text{ kN} \cdot \text{m}$$

Table A-6 Flexural crack strength of bearing walls

X -direction			Y -direction		
Wall	Length(mm)	Flexural crack Strength(kN·m)	Wall	Length(mm)	Flexural crack Strength(k·Nm)
X1	6,975	1,149	Y1	1,700	68
X2	2,550	154	Y2	3,650	315
X3	7,750	1,419	Y3+Y4	6,650	1,045
X4	3,000	213			
X5	4,175	412	Y5	2,450	142
$\sum M_f$		3,346			1,570
Demand	1,946		1,946		
Result	O·K		N·G		

(4) Flexural strength (reinforced ALC wall)

The flexural strength of the ALC wall is determined according to ACI 523.4R as follows: the maximum compressive strain of the ALC block is assumed as 0.003, the compressive stress block height is $0.85f_{ALC}$, the width is $\beta_1 c$ (β_1 = 0.67) and the flexural strength reduction factor., it was assumed that the tensile Re-bar was yielded and the force of compressive Re-bar was 0 to simplify the calculation below equation.

$$M = T_s(L_1 - L/2) - C_S(L/2 - L_2) + C_{ALC}\left(\frac{L-a}{2}\right)$$

Where T_S is compressive force of Re-bar in tension zone, C_s is tensile force of Re-bar in compression zone, L_1(=150 mm) is distance of compressive Re-bar from the end of wall, L_2(=L - 150 mm) is distance of tensile Re-bar form the end of wall, C_{ALC} is compressive force of ALC, a is width of compressive force of ALC.

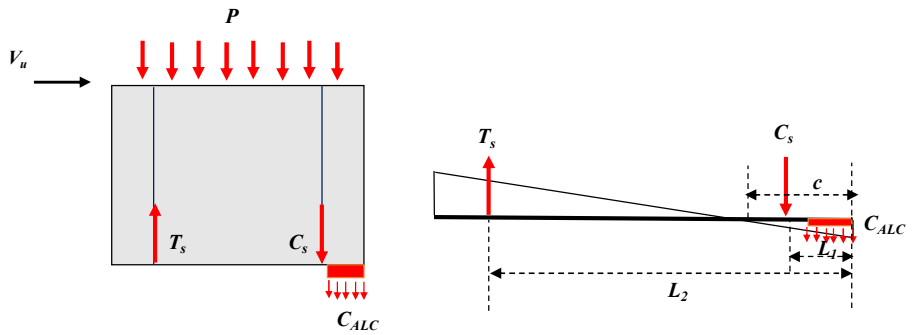

Figure A-7 . Forces in reinforced ALC walls

(i) Calculation of neutral axis*(c)*

$$P + T_S - C = 0$$

☞ $f_{ALC} A \times \text{axial load ratio} + A_{st} f_y - 0.85 \beta_1 f_{ALC} c t = 0$

☞ $3.0 \times 6975 \times 350 \times 0.02 + 198.6 \times 400 - 0.85 \times 0.67 \times 3.0 \times c \times 350 = 0$

C=377.8 mm

(ii) flexural strength

$$M = T_s (L_1 - L / 2) + C_{ALC} \left(\frac{L - a}{2} \right)$$

☞ $M_n = 79.4(6.825 - 3.487) + (0.85 \times 0.67 \times 3.0 \times 377.8 \times 350 \times 10^{-3}) \times \left(\frac{6.975 - 0.253}{2} \right)$

$= 1,024$ kN

Table A-7 Flexural strength of bearing walls reinforced with 1-D16

X -direction			Y -direction		
Wall	Length(mm)	Flexural Strength(kN·m)	Wall	Length(mm)	Flexural Strength(k·Nm)
X1	6,975	1,024	Y1	1,700	146
X2	2,550	249	Y2	3,650	404
X3	7,750	1,202	Y3+Y4	6,650	891
X4	3,000	310			
X5	4,175	419	Y5	2,450	208
$\sum M_n$		3,204			1,649
$\sum \phi M_n$	2,723		1,401		
Demand	1946 kN·m				
Result	O·K		N·G		

Table A-8 Flexural strength of bearing walls reinforced with 2-D16

X -direction			Y -direction		
Wall	Length(mm)	Flexural Strength(kN·m)	Wall	Length(mm)	Flexural Strength(kN·m)
X1	6,975	1,543	Y1	1,700	255
X2	2,550	424	Y2	3,650	665
X3	7,750	1,780	Y3+Y4	6,650	1,361
X4	3,000	520			
X5	4,175	700	Y5	1,700	255
$\sum M_n$		4,967			2,645
$\sum \phi M_n$	4,222		2,248		
Demand	1,946 kN				
Result	O·K		O·K		

(4) Comparison of Demand and Capacity

The demand strength and the capacity of the example were compared as shown in Table A-9. In the unreinforced building, the sliding strength and the flexural crack strength were lower than the demand strength. In the building reinforced with 1-D16 at ends of bearing walls. the flexural strength in y direction was lower than the demand strength. Therefore, to safely design building with 0.22 g ground accrelation, 2-D16 rebars at both ends of the bearing wall must be reinforced to satisfy the flexural strength as shown in Fig. A-8.

Table A-9 Comparason with the capacity and the demand strength

Classification	No Rebar		1-D16		2-D16	
	X-Dir.	Y-Dir.	X-Dir.	Y-Dir.	X-Dir.	Y-Dir.
Sliding strength(kN)	327	327	642	584	956	842
Shear strength (kN)	757	448	757	448	757	448
Flexural crack strength (kN·m)	3,005	1,570	-	-	-	-
Flexural strength (kN·m)	-	-	2,723	1,401	4,222	2,248
Demand strength	· V_u=389.2 kN, M_u=1,946kN·m					

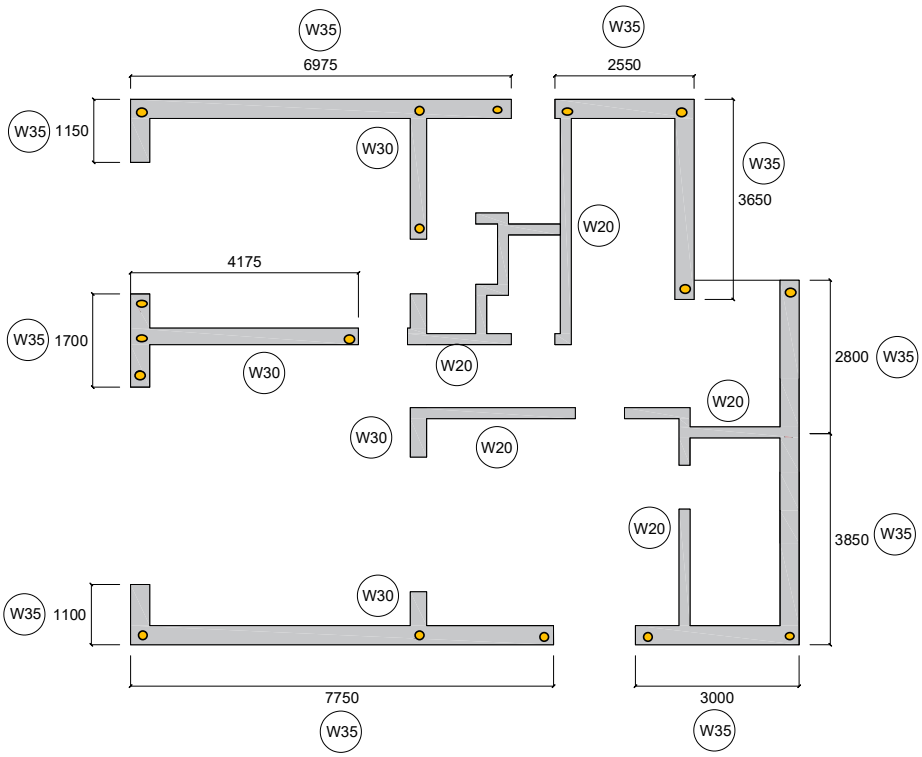

Figure A-8 . Plan View of 1st floor reinforced with 2-D16 Re-bar

References

[1] MOCT 376 : 1997, “Design standard for ALC block”, Ministry of Construction & Transportation

[2] MOCT 377 : 1997, “Design standard for ALC Design standard for ALC panel”, Ministry of Construction & Transportation

[3] KS F 2701 : 2012, “ALC block”, Korean Industrial Standards

[4] KS F 4914 : 2012, “ALC Panel”, Korean Industrial Standards

[5] ACI 523.4R : 2009,“Guide for Design and Construction with Autoclaved Aerated concrete Panels”

[6] DIN EN 12602 : 2013, “ Prefabricated Reinforced Components of Autoclaved aerated concrete”

[7] BCRSM : 2013, “Building Code Requirements and Specification for Masonry Structures”

[8] Eurocode 6 : 2005, “Design of Masonry Structures”

[9] RILEM : 1993, “Autoclaved Aerated Concrete Properties, Testing and Design”

[10] ASTM : 2011, “Standard Test Methods forSampling and Testing Brick and Structural Clay Tile(C67)”

[11] ASTM : 2016, “Standard Test Method for Flexural Strength of Concrete (Using Simple Beam with Third-Point Loading), (C78/C78M) ”

[12] ASTM : 2016, “Standard Specification for Masonry Cement(C91/C91M)”

[13] ASTM, “Standard Test Method for Compressive Strength of Hydraulic Cement Mortars(C109/C109M)”, 2016

[14] ASTM, “Standard Specification for Mortar for Unit Masonry(C270), 2014

[15] ASTM, “Standard Specification for Grout for Masonry”, 2016

[16] ASTM, “Standard Test Methods for Flexural Bond Strength of Masonry(E518/E518M)”, 2015

[17] ASTM, “Standard Test Method for Diagonal Tension (Shear) in Masonry Assemblages(E519/E519M), 2015

[18] ASTM, “Standard Specification for Thin-bed Mortar for Autoclaved Aerated Concrete (AAC) Masonry(C1660)”, 2010

[19] ASTM, “Standard Practice for Construction and Testing of Autoclaved Aerated Concrete (AAC) Masonry(C1692)”, 2011

[20] ASTM, “Standard Specification for Unreinforced Autoclaved Aerated Concrete (AAC) Masonry Units(C1691)”, 2011

[21] ASTM, “Standard Specification for Autoclaved Aerated Concrete (AAC)(C1693)”, 2011

[22] Tanner, “Design provisions for autoclaved aerated concrete(AAC) structural systems”, 2003

[23] Cancino, “Behavior of autoclaved aerated concrete shear wall with low-strength AAC)”, 2003

[24] A.Penna et al.“Experimental assessment of the in-plane lateral capacity of autoclaved aerated concrete (AAC) masonry walls with flat-truss bed-joint reinforcement, 2015”

[25] Portland Cement Associaition(PCA),“Masonry Information (Masonry cement:product data sheet), 2002

[26] L.Berto et al, “Failure mechanism of masonry prism loaded in axial compression: computational aspects”, 2004

초 록

반복 횡 하중을 받는 경량기포콘크리트 조적벽체의 구조적 성능

김 영 문

서울대학교 건축학과 대학원

ALC (Autoclave lightweight concrete)는 고온 고압 증기 양생 과정을 통해 제작된 기성콘크리트이다. ALC 물보다 가볍기 때문에 일반 블록보다 시공하기가 쉽고, 내부에 기공이 많아 단열성능도 우수하다. 세계2차대전 이후, 독일의 주택복구에 ALC가 널리 사용되었고, 이후 유럽을 중심으로 여러나라에서 많이 사용되었다. 현재 우리나라에서도 높은 시공성과 우수한 단열 성능으로 소규모 주택에서 구조재로 사용되고 있다.

경주 지진과 포항 지진이 발생한 이후, 우리나라에서는 내진 법규가 강화되었고, ALC 건물 또한 내진 법규를 적용대상이 되었다. 현재 우리나라에는 내진과 관련된 ALC 기준은 없고, ALC에 대한 구조적 실험과 연구가 거의 진행되지 않았다. 그래서 국내 ALC 건물이 어느정도의 내진능력을 갖고 있는지 예측하기는 힘들다.

따라서 본 연구에는 ALC 재료, 프리즘, 벽체 실험을 통하여 재료의 성능부터 벽체의 성능까지 검증하였고, 이를 국외기준(ACI 523.4R)과

비교하였다. 또한 ALC의 낮은 인장강도를 보완하고 내진성능을 높이기 위해서, 유리섬유를 보강 따른 성능평가를 병행하여 진행하였다. 그 결과, 기본적인 재료의 강도, 내진성능을 만족하기 위한 수직철근 보강법, 유리섬유 보강법을 확인 및 제안할 수 있었고, 유리섬유보강이 벽체의 전단강도에 미치는 효과도 확인할 수 있었다.

본 연구는 ALC벽체의 구조적 성능을 횡가력 반복실험을 통해 평가하고, 보강방법에 따른 효과를 검증함으로써 소규모 ALC 주택 설계시 내진성능을 평가할 수 있는 근거를 제공할 수 있을 것으로 기대된다. 그리고 유리섬유 보강을 통한 내진보강효과가 ALC 구조뿐만 아니라 다른 조적조에 구조의 내진보강에도 도움이 될 것으로 예상한다.

주요어 : 경량기포콘크리트, 유리섬유, 전단강도, 전단벽체, 조적조

학 번 : 2017-22064

감사의 글

군인으로서 9년간의 군복무를 수행한 후, 늦은 나이로 입학한 석사과정 2년은 저에게는 쉽지만은 않은 시간이었습니다. 하지만 교수님의 지도와 연구실 동료들의 도움으로 석사과정을 잘 마칠 수 있었습니다. 이렇게 보람있는 배움의 기회를 준 조국에 감사하며, 군에 돌아가서도 석사과정에서 습득한 지식이 국가에 도움이 되도록 복무하겠습니다.

먼저 부족한 저를 가르쳐주시고 연구를 맡기고 지도해 주신 박홍근 교수님께 진심으로 감사드립니다. 그리고 항상 응원의 메시지를 주시며 연구를 지도해주신 홍성걸 교수님, 신영수 교수님 감사드립니다. 또한 열정적인 강의로 구조에 흥미를 갖게 해주신 이철호 교수님, 강현구 교수님 감사드립니다.

같이 연구를 하고 큰 도움을 준 동갑내기 친구이자 나의 사수인 김철구 교수, 언제나 두꺼운 대화를 즐기던 백장운 교수, 자기 관리가 철저한 호준이, 행복 바이러스 멋진 정일이, 육사동기 여동생인 성실한 주옥이, 같이 쉬는 시간을 보내던 열정적인 방장 현진이, 연구실의 브레인 성현이와 다정한 주형이, 육사 후배 착한 광원이, 졸업 후 더 멋있어진 환철이, 입학동기 현근이, 요즘 실험으로 바쁜 해빈이와 듬직한 종훈이, 연구실 막내 진영이, 연구실 식구들 모두 감사드립니다.

항상 남편이 늦게 퇴근해도 불평없이 옆자리를 지켜준 사랑하는 아내 소이, 귀여운 아들 민준, 예쁜 딸 민하 미안하고 사랑하고 감사합니다. 그리고 절 항상 믿어 주시고 응원해 주신 아버지, 어머니, 장모님 감사드립니다.

그 외 저에게 도움과 힘을 주신 분들이 많습니다. 이 모든 분들께 감사드립니다. 석사 2년동안 이러한 분들과 같이 했다는 것을 영광과 행운으로 여기며, 군에 복귀해서는 조국에 도움이 될 수 있도록 최선을 다해 노력하겠습니다.